DOKUZ EYLÜL UNIVERSITY

GRADUATE SCHOOL OF NATURAL AND APPLIED SCIENCES

SLOPE STABILITY OF THE OPEN PITS-ROCK SLOPE

by

Dramane SOGORE

July, 2018

İZMIR

SLOPE STABILITY OF THE OPEN PITS-ROCK SLOPE

A Thesis Submitted to the
Graduate School of Natural and Applied Sciences of Dokuz Eylül University
In Partial Fulfillment of the Requirements for the Degree of Master of Science in Geological Engineering, Applied Geology Program

by
Dramane SOGORE

July, 2018
İZMİR

M.Sc THESIS EXAMINATION RESULT FORM

We have read the thesis entitled **"SLOPE STABILITY OF THE OPEN PITS-ROCK SLOPE"** completed by **DRAMANE SOGORE** under supervision of **PROF. DR. NECDET TÜRK** and we certify that in our opinion it is fully adequate, in scope and in quality, as a thesis for the degree of Master of Science.

....

Prof. Dr. Necdet TÜRK

Supervisor

....

Prof. Dr. A. Bahadır Yavuz

(Jury Member)

....

Prof. Dr. Halil KUMSAR

(Jury Member)

Prof. Dr. Latif SALUM

Director

Graduate School of Natural and Applied Sciences

ACKNOWLEDGEMENT

I express my sincere gratitude and sincere thanks to my supervisor **Prof. Dr. Necdet TÜRK** for his guidance and constant encouragement and support during the course of my Research work. I truly appreciate and values his esteemed guidance and encouragement from the beginning to the end of this works.

I sincerely thank to **Prof. Dr. Mümtaz ÇOLAK** Head of the Department Geology, and all the authorities of the institute for providing nice academic environment and other facility in the Campus. Also I would like to thanks all Professors of Geological Engineering Department who helped me directly and indirectly.

I am also thankful to all the staff members of **Geotechnical Section in Sadiola Open Pit Gold Mine** for their assistance and co-operation during the course of experimental works. I also thank all my mates who have directly or indirectly helped me in my work and shared the moments of joy and sorrow throughout the period of work.

To my family and loved ones for their constant words of encouragement, support and unfailing love, without which I could not have completed this study, I say a big thank you.

Dramane SOGORE

SLOPE STABILITY OF THE OPEN PITS-ROCK SLOPE

ABSTRACT

The stability of slopes in Sadiola Open Pit Gold Mines is an issue of great concern because of the significant detrimental consequences instabilities can have. To ensure the safe and continuous economic operation of these mines, it is necessary to systematically assess and manage slope stability risk. This however has not been traditionally easy due to the fact that measuring the parameters needed to assess the stability of slopes can be laborious, expensive, and cause disruption to mining operations.

Slope stability is affected by many factors, their effects on the slope stability may be big or small. It is more important to identify the main influencing ratio factors in the process of analyzing the slope stability.

Keywords: Slope stability, Simplified Bishop Method, Fellenius Method, factor of safety, Hoek diagram, Sadiola open pit gold mine (Mali)

AÇIK İŞLETMELERDE-KAYA ŞEVLERİNDE ŞEV STABİLİTESİ

ÖZ

Sadiola Açık Altın Madenlerinde yamaçların stabilitesi, istikrarsızlıkların sahip olabileceği önemli zararlı sonuçlardan dolayı büyük bir endişe konusudur. Bu madenlerin güvenli ve sürekli ekonomik çalışmasını sağlamak için, şevlerin stabilite riskini sistematik olarak değerlendirmek ve yönetmek gereklidir. Ancak bu, eğimlerin stabilitesini değerlendirmek için gerekli parametrelerin ölçülmesinin zahmetli, pahalı ve madencilik işlemlerine zarar verebilmesinden dolayı geleneksel olarak kolay olmamıştır.

Şev stabilitesi birçok faktörden etkilenir, şev stabilitesi üzerindeki etkiler büyük veya küçük olabilir. Şev stabilitesini analiz etme sürecinde ana etkileme oranı faktörlerini tanımlamak daha önemlidir.

Anahtar kelimeler: Şev stabilitesi, Simplified Bishop Metodu, Fellenius Metodu, güvenlik faktörü, Hoek diyagram, Sadiola açık altın Maden (Mali)

CONTENTS

Page

LIST OF FIGURES

Page

LIST OF TABLES

Page

CHAPTER ONE
INTRODUCTION

1.1 Introduction

This study was conducted as a Master of Science Thesis in partial fulfillment of the requirements necessary for the award of a Master of Science Degree in Geological Engineering by the Graduate School of Natural and Applied Sciences, Dokuz Eylül University, Turkey.

1.2 Location and Physiography

The Sadiola Hill gold mine is situated in the Sadiola goldfield, in western Mali at about 77km south of the regional capital, Kayes, near the international border of Mali with Senegal (Figure 1.1). Mali is a landlocked country bordered by Niger to the east, Burkina Faso to the east, Algeria to the north, and Senegal and Mauritania to the west in the West African Savannah-Sahel region. The official language in Mali is French with 80% of the population speaking Bambara. Muslim is the dominant religion in Mali with a small group being Christian, with the remainder practising African religions.

The climate is subtropical to arid with distinct dry and rainy seasons and the dry season is warm from November to February (15˚ to 30˚C) and hot from March to June (25˚ to 45˚C) (IAMGold.com). The rainy season lasts from July to October. The dominant infrastructure in the study area is the mining operations and a mine town that includes schools, clinics and shops for the Sadiola mine employees and their dependent.

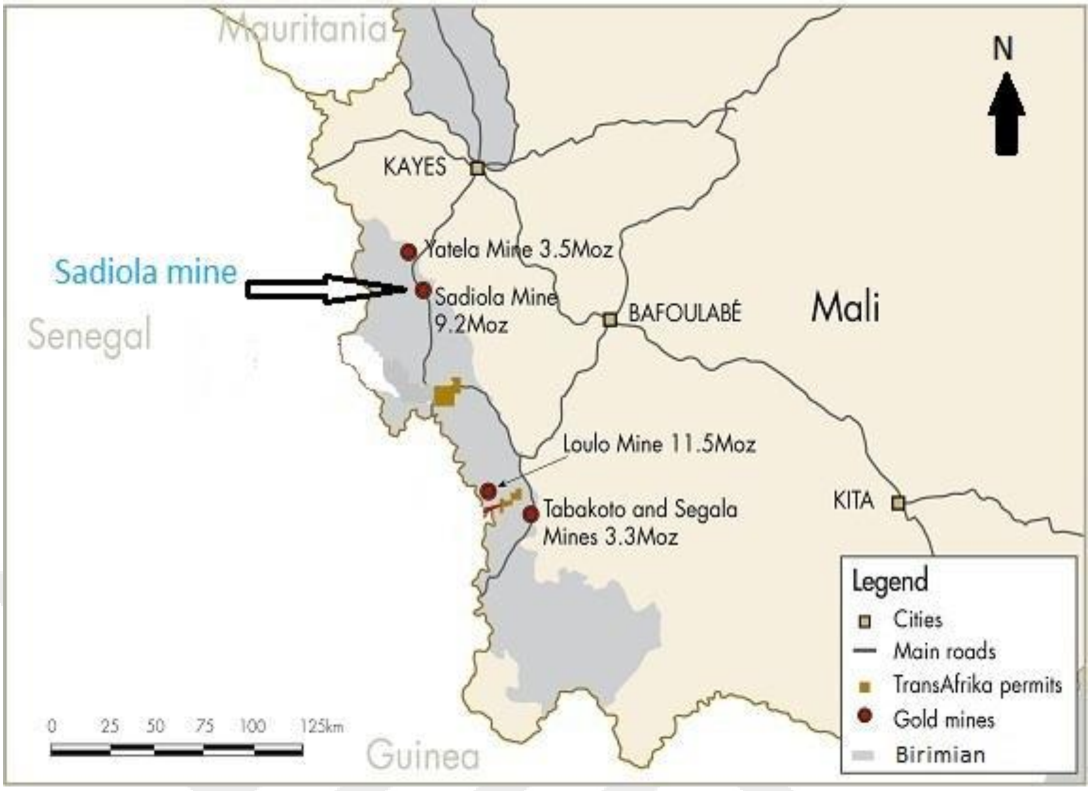

Figure 1.1 Locality map of Mali showing neighbouring countries, Sadiola and other gold Mines with estimated reserves, and the occurrence of the Birimian rocks (Iamgold, 2007)

1.3 Aims of the study

Excavation usually takes place in a series of benches, each of which may be many meters high, so the geotechnical engineer must evaluate the stability of individual benches as well as the overall slope.

This implies, on the one hand that the slopes of the pit be as steep as possible, but on the other hand, the steeper the slopes, the greater the danger of slope failures. Slope instabilities can have detrimental consequences, both in terms of economic damage, and sometimes even loss of life. To ensure the safe and economic operation of these mines, it is necessary to systematically assess and manage slope stability risk.

This document presents a framework based on decision theory by which risk can be systematically assessed and managed. The risk assessment involves estimating the properties of the materials in the slopes, calculating the stability of various slope geometries, and monitoring the performance of the slopes as the pit is developed.

CHAPTER TWO

REGIONAL GEOLOGY AND MINE GEOLOGY

2.1 Regional Geology

2.1.1 Geology of the West African Craton

The West African Craton (WAC) is composed of an Achaean and Palaeoproterozoic basement that is divided into two shields which are the Reguibat shield in the north and the Man shield in south (Potrel et al., 1998). These two shields are separated by the Taoudeni basin, which is Neoproterozoic to Devonian in age and are entirely surrounded by Pan African and Hercynian belts (Matthias and Hein 2002). The Reguibat shield contains Palaeoproterozoic assemblages in the eastern part as well as Archean relicts which include kimberlites (Ennih and Liegeois, 2008). Large parts of the WAC in the Man Shield consist of Palaeoproterozoic rocks referred to as the Birimian Supergroup (Abouchami et al. 1990; Beziat et al., 2000). The Birimian Supergroup represents a juvenile crust without any influence of surrounding Archean continents (Abouchami et al. 1990; Pawlig et al. 2006). The Man Shield has been divided into three age provinces (Marcfarlane et al. 1981): Leonean (~ 3.0 Ga), Liberian (~ 2.7 Ga), and Eburnean (~ 2.0 Ga), but there is a debate as to whether the Leonean and Liberian are two separate events or a single event due to limited radiometric dating (Matthias and Hein 2002). The Man Shield crops out in the Kedougou-Kenieba Inlier in the western part of the Birimian Supergroup.

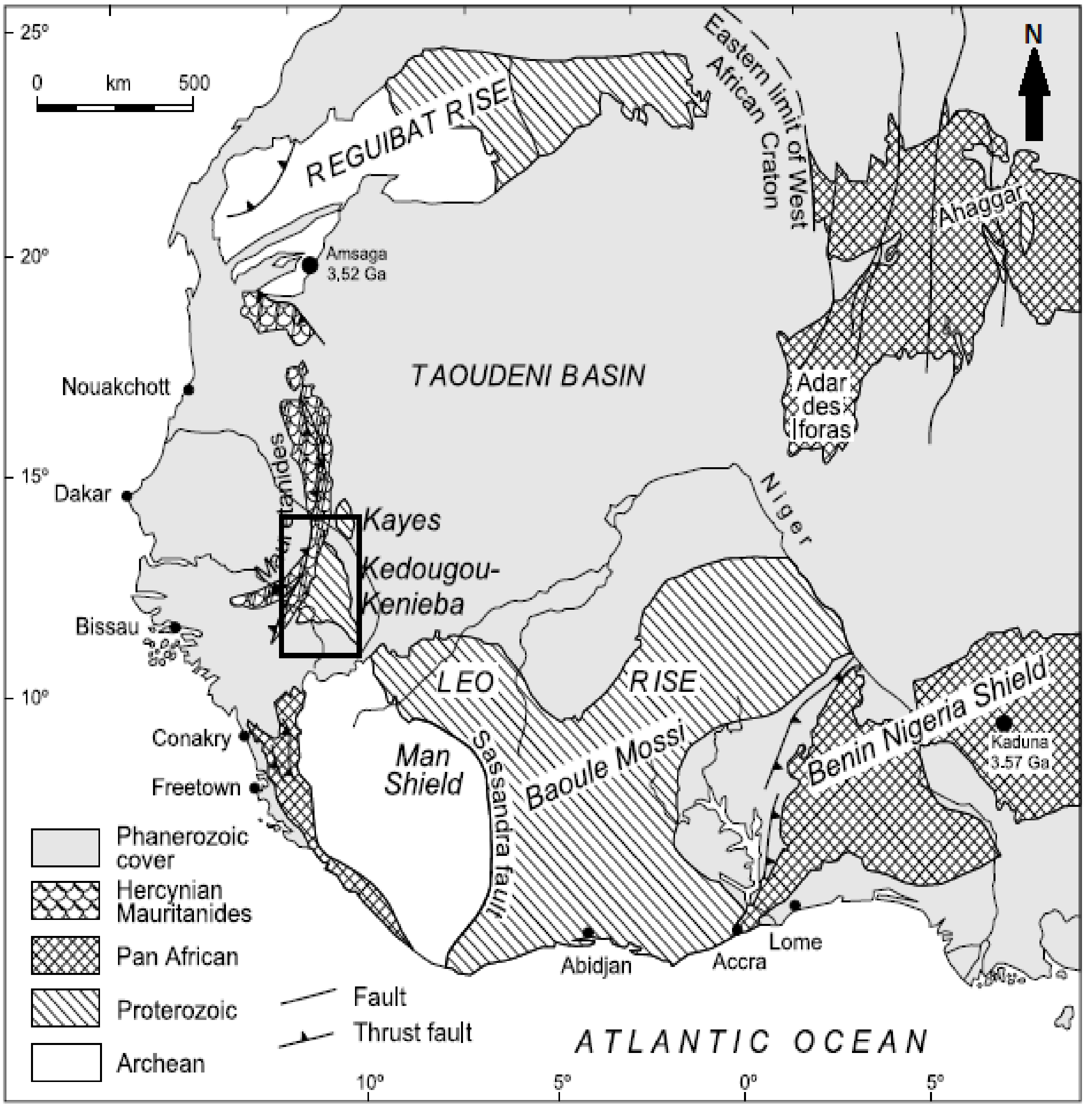

Figure 2.1 Geological sketch map showing major tectonic units of the West African Craton (After Boher et al. 1992) and location of the Kedougou-Kenieba Inlier (rectangle)

2.1.2 Geology of the Kedougou-Kenieba Inlier

The Kedougou-Kenieba Inlier (KKI) is the westernmost exposed part of the WAC in eastern Senegal and western Mali (Dia et al., 1997). The KKI is a triangular-shaped area bounded by the Mauritanide Hercynian Belt on its western side and is covered to the north, east and south by Neoproterozoic and Palaeozoic formations of the Taoudeni basin (Gueye et al. 2007). The KKI consist of Birimian formations formed during the Eburnean orogeny at ca. 2.2 -2.0 Ga (Abouchami et al. 1990; Liégeois et al. 1991).

The KKI consist of volcano-sedimentary greenstone belts intruded by granites (Gueye et al 2007). The volcano-sedimentary units are separated into two lithostratigraphic supergroups, the Mako Group in the west and the Diale-Dalema Group in the east (Bassot and Cen-Vachette, 1984; Bassot, 1987).

The Mako Group was defined by Witschard (1965) and Bassot (1966) as being made up of metamorphosed and deformed volcanic and volcano-sedimentary sequences which have been intruded by granitoids of the Kakadian Batholith and smaller massifs. The Mako Group is dominated by basaltic, volcano-sedimentary and sedimentary complexes. The volcanic rocks are dated between 2160 Ma and 2200 Ma (Boher et al, 1992; Dia et al., 1997).

The Diale-Dalema Group consists of platform-type sediments (e.g. carbonates) which were intruded by peraluminous granites which were emplaced at synchronous to the TTG intrusive along the belts (Gueye et al. 2007; Hirdes and Davis, 2002). The Diale and the Dalema formation are separated by the Saraya Batholith (Hirdes and Davis, 2002). The Diale formation comprises basal limestones and dolomitic marbles followed by greywacke and sandstones, whereas the Dalema formation consists of interlayered quartzites, greywackes, schists and marbles that contain rare slump breccias (Gueye et al, 2007; Hirdes and Davis, 2002). The Mako and the Diale-Dalema Groups are separated by a regional crustal scale shear zone, the Main Transcurrent Shear Zone (MTZ) which trends northeast to southwest (Milési et al. 1989). The Diale-Dalema Group and the Dalema formation, also referred to as the Kofi Supergroup, are separated by the Senegalo-Malian Shear Zone (SMFZ).

During the late Eburnean, the KKI underwent transcurrent deformation along a network of ductile shear zones and almost all lithostratigraphic units were metamorphosed under greenschist-facies conditions (Ledru et al. 1991; Milési et al. 1992). Amphibolite-facies metamorphism is only observed in the contact aureoles around granitic intrusions (Gueye et al. 2007). Three deformational events have been recorded and include a compressional D1 event related to early thrust formation and two late transcurrent deformation events (D1-D2), which led to the development of the

MTZ and the SMFZ (Ledru et al. 1991; Dabo and Aifa, 2010, 2011; Lawrence et al. 2013).

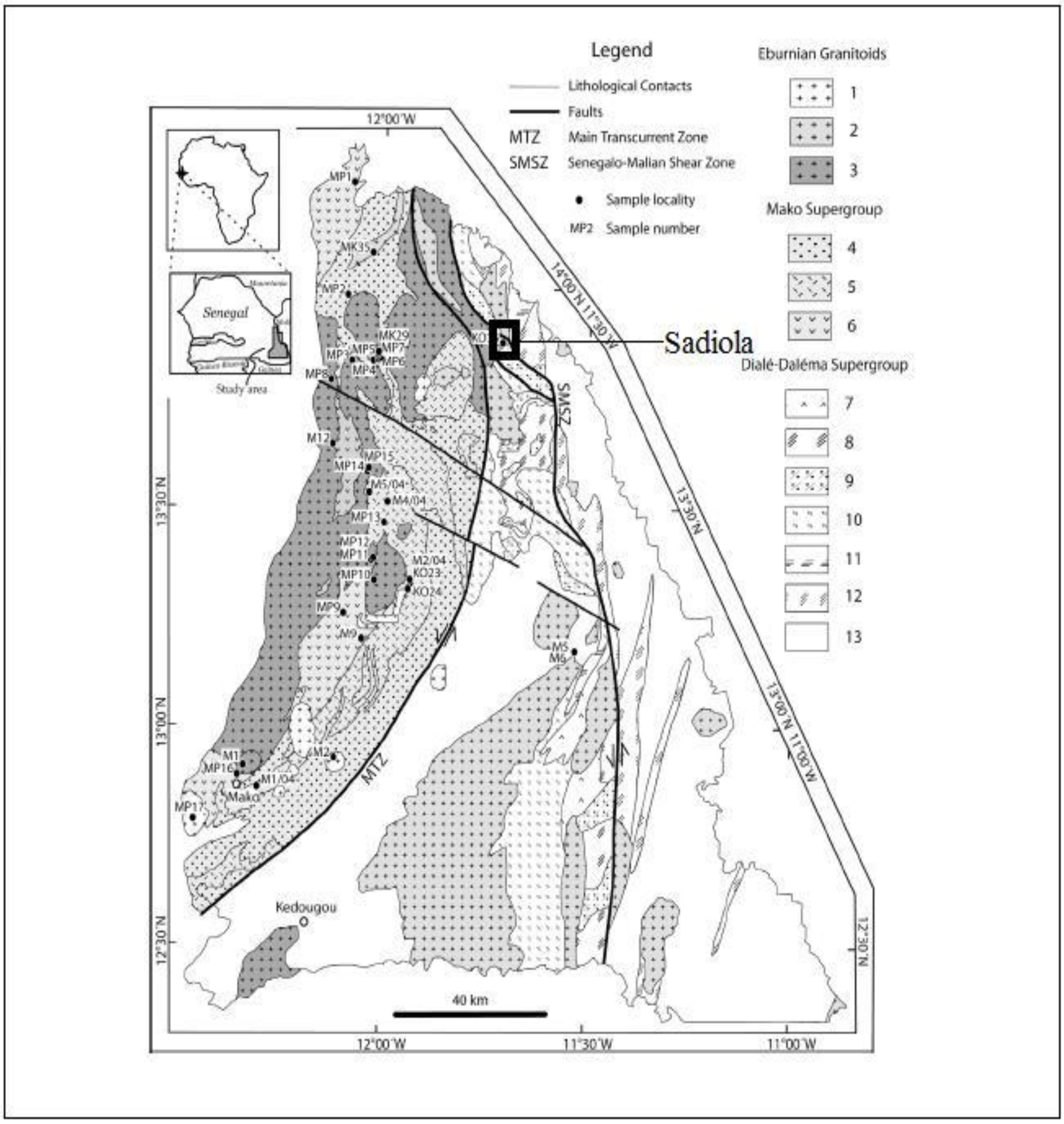

Figure 2.2 Geological map of the KKI located in the eastern part of Senegal (West Africa) with sample localities (modified after Ledru et al. 1991)

Symbol explanation: Eburnian granitoids: 1-4; Mako Group: 4 = volcano-sedimentary series; 5 = intermediate to mafic volcanics; 6 = mafic volcanics; Dialé-Daléma Group: 7 = intermediate volcanics; 8 = volcanogenic sediments and tuff; 9 = intermediate volcanics; 10 = undifferentiated detrital sediments; 11 = limestone; 12 = tourmaline-bearing sediments; 13 = undifferentiated flyschic sediments.

2.2 Mine Geology

The Sadiola Hill deposit is situated in the Sadiola goldfield. The goldfield is a mine camp which hosts several deposits which include the FE3 and FE4 open cast pits. These together with the Sadiola Hill mine are mined by Société D'Exploitation des Mines d'Or de Sadiola S.A (SEMOS), which is a Joint Venture between AngloGold Ashanti, IFC and the government of Mali.

The Sadiola goldfield is located within folded and altered sedimentary rocks of the Kofi Supergroup, which have been intruded by a number of felsic intrusions. The metasedimentary rocks consist of fine grained greywacke and impure carbonates with minor tuffs and acid volcanics (Hanssen et al., 1998). These lithologies show evidence of macroscopic to mesoscopic slump structures (Hein and Tshibubudze, 2007a, b). Carbonate, greywacke, quartz-feldspar-porphyry and diorite are the main host to the Sadiola deposit (Boshoff et al., 1998). The Sadiola Hill deposit is located along a diorite intruded marble-greywacke contact east of the SMFZ (Hanssen et al., 1998).

The Kofi Supergroup is obliquely cut by the N-S to NNW trending Senegalo-Malian Shear Zone, whereas the Sadiola deposit occurs along the NNE striking Sadiola Fracture Zone (SFZ) (Robins, 2006). The SFZ follows the steeply westerly dipping contact between greywacke to the west and impure carbonates to the east and its wallrock are intruded by discontinuous diorite and quartz-feldspar-porphyry dykes (Hanssen et al., 1998; Robins, 2006).

The Sadiola Hill deposit is also located at the margin of the inner and intermediate contact metamorphic aureole of the Alamoutala-Sekekoto plutonic system identified by (Hein and Tshibubudze, 2007b). Dating of the Alamoutala-Sekekoto granodiorite gave an age of 2083 ± 7 Ma and is taken as the age of gold mineralisation in the Sadiola goldfield (U-Pb zircon) (WAXI, 2013). Based on geophysical data, the plutonic system is interpreted to be situated directly below the Sadiola goldfield and is represented by projections of tonalite dykes in pits from the upper surface of the pluton, and it crops out at Alamoutala (Hein and Tshibubudze, 2007b).

Alteration assemblages identified include calc-silicate, potassic, chlorite–calcite, carbonate and silicification with gold mainly associated with both arsenic and antimony dominated sulphide assemblages including arsenopyrite, pyrrhotite, pyrite, stibnite and gudmuntite (Hanssen et al., 1998; Hein and Tshibubudze, 2007b).

Ore reserves and resources at the Sadiola Hill deposit have been estimated as of 31 December 2012, using an average of $2000/oz. gold price in accordance with JORC (IAMGold.com). In Sadiola Hill, mining is carried using conventional open-pit techniques with a carbon-in pulp processing plant (InfoMine.com). The processing plant is capable of treating 5.3 Mt of saprolite ores per year and has a 75% sulphide recovery (IAMGold.com). The table below shows the estimated ore reserves and resources from IAMGold Corp.

Table 2.1 Estimated ore reserves

Category	Tonnes (10^3)	Grade (g/t)	Gold(oz)
Reserves			
Proven	2,213	1.3	101477.95
Probale	34,809	1.8	2210095.24
Resources			
Measured	7,084	0.9	224888.88
Indicated	51,519	1.8	3271047.62
Inferred	10,993	1.7	659192.239

2.2.1 Lithology

The steeply west dipping lithologies of the Sadiola Hill gold deposit are dominated by greywacke, carbonate, marble and volcanics as recorded by Hanssen et al. (1998). The greywacke forms the hangingwall of the deposit. Greywacke and feldspathic greywacke are biotite bearing (Hanssen et al., 1998; Hein and Tshibubudze, 2007b). These greywacke units are massive with sharp bases (to the west), show an upward gradation and cross bedding at all scales, and are best developed to the west of the SFZ (Hein and Tshibubudze, 2007b; Boshoff et al., 1998).

Carbonate rocks in the Sadiola deposit are impure marble which consists of alternating beds of dark pelite-rich carbonate and light coloured carbonate rich beds (Hanssen et al., 1998). The carbonates include a massive, grey dolomite-marble and carbonaceous greywacke, and siltstone units which occur in a number of pits within the Sadiola goldfield (Hein and Tshibubudze, 2007a, b).

The igneous rocks at the Sadiola mine include diorite, lamprophyre dykes and quartz-feldspar porphyry. The diorite is composed of alkali-rich plagioclase and hornblende, and grades into coarse biotite-rich diorite which contains sulphides (Hanssen et al., 1998; Hein, 2008). This intrusion was characterized by Theron (1997a) as having similar composition as the TTG suite rocks, which are widespread across the WAC (WAXI, 2013).

The quartz-feldspar-porphyry (QFP) dykes have been recorded in outcrop in the Sadiola opencast (Hein and Tshibubudze, 2007a).The quartz porphyry host rare tourmaline crystals (Hanssen et al., 1998). QFP dykes often intrude along steep west dipping, NNE trending faults and crosscut the diorites (Robins, 2006).

2.2.2 Structure

The Sadiola deposit occurs in the steeply dipping, NNE striking SFZ and NE-trending fault splays Voet (1997). Hanssen et al. (1998) stated that the SFZ crosscuts all pre-existing structures and forms a fault contact between greywacke units on the west and marbles on the east of the pit. Hanssen et al. (1998) concluded that NE and NW-trending stacking faults crosscut the orebody; in contrast Voet (1997) stated that the NE trends are due to folds cross-cutting the orebody.

Hein and Tshibubudze (2007b) recorded that the Sadiola opencast contains an N-trending zone of north and NE-trending fractures, faults, and quartz-sulphide veins which cross-cut all metasedimentary sequences, NE-trending folds in the metasedimentary sequence, and tonalite dykes. The folds are crosscut and intruded by tonalite dykes indicating that folding preceded dyke emplacement whereas the tonalite dykes are crosscut by mineralised veins suggesting that quartz-sulphide vein were formed at a later stage (Hein, 2008).

2.2.3 Metamorphism

The Birimian sequence in which the Sadiola Hill deposit has been affected by metamorphism associated with the Eburnean orogeny (Hasting, 1982) with regional metamorphism to greenschist facies and contact metamorphism to hornblende-hornfels and epidote-chlorite facies (Hein and Tshibubudze, 2007a, b). The low-pressure greenschist facies is indicated by the mineral assemblage muscovite, chlorite ± biotite (Ledru et al., 1991). The greenschist facies mineral assemblage is fine grained and shows a granoblastic texture, and indicates biotite-chlorite alteration (Liégeois et al., 1991).

The contact metamorphism contains two zones, the inner and the middle aureole which is a result of the emplacement of tonalite-granodiorite plutons and the tonalite dykes (Hein and Tshibubudze, 2007a, b). The carbonates in the Sadiola Hill deposit are recrystallized to marbles and attained hornblende-hornfels facies in the inner aureole (Ledru et al., 1991; Hein et al., 2008). The middle aureole is characterized by epidote-albite facies and within it, primary sedimentary features are preserved (Hein and Tshibubudze, 2007b; Hein et al., 2008).

2.2.4 Gold Mineralisation and Metallogenesis

Gold mineralisation has been closely associated with the steep dipping SFZ, sub-parallel structures and minor faults splaying off the SFZ (Hanssen et al. 1998). Ranson (1998) further suggested that the main zones of mineralisation underlies the large diorite sill which intruded along thrust planes of the feeder zone within the SFZ, and because the SFZ has been modelled as the principle displacement zone of the D2 event, therefore both the diorite intrusion and mineralisation were related to the D2 event. In both cases, mineralisation has been recorded as to have occurred as disseminated around veins in wallrock and as massive lodes in quartz veins. Sulphides recorded in the deposit include pyrite, arsenopyrite, and minor chalcopyrite, sphalerite and galena (Hanssen et al. 1998).

Two metallogenic styles have been recorded in the Sadiola Hill deposit by Hein and Tshibubudze (2007a, b). This metallogenic styles include:

1. Placer gold in palaeochannels and screes in pits at FE3-1, FE3-3, and FE4. The palaeochannels in the deposit represent the Pan African erosional surface.

2. Gold mineralisation in breccia's and stockwork veins which formed as a consequence of dilation of thrusts and faults, and fracturing of tonalite dykes.

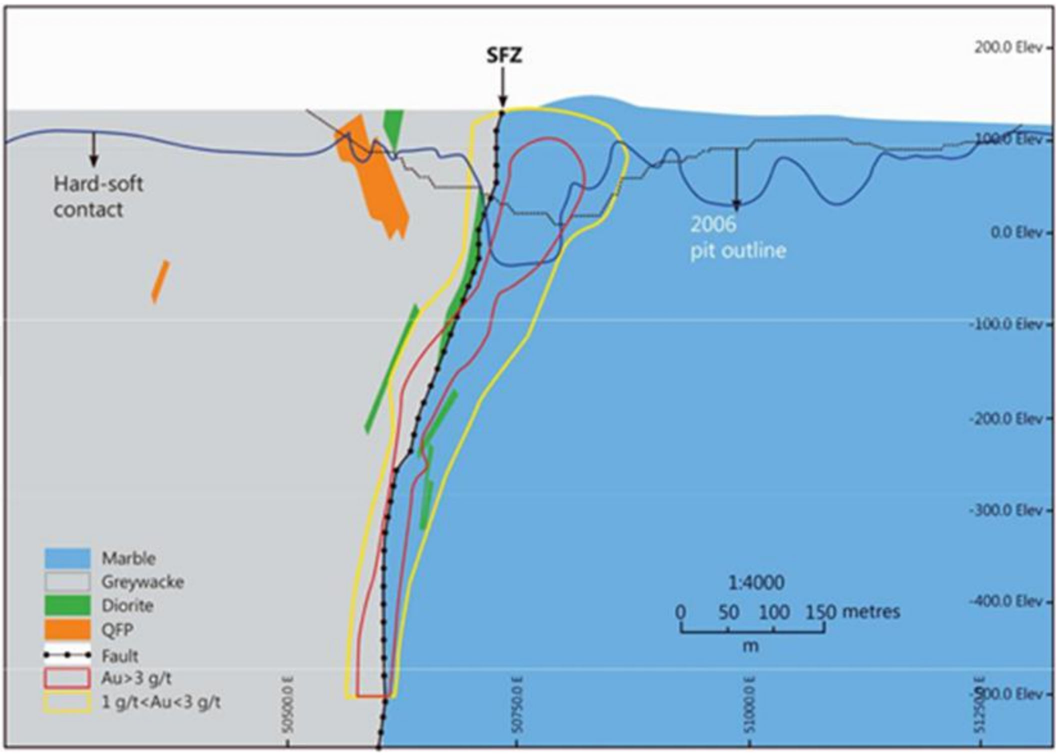

Figure 2.3 Section through the Sadiola orebody. Mineralisation is focused along the greywacke-marble contact (Sadiola Fracture Zone) (Robins, 2006)

CHAPTER THREE
THE ACTIVITIES IN THE SADIOLA OPEN PIT GOLD MINE

3.1 Safety First

The safety is the most important thing in Sadiola mine and more particularly at mining department, each person who must work in the pit has to do a pit induction (driving induction if necessary) in addition to the site induction because the pit is more dangerous than you can imagine (trucks, digger, sump, rock falls ...).

During these inductions we will tell you the personal protective equipment (PPE) required to work (helmet; shoes; glass; light short.....), the good behavior in the pit and mandatories equipment for a vehicle (radio; giro light; flag; head light).

This induction saves lives, prevents accidents and maximizes profit.

3.2 Grade Control (GC)

As its name indicates Control of Grade after exploration and development stages, it's done for:

- Block model confection
- quantified mineralization
- minimized dilution
- Better mining.

3.2.1 Grade Control (GC) Procedure

3.2.1.1 Planning

This planning is done in the office using software called Surpac. The grid is generally 10mx5m to better define grade. Holes depths depend on the desired bench and topography.
Holes orientations and dip depend on mineralization characteristics.

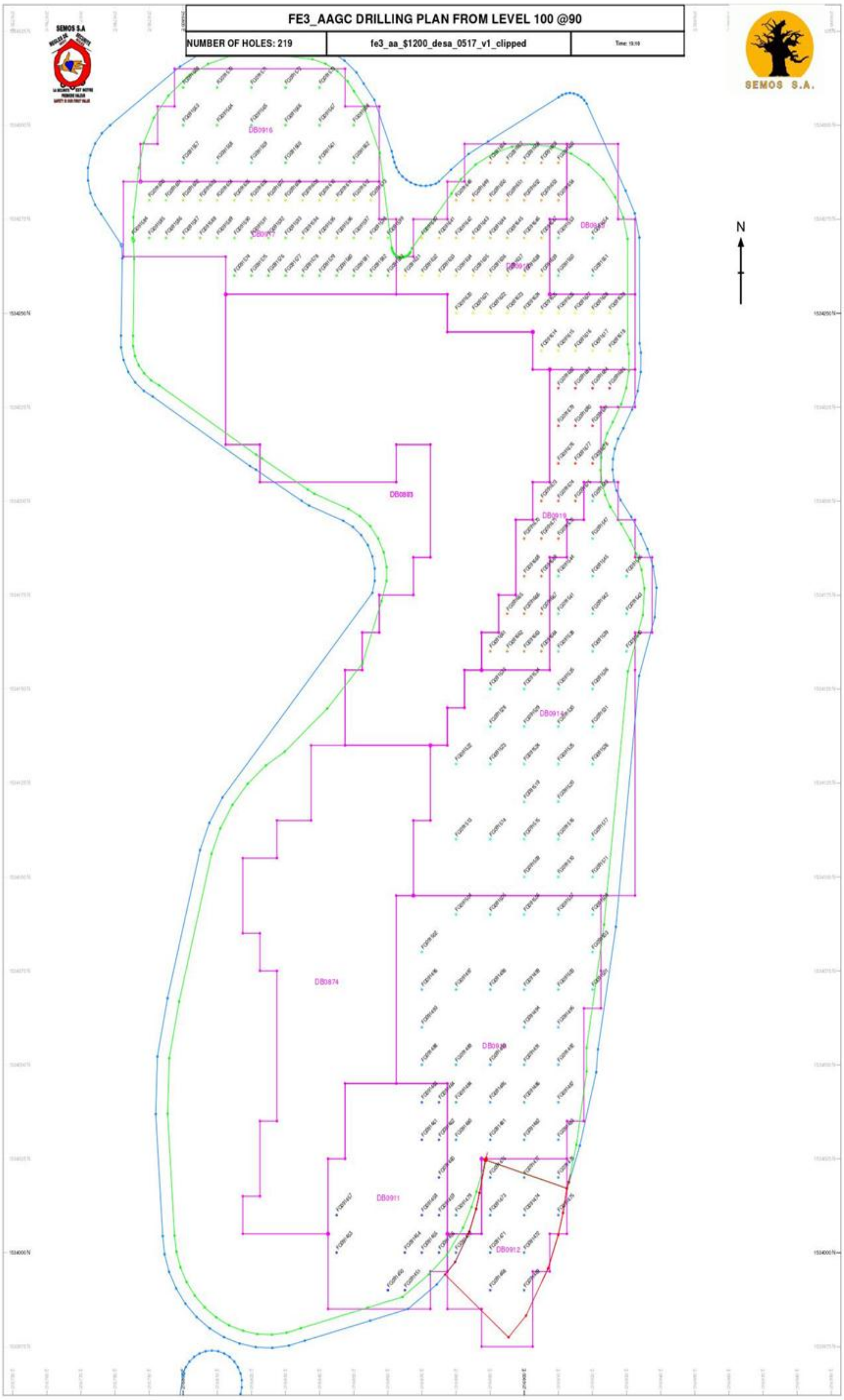

Figure 3.1 Priority GC holes planed in Farabakouta East (FE) (SEMOS, 2009)

3.2.1.2 Implantation

For the best accuracy surveyors are mandated to do implantation using the GPS. The area will be rename drill pattern and barricade by safety cones.

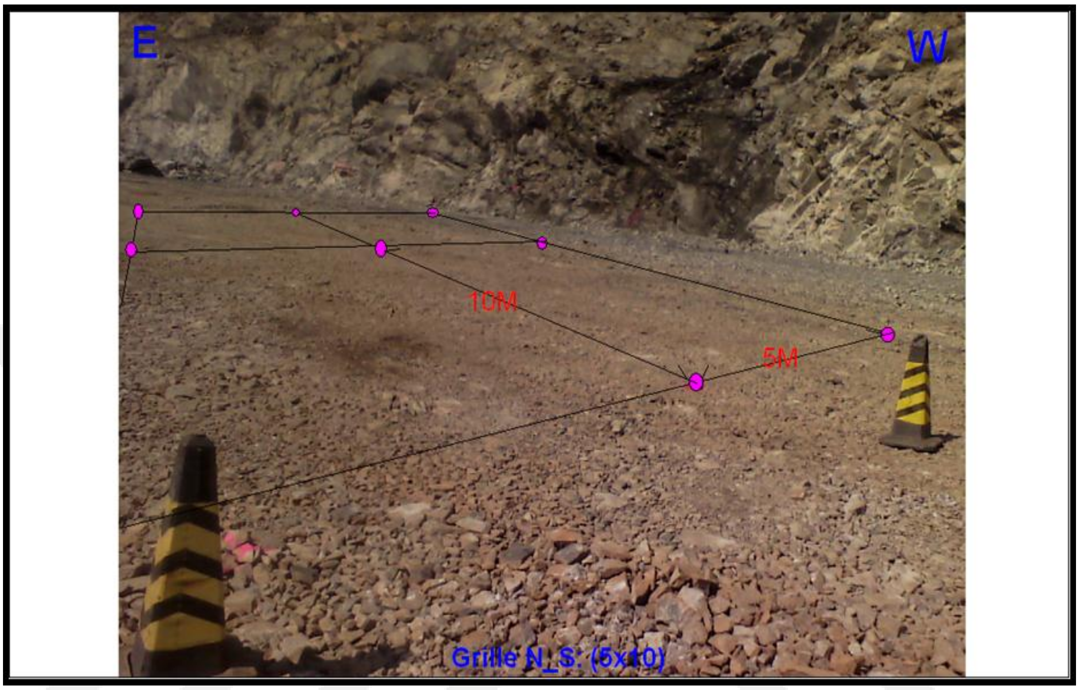

Figure 3.2 Grid NS (5x10m) of grade control Farabakouta East (FE) (Personal archive, 2017)

Figure 3.3 GC holes implanted Farabakouta East (FE) (Personal archive, 2017)

3.2.1.3 Drilling

Drilling is generally a circular hole (with different diameter) through the geological formations in order to provide information. RC drilling is a destructive Reverse Circulation.

- **drilling execution**

The drilling is carried out with the machine called * schramm11 * by a contractor company (Aveng Moolman).

Drilling works are executed as follows:

- sub-delimited drilling holes
- orientation (AZ) set up
- set up drill rig following azimuth
- dip Adjustment by driller and geologist
- drill until the programmed depth.

NB: Sometimes it happens to change the dip scheduled because of some constraints (slope, wall, pit...).

Figure 3.4 Drilling and sampling in progress (Personal archive, 2017)

- **Sampling and Quality Analyze, Quality Control (QAQC) Insertion**

Samples are recovered at each 1.5m (i.e. a 9m hole must give a total of 6 normal samples) and dividing with the splitter to take 2.5Kg.

It assigns each sample a number (ex: GC515503) that follows it up to data base.

For this sampling we use a GC sampling sheet which:

- shows the various holes with their sample numbers
- shows you QAQC insertion.

- **Logging**

The logging consists to describe rock chips (depth; color; weathering, rock types, alteration, sulphides %, quartz% ...) with different codes recognizable by the data base in order to create a possible relationship between gold mineralization and logging parameters (rock types, alteration, sulphides % ...).

For this, the geologist has:

- a code sheet established by the company
- a log sheet fairly detailed.

- **Holes fill back**

Once the drilling and sampling ended; the hole must be backfilled and re-pegged in order to:

- optimize the blast energy since blast holes are vertical
- facilitate the surveyors pick up.

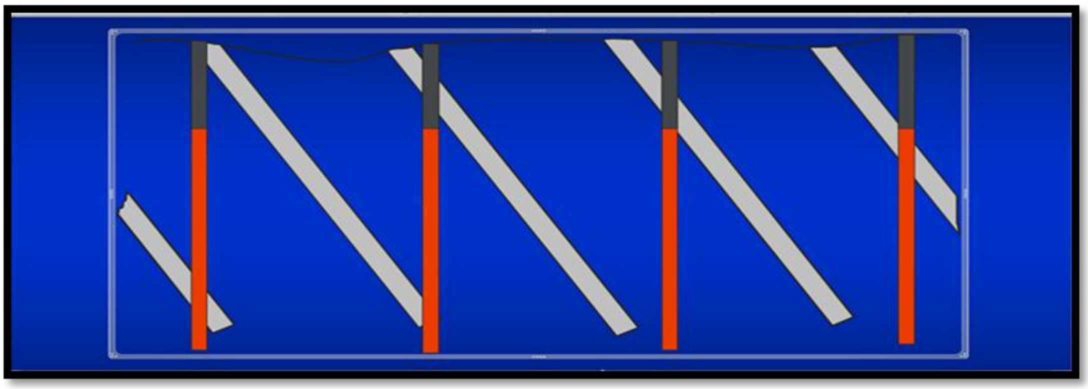

Figure 3.5 Relation GC and blast holes (red are blast holes) (Personal archive, 2017)

Figure 3.6 GC holes back filled and re-pegged (Personal archive, 2017)

- **Survey Pick up**

Surveyors pass every afternoon to:

- pick up the holes drilled in order to provide the exact coordinates to data base
- implant the holes should be drilled soon.

Daily REPORT

Every afternoon geologist or field technician has to make a daily report which aims to:

- inform chief geologist of drilling progression
- a quick data base update.

- **Sample submission**

Generally samples are sent to Sadiola mine lab for AU analyze.

3.2.2 Grade Control Result

After results reception from lab, data are treated with Surpac and MP3 softwares to make ore block which is the main purpose of grade control.

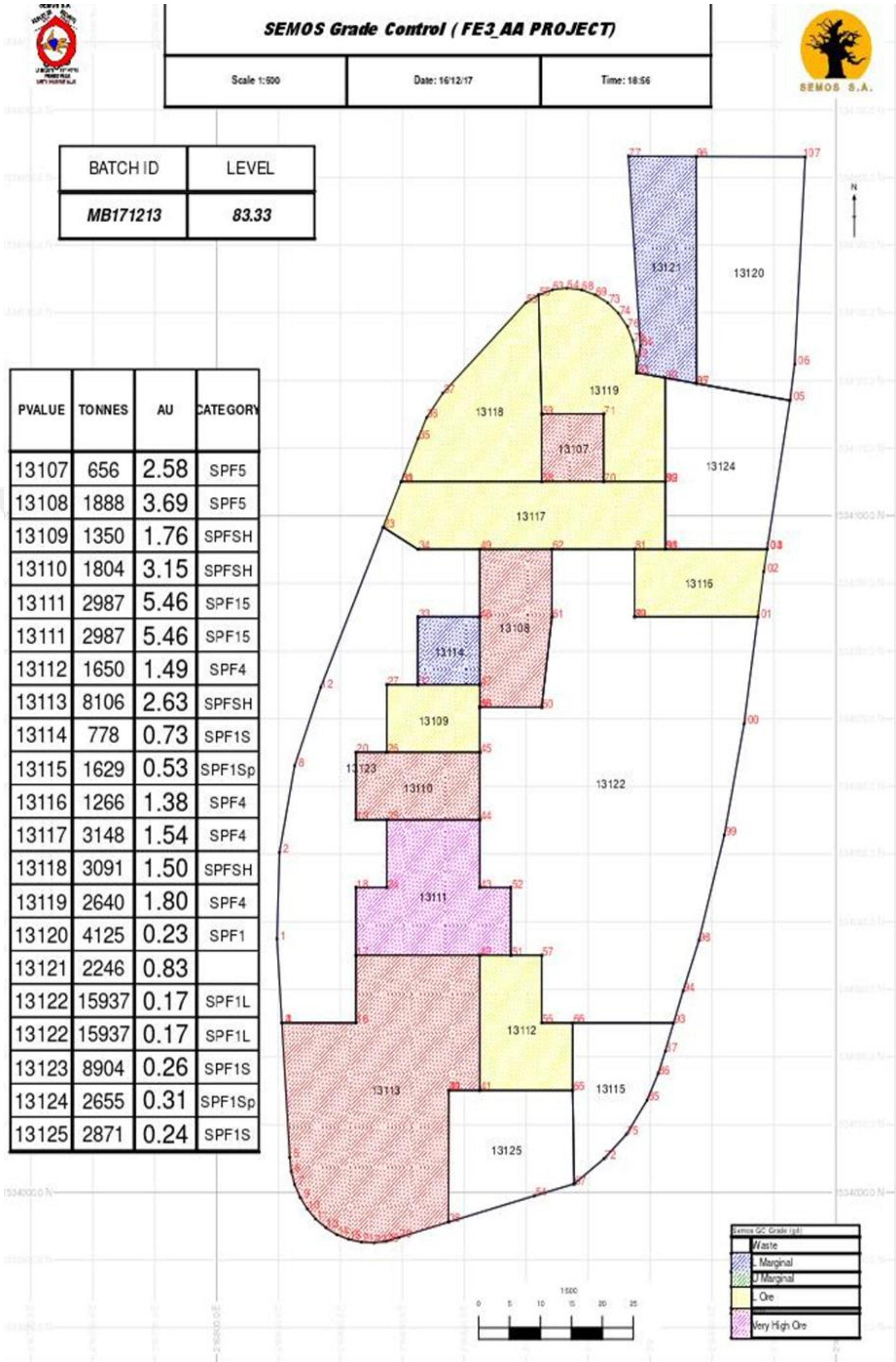

PVALUE	TONNES	AU	CATEGORY
13107	656	2.58	SPF5
13108	1888	3.69	SPF5
13109	1350	1.76	SPFSH
13110	1804	3.15	SPFSH
13111	2987	5.46	SPF15
13111	2987	5.46	SPF15
13112	1650	1.49	SPF4
13113	8106	2.63	SPFSH
13114	778	0.73	SPF1S
13115	1629	0.53	SPF1Sp
13116	1266	1.38	SPF4
13117	3148	1.54	SPF4
13118	3091	1.50	SPFSH
13119	2640	1.80	SPF4
13120	4125	0.23	SPF1
13121	2246	0.83	
13122	15937	0.17	SPF1L
13122	15937	0.17	SPF1L
13123	8904	0.26	SPF1S
13124	2655	0.31	SPF1Sp
13125	2871	0.24	SPF1S

Figure 3.7 Ore blocks Farabakouta East (FE) (SEMOS, 2009)

3.3 Excavation of Ore

The excavation of ore involves removing the ore deposit and its delivery to different deposits: the ROM Pad, the Stock pile (Sp) or Finger (F) to feed the crusher. To make this work, we need:

- Having an outline map of the mineralized perimeters (Ore Block)
- Make marking mineralized perimeter with spray paint (Ore mark out)
- Excavate ore (Ore Mining)
- Transport ore to different deposits (Rom pad).

3.3.1 Ore Block Map

This is a map drawn by geologists of production. It shows us the boundaries of the mineralized zone.

Physical plane:

After this map is subject to surveyors in the aim of making a new map (Ore markup) on which are located the points to mark the contours of minerals.

Each ore block is defined by five elements which are: The name of the block, the gold grade, carbon organic and sulfide grade and ore tonnage.

After, this map is subject to surveyors in the aim of making a new map (Ore markup) on which are located the points to mark the contours of minerals.

Each ore block is defined by five elements which are: The name of the block, the gold grade, sulphide, organic carbon and tonnage.

3.3.2 Ore Mark Out

This step is to materialize on the ground ore block obtained from grade control results.

It is realized (with map in hand) as follows:

- Surveyors implant contour points of each ore block
- These contour points are connected with corresponding ore block colour flagellum (red, blue, green)
- We materialize each ore block on the floor with the pray mark to be able to find the place in case of problems with the flagellum.

This step is crucial because it allows:

- to differentiate the different field area based on their grade
- to make a fair and organized mining.

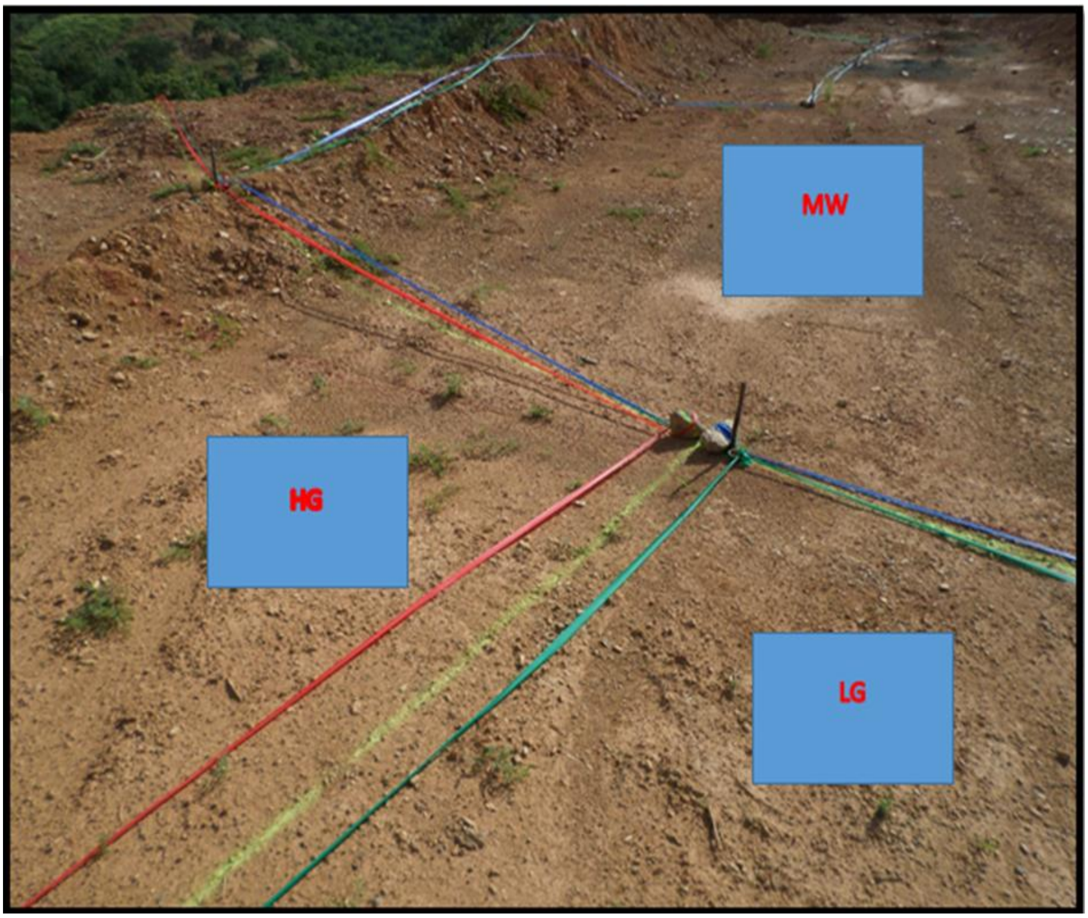

Figure 3.8 Ore block marked out on ground Farabakouta East (FE) (Personal archive, 2017)

3.3.3 Extraction of Ore (Ore Mining)

The company of AVENG MOOLMAN provides the extractive activities and transportation of ore controls the excavated using a device. Technicians in geology must remain at all times to monitor carefully the right approach activities of the last excavation to update progressive excavated areas. They are responsible to indicate the mineralized or barren excavation, the number of travel days, and the deposit of ore stockpile blocks and ensure that it is less dilution or ore loss.

Figure 3.9 Bulldozer cleanup wall (Personal archive, 2017)

Figure 3.10 Charger in activity ore extraction (Personal archive, 2017)

3.3.4 Ore Deposit or Rom Pad

This is the storage of minerals to feed the crusher. The ROM pad is distributed in different parts as follows:

Deposit A, deposit B, deposit C, deposit D and deposit E.

A geologist helper is still using the ROM pad to monitor and report the activities of trucks transporting minerals and followed dilution.

In addition, there is also a ROM pad for mobile crusher which is also provided as needed ore.

Figure 3.11 Ore deposits (Personal archive, 2017)

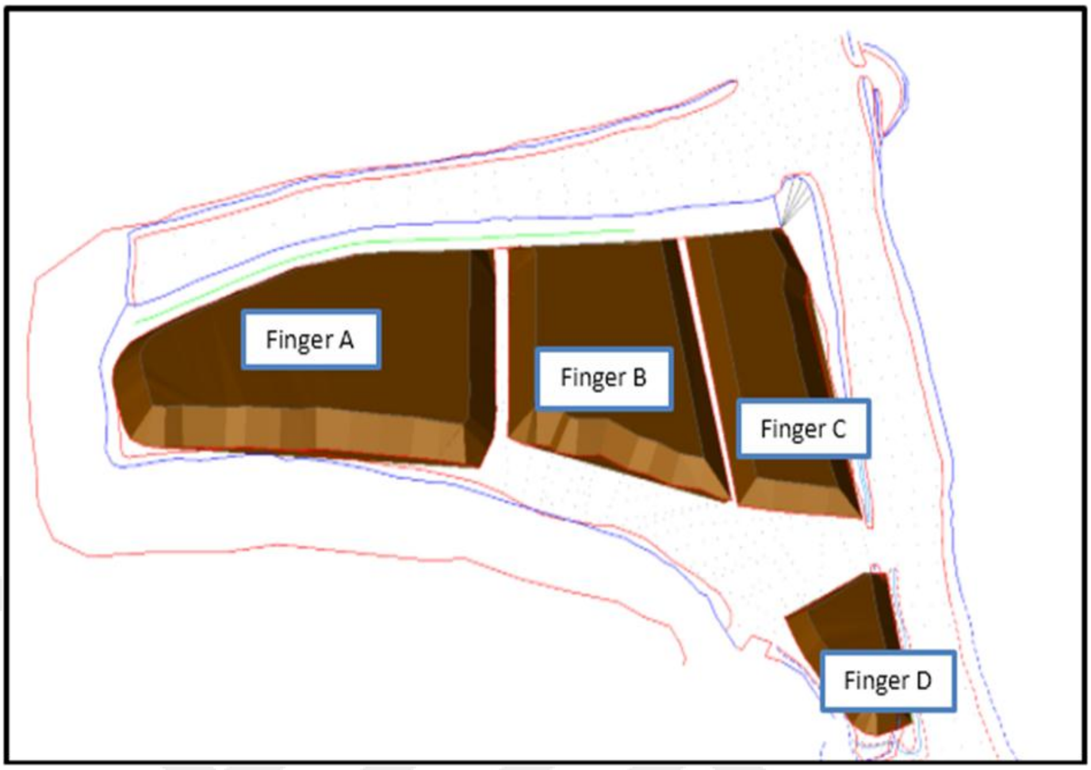

Figure 3.12 Deposit ore sketch (SEMOS, 2009)

Figure 3.13 Loader ROM pad and Feeding crusher (Personal archive, 2017)

3.4 Mapping

Mapping is the litho-structural representation of the land and its events (alteration, mineralization ...) on a plane or section.

This mapping allows to identify a possible relationship between the ore body and the different elements such as:

- Lithology
- Structure (shear, fault ...)
- Alteration
- Mineralization.

Materials used for this mapping are: graph paper; spray paint; hammer; compass; pencil; tape…

There are two kinds of mapping.

3.4.1 Floor Mapping

The purpose of this mapping is to see how “geology and mineralization” behave on the ground because we can see a lot of things in plan at this level.

It is realized as follows:

- Plan and locate the area in the pit
- Mark different limits (geology, alteration, structure) by the paint spray
- Do correctly the sketch on graph paper, which will help us a lot in digitalization
- Notified surveyors to pick up limit letters
- Digitalize map with Gemcom Surpac from the sketch and surveyors pick-ups.

3.4.2 Face Mapping

The main purpose of this face mapping is structure characteristics measurement (dip, dip direction, azimuth) because we see things in section at this level.

For this we process as follows:

- Plan and located the area
- spread the tape out in face mapped ground and mark both ends

- Make lithology, structures, alterations limits on the face with different letters (lithology = L1, L2 ...; structure = S1, S2 ..., and alteration = A1, A2) by the paint spray paint
- Measure Structural elements (dip, dip direction, AZ) by a compass
- Make a correct sketch on mapping sheet
- Notify Surveyors for the pick-ups
- Digitalize map with Gemcom Surpac from the sketch and surveyors pick-ups.

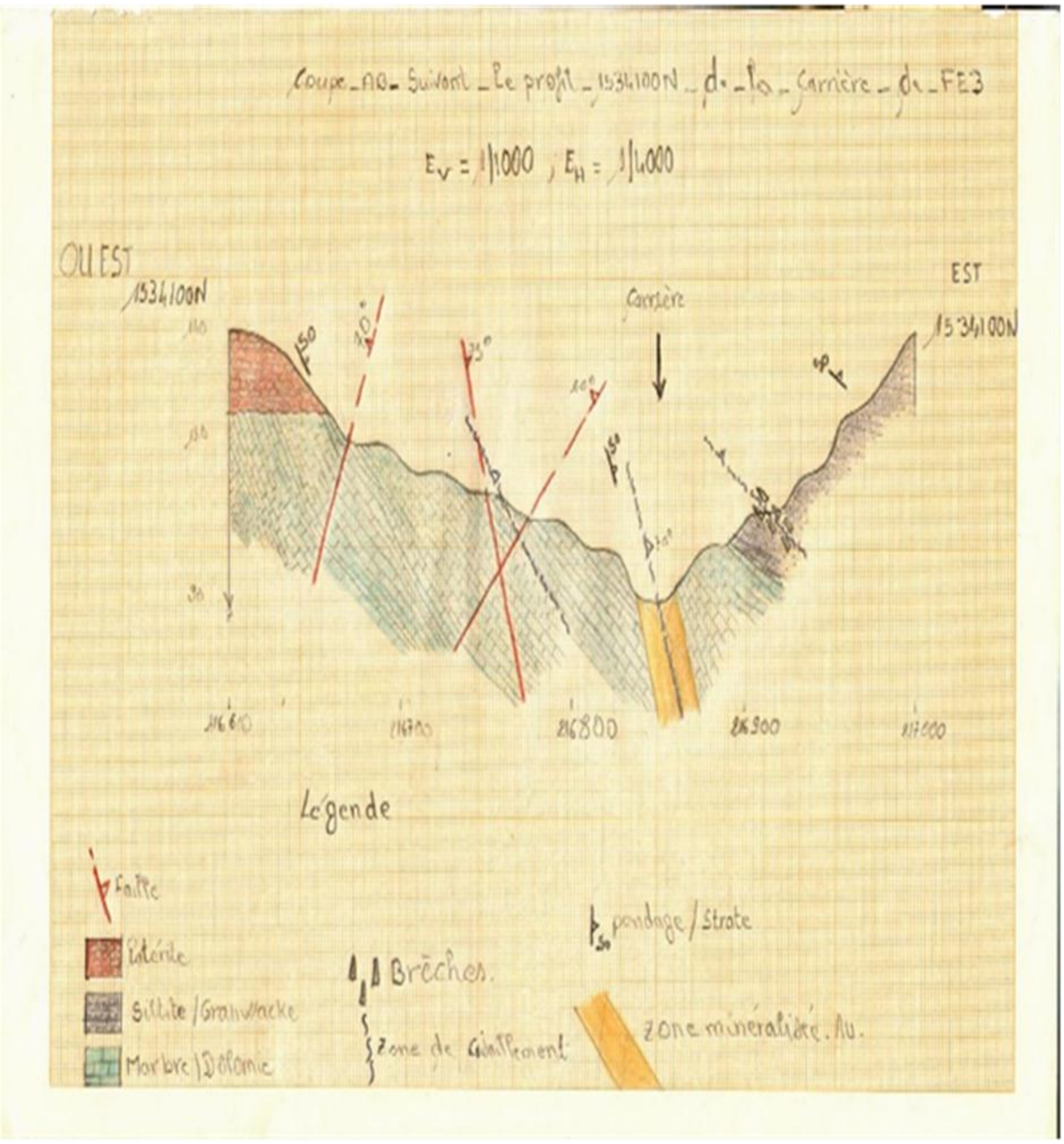

Figure 3.14 Cross-section West-East (Mamadou, 2017)

Digitizing

It was traced to a (drawing) geological formations from a data set (points) in a computer through the software Surpac.

The steps are:

- Make the outline from the survey points refer to the master sheet on the ground.
- Assign lithologies according to grade control legend.

CHAPTER FOUR
GEOTECHNICAL INVESTIGATIONS

4.1 Geological Setting

4.1.1 Local Geology

The concession area is underlain by metamorphosed sediments of carbonate (marbles) and silicate composition (pelites, sandstones, greywackes) of lower Proterozoic age. Igneous plutons and dykes (diorite and dolerite) intrude these sediments and form linear north northeast trending features. On a regional scale, deep tropical weathering has resulted in the formation of saprolitic soils, to an average depth of approximately 20 m, with the occurrence of superficial caps of iron laterite in places.

Circulating groundwater that has come into contact with sulphide mineralisation has increased the acidity resulting in extensive decalcification of the marble host rock. Along the southern margin of the ore deposit, this decarbonated marble (DCMB) attains a maximum depth of 200 m. The contact zone between the decarbonated and unaltered marble (CAMB) is highly irregular and is characterized by extensive fracturing and oxidation across a 4m to 6m wide zone. A simplified geological map of the contact zone is presented in Figure 4.1.

Major lithological units within the current Sadiola main pit comprise meta-sandstone (MGWK) in the west and carbonated marbles (CAMB) in the east. An intrusive diorite (DIOR) is present in the south. Quartz porphyry (QFP) and diorite stringers cross the major lithologies from the southwest to northeast, mimicking the major faulting.

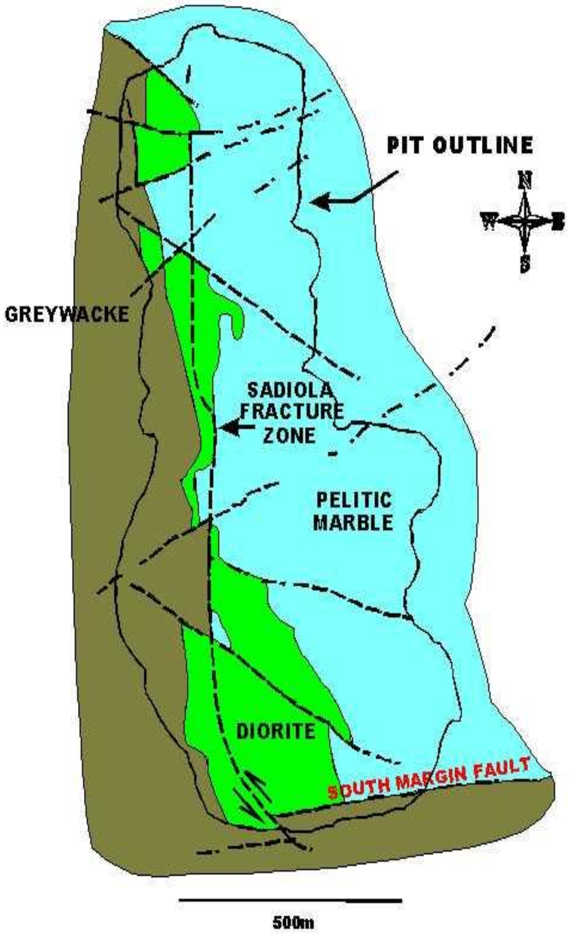

Figure 4.1 The decarbonated/unaltered marble contact zone (SRK, 2009)

4.1.2 Structural Geology

The Sadiola deposit coincides with the Sadiola fracture zone (SFZ), which is a splay of the Senegalo-Malian shear zone. The SFZ follows the steeply westerly dipping contact between greywacke to the west and carbonated marble to the east. Along the fracture zone both greywacke and carbonate marble are transposed. The SFZ and its wall rock are intruded by discontinuous diorite dykes, which may show a weak mineral foliation and sometimes intense ductile deformation. Silicified quartz-feldspar porphyry (QFP) dykes often intrude along steeply west dipping structures.

Steeply dipping southwest and northeast trending faults traverse the rock mass (Figure 4.2). The faults tend to be continuous through the pit and typically have a normal faulting mechanism. Generally, the faults range in width from 5m to 10m, and are characterised by the presence of chlorite infill. Typically, water seepage associated with the faults is seasonal. A summary of the characteristics of major faults is presented in Table 4.1.

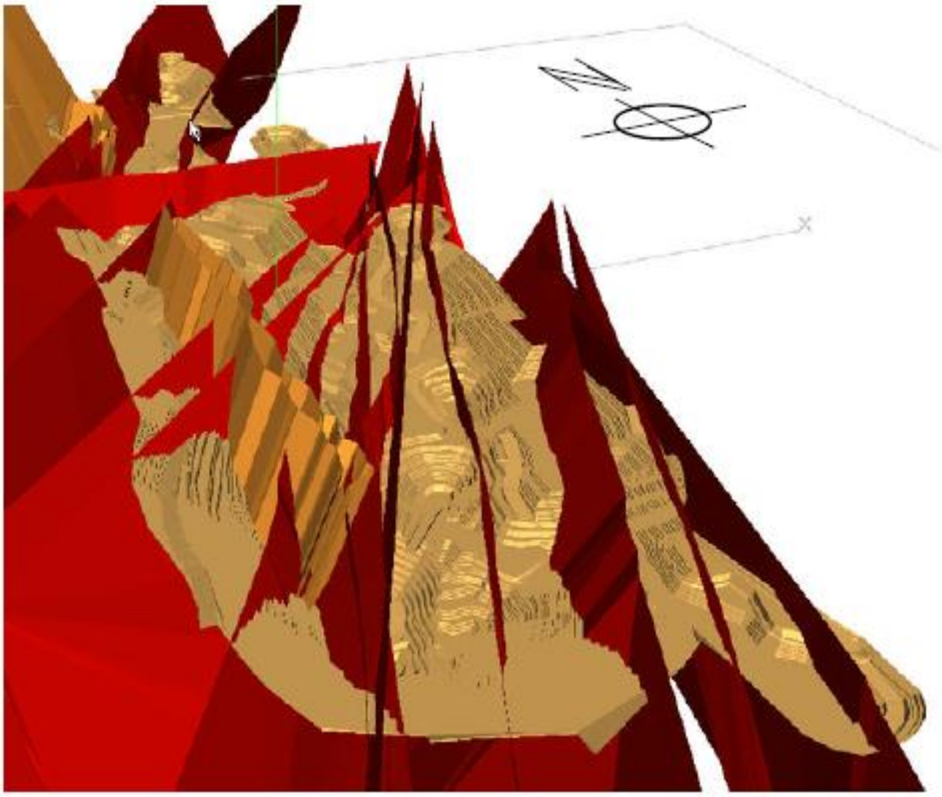

Figure 4.2 Major faulting developed in current Sadiola main pit (SRK, 2009)

Table 4.1 Summary of major faults in Sadiola main pit (SRK, 2009)

Fault Identification	Fault Width (m)	Infill Description	Dip (°)	Dip Direction (°)
SFZ	20 – 60	Calc-silicate; biotite; sulphides; quartz	72	274
NB3	10	Biotite; antophyllite; quartz; sulphides	71	134
NB6	10 - 15	Biotite; QFP; diorite; quartz; chlorite; sulphides	74	129
NB7	20	QFP; diorite; quartz; chlorite	70	293
NB16	20	Antophyllite; chlorite; biotite;	74	2
NE3	10 – 15	Antophyllite; chlorite; quartz; sulphides	76	114
NE7	10 – 20	Chlorite; biotite; quartz; diorite; sulphides	86	126
NE9	7 – 10	Biotite; antophyllite; quartz; sulphides; QFP; diorite	84	114
NE11	7 – 15	Biotite; antophyllite; quartz; sulphides; QFP; diorite	84	294
NE13	4 – 7	Biotite; antophyllite; mica ; quartz ; sulphides	72	117

The large number of faults mapped in the current pit, together with extrapolation from exploration drilling to the east and west of the pit is a concern due to the potential for fault interaction. Although current interpretations do not indicate any major interaction between the faults for the proposed final pit geometry, it should be noted that this does not exclude the possibility of interaction, and an adverse kinematic reaction, where faults intersect prominent joints.

4.1.3 Weathering

The weathering zone comprises a trough coinciding with the Sadiola shear zone along the MGWKCAMB contact. The trough deepens rapidly from the west, but gradually from the north to the south, attaining a maximum thickness of 200m in the south shallowing to 30m in the north. The trough is filled by completely weathered marble, diorite and meta-sandstones; these units being loosely termed the saprolites, and still retaining the original structures of the parent rock. The saprolites are overlain by a laterite cap, which has a maximum thickness of 30m, thinning to less than 10m.

The boundary between the weathered and fresh rock horizons is not a sharp surface but rather a transitional zone. However, an indication of the extent of the weathering profile can be obtained from a surface constructed as the lower from the soft-hard and oxide-sulphide rock boundaries included in the geological model and derived from the exploration boreholes. The extent of the weathering profile across the current pit area interpreted in this manner is illustrated in Figure 4.3.

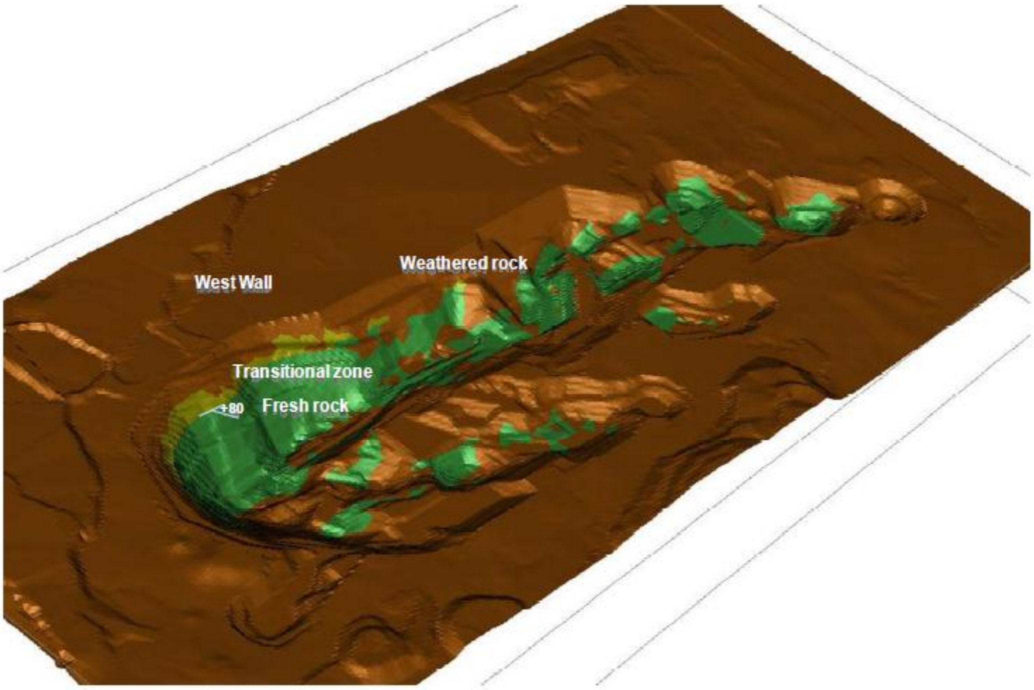

Figure 4.3 Extent of weathering across the current Sadiola pit (SRK, 2009)

4.1.4 Seismological Setting

The area where the mine is located is not prone to large earthquake events, as indicated by the distribution of large seismic events across the African continent. Although local stress regime data are unavailable, residual stresses are not anticipated due to the highly faulted and weathered nature of the terrain in the area.

4.2 Geotechnical Drilling Programme

The recording and assimilation of geotechnical data was conducted and supervised by mine personnel. A comprehensive data base was provided containing the geotechnical logging of borehole core collected through different stages of the mine life. This data was processed and the pertinent information extracted for the purpose of the slope design.

The historical geotechnical site investigation for the pit design included the drilling of 159 rotary-cored boreholes, which were drilled in several campaigns (phases) including the previous prefeasibility investigations. The location of the borehole collars is shown in Figure 4.4, together with the outline of the current pit.

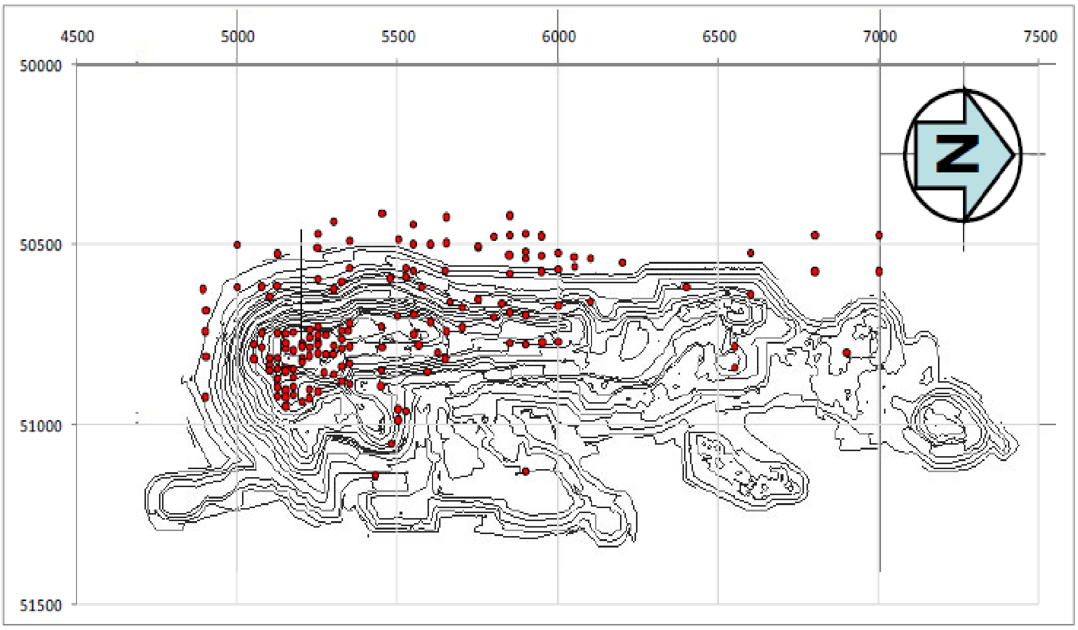

Figure 4.4 Sadiola mine plan showing the positions of the Sadiola deep sulphide project geotechnical boreholes (SRK, 2009)

Many of the historical geotechnical boreholes were used to collect joint orientation data for the assessment of the structural patterns of the rock mass. However, difficulties in the collection procedures of this type of data and the fact that the majority of the boreholes were oriented in an easterly direction (Figure 4.5) as they were primarily planned for exploration purposes resulted in poor definition of joint patterns for the stability analysis.

In order to cover existing gaps of information on structural patterns, three oriented core holes were drilled on the west wall of the pit as part of the present study. The boreholes were used to assess rock mass quality with RMR values and to collect reliable data on structure orientations relevant for the stability analysis of the west wall of the pit. The location and general characteristics of the holes are indicated in Figure 4.6 and Table 4.2. The boreholes were logged geotechnically on site by a Steffen, Robertson and Kirsten (SRK) company geologist and were also used for the recovery of undisturbed samples of weathered and unweathered rock as well as core specimens with natural joint planes, for laboratory testing.

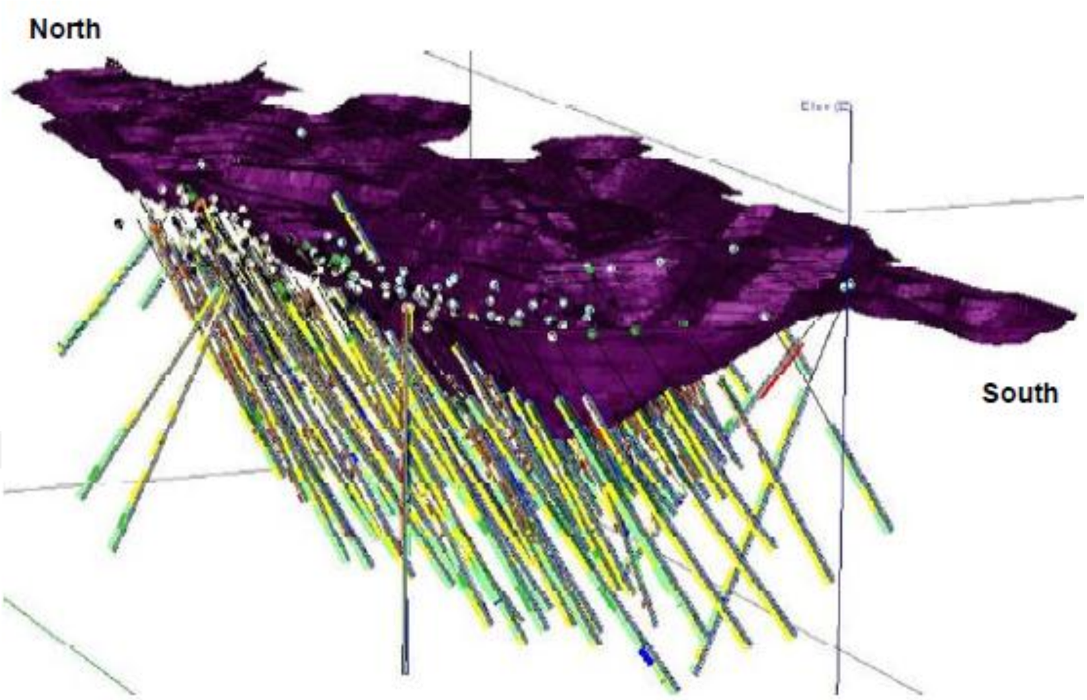

Figure 4.5 Predominant orientation of historical geotechnical boreholes (SRK, 2009)

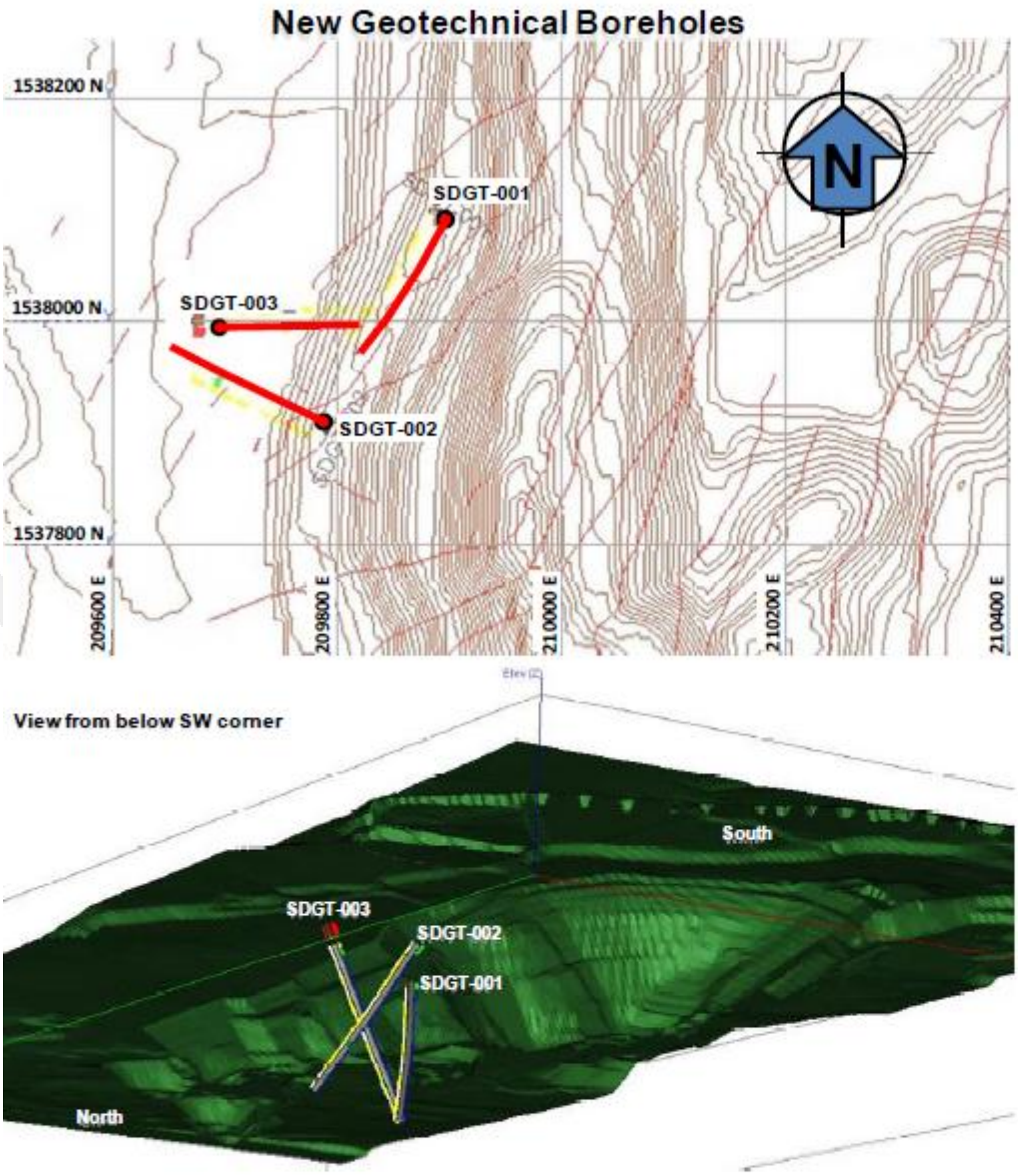

Figure 4.6 Location and orientation of new geotechnical boreholes (SRK, 2009)

Table 4.2 Characteristics of new geotechnical boreholes (SRK, 2009)

No.	BHID	XCOLLAR	YCOLLAR	ZCOLLAR	Final Depth (m)	Average Bearing (º)	Average Dip (º)
1	SDGT-001	209,892.196	1,538,097.956	76.190	301	213	-61
2	SDGT-002	209,789.572	1,537,900.135	98.482	301	296	-58
3	SDGT-003	209,670.285	1,538,000.663	127.789	350	89	-62

Overall, a total of 40,260 m of core drilling was completed with the site investigation campaigns and the corresponding geotechnical logs were collated in an Excel database that contains 3,166 records of core descriptions.

4.3 Rock Mass Characterisation

The geotechnical characterization of the lithological units in the Sadiola pit area was carried out utilising Laubsher's Rock Mass Rating (RMR) classification system. The older version of the system is based on the calculation of the RMR and MRMR indexes as described by Laubscher (1990). The rock mass strength characterization for the purpose of the slope stability analysis included in the present report is based entirely on the RMR values.

The borehole log data base used for the estimation of rock mass properties. It is believed that this information has the adequate level of confidence to support the rock mass characterisation for design. The database includes the identification of the geotechnical interval, the rock type unit, and the values of the Laubscher's parameters IRS, RMRL90, FFr and JC. Data corresponding to materials described as overburden, soils and core losses were excluded for the rock mass characterisation analysis.

The rock types were grouped into the four basic lithological units indicated in Table 4.3, which were also used as geotechnical units for slope design.

Table 4.3 Summary of lithological units (SRK, 2009)

No.	Code	Lithological / Geotechnical Unit
1	DIOR	Diorites
2	CAMB	Carbonated marbles
3	MGWK	Meta-sandstones and meta-greywackes
4	QFP	Quartz feldspar porphyries

4.4 Jointing Orientation

Seven joint sets were identified within the current Sadiola main pit based on the analysis of surface mapping data. Four of them constitute the predominant joint sets developed in the pit and the remaining three correspond to more randomly developed discontinuities. The frequency distribution graphs of dip and dip direction for the joint sets identified at Sadiola are presented as Figure 4.7 and Figure 4.8, respectively. The main joint set characteristics are summarised in Table 4.4.

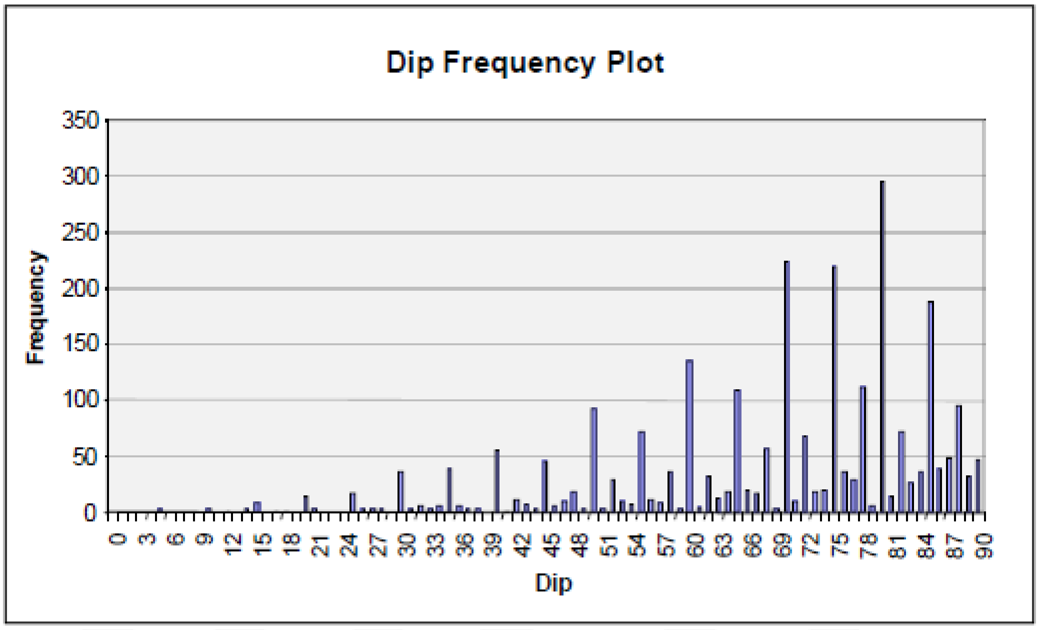

Figure 4.7 Dip frequency plot for the Sadiola joint sets (SRK, 2009)

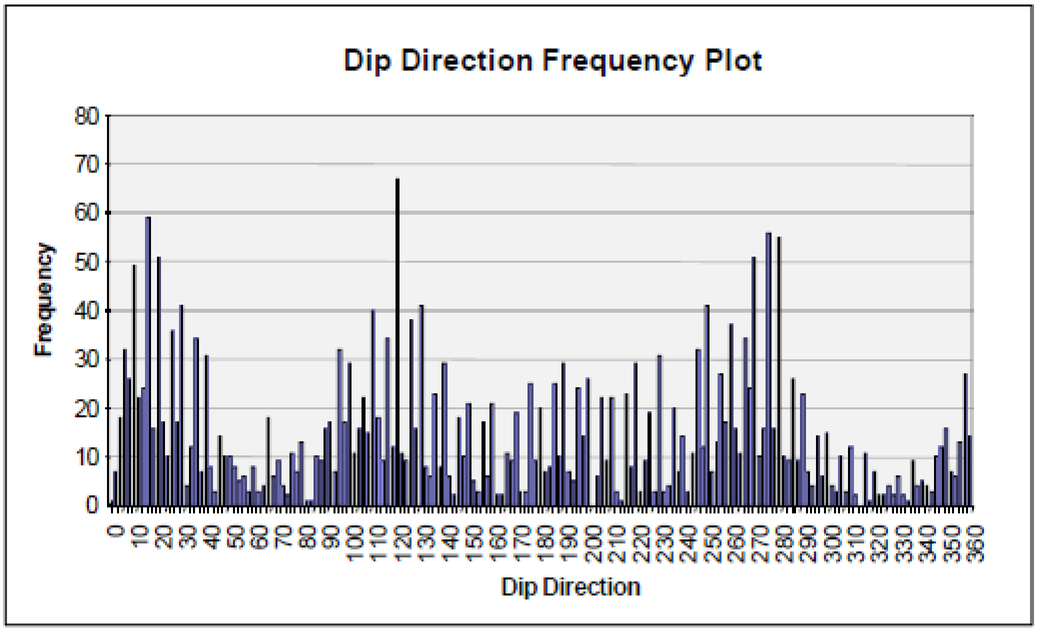

Figure 4.8 Dip direction frequency plot for the Sadiola joint sets (SRK, 2009)

Table 4.4 Summary of joint set characteristics (SRK, 2000)

Joint Set No.	Dip (°)	Dip Direction (°)	Micro Roughness	Macro Roughness	Joint Alteration	Dip Continuity (m)	Strike Continuity (m)
J1	60 - 90	085 - 146	Rough/Smooth Undulating	Undulating	Soft sheared chlorite	6 - >10	>10
J2	65 - 90	344 - 046	Smooth Planar	Undulating	Chlorite staining	1.5 - >10	>10
J3	60 - 90	240 - 310	Smooth Planar	Undulating	Clean	0 - 10	>10
J4	70 - 90	175 - 220	Smooth Planar	Undulating	Soft sheared chlorite	0 - 2	<3
J1 (a)	20 - 60	085 - 146	Rough Undulating	Undulating	Clean	0 - 5	<10
J3 (a)	20 - 60	240 - 310	Rough Undulating	Undulating	Clean	0 - 2	<10
J5	50 - 70	175 - 220	Rough Undulating	Undulating	Soft sheared chlorite	<3	<10

Analysis of the joint orientation data indicates that the majority of joints developed in the Sadiola main pit have a dip between 70° and 85°. Similarly, analysis of the joint orientation data indicates four prominent dip directions, with one to two random sets. The unweathered rock comprises very competent rock; consequently, instability most likely will be kinematically controlled. Potential modes of failure include wedge, planar, toppling or complex step-path failures.

4.5 Laboratory Testing

The historic laboratory data base used for the present study include the results of the laboratory testing programmes carried out to investigate the properties of both, soft rock saprolites and hard rocks. In addition to this information, the results of the laboratory tests carried out on samples collected as part of the site investigation for the present study were considered for the analysis.

The historic testing programme on soft rock saprolites was conducted in 1999 and early 2000 at the Civilab laboratory in Johannesburg (SRK, 2000). The testing programme of soft rock saprolites included:

- Index tests, including Atterberg limits and particle size distribution. The results of these tests were used to classify the material according to the Unified Soil Classification System (USCS).

- Effective stress triaxial tests with pore pressure measurements on soaked specimens.
- Total stress triaxial tests, unconsolidated, undrained on natural moisture content specimens.
- Shear box tests drained at natural moisture content.

A summary of the results of the historic testing programme on weathered rock saprolites is shown in Table 4.5 and the detailed support information can be consulted in the Sadiola Cut III pit slope design report by SRK from May 2000.

Table 4.5 Results of the historic soft rock testing programme (SRK, 2000)

Rock Unit	Sample No.	BH No.	Depth (m)	USCS	Shear Box		Triaxial Eff. Stress		Triaxial Total Stress	
					c (kPa)	Φ (°)	c (kPa)	Φ (°)	c (kPa)	Φ (°)
CAMB	F489	1	Elev.+127m	ML	152	25	25	29	171	27
MGWK	F491	2	Elev.+123m	ML	30	37	35	22	168	27
DIOR	F649	6	Elev.+90m	ML	28	39	74	20	77	37
MGWK	H238	S655	27.0-42.0m	ML-ML	0	52			39	22
MGWK	H239	S656	14.5-30.1m	ML	0	42	28	26	129	18
MGWK	H355	S656	13.1-23.0m	ML	54	39			117	24
DIOR SAP	H416	S657	64.2-76.0m	ML	0	46			90	0
QFP SAP	H415	S663	102.1-108.4m	ML	71	46	0	25	0	32
DIOR SAP	H414	S661	78.0-81.0m	ML	49	50			230	35
QFP SAP	H413	S661	36.0-43.0m	ML	0	54	83	26	0	26
DIOR	H706	S665	54.2-65.9m	ML					207	14
CAMB	H707	S666	153.8-165.2m	ML					25	14
Mean					38	43	41	25	104	23
Standard Deviation					47	9	32	3	79	10

The historic hard rock testing programme includes three phases of investigation completed by the CSIR Miningtek laboratory in Johannesburg, with testing being undertaken during January 2000, January 2001 and June 2003, respectively. The testing programme of unweathered (hard) rock included:

- Uniaxial Compressive Strength (UCS) tests (including Young's Modulus and Poisson's Ratio determinations).
- Triaxial Compression Strength (TCS) tests.
- Point Load Strength (IS50) tests.
- Shear Box Strength (SHS) tests.

The complete historic hard rock laboratory data base used for the present study and a summary of the main results is presented in Table 4.6. The results of the triaxial tests are shown in Figure 4.9.

Table 4.6 Summary of historic hard rock laboratory test results (SRK, 2000)

Rock Unit		CAMB	MGWK	DIOR	QFP
Density (T/m3)	No. tests	63	68	35	11
	Minimum	2.60	2.43	2.66	2.35
	Average	**2.75**	**2.71**	**2.85**	**2.63**
	Maximum	2.86	2.82	3.15	2.69
	Standard Deviation	0.04	0.06	0.09	0.10
	Coefficient Variation	0.01	0.02	0.03	0.04
UCS (MPa)	No. tests	54	59	35	11
	Minimum	74	9	7	81
	Average	**136**	**151**	**126**	**166**
	Maximum	222	295	220	262
	Standard Deviation	36	64	53	68
	Coefficient Variation	0.27	0.42	0.42	0.41
Young's Modulus (Gpa)	No. tests	3	3		
	Minimum	73	71		
	Average	**79**	**75**		
	Maximum	87	81		
	Standard Deviation	7	5		
	Coefficient Variation	0.09	0.07		
Poissons's Ratio (υ)	No. tests	3	3		
	Minimum	0.25	0.30		
	Average	**0.26**	**0.32**		
	Maximum	0.27	0.36		
	Standard Deviation	0.01	0.03		
	Coefficient Variation	0.04	0.10		
IS50 (Mpa)	No. tests	342	77	99	11
	Minimum	0.5	1.1	0.8	1.0
	Average	**5.8**	**9.3**	**9.1**	**6.2**
	Maximum	14.4	17.2	14.8	11.6
	Standard Deviation	1.8	3.6	2.7	3.6
	Coefficient Variation	0.31	0.39	0.30	0.59
SHS Friction Angle (°)	No. tests	11	15	3 (*)	2 (*)
	Minimum	25	31	42	51
	Average	**35**	**36**	**47**	**53**
	Maximum	42	50	53	54
	Standard Deviation	4	6	5	3
	Coefficient Variation	0.12	0.16	0.12	0.05

CAMB: Carbonated marbles **MGWK**: Meta-sandstones and meta-greywackes

DIOR: Diorites **QFP**: Quartz feldspar porphyries

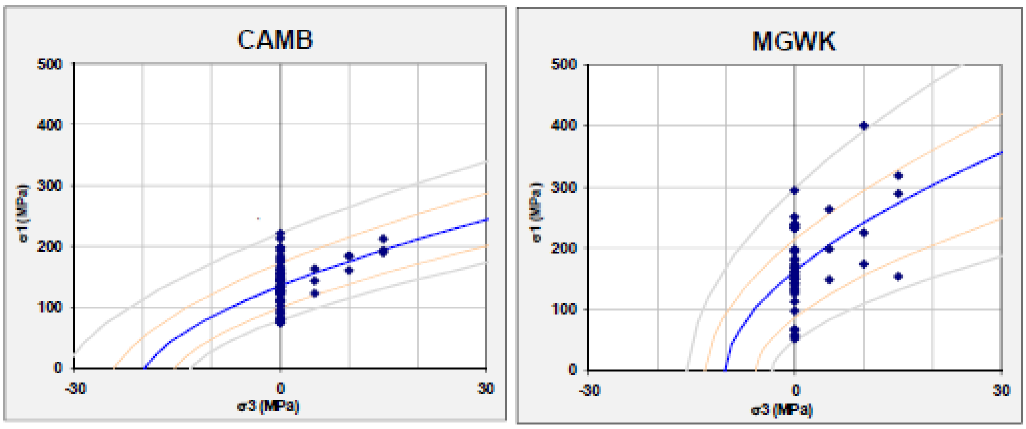

Figure 4.9 Plots of σ3 versus σ1 from the UCS and triaxial test results (SRK, 2000)

A supplementary laboratory testing programme was completed with samples collected during the site investigation carried out in March 2010 as part of the present study (SRK, 2010). The testing was executed in the Rocklab laboratory in Johannesburg and included the following tests:

- Uniaxial Compressive Strength (UCS) tests on diorite and metasandstone samples.
- Triaxial Compression Strength (TCS) tests on weathered and transitional metasandstone samples.
- Base friction angle (BFA) tests on diorite and fresh metasandstone samples.
- Shear Box Strength (SHS) tests on open joints in metasandstone with various roughness characteristics.

A summary of the results of the supplementary laboratory testing programme is presented in Table 4.7. The results of the triaxial tests carried out on saprolite samples are included in Figure 4.10 in the form of graphs of normal stress (σn) versus shear strength (τ). In this figure the results of previous testing completed in year 2000 is included for comparison purposes.

Table 4.7 Summary of supplementary laboratory test results (SRK, 2010)

Rock Type	Item	Density (T/m3)	UCS (MPa)	BFA (º)	SHS Friction Angle (º)			
					Φ peak			Φ res
				Φ base	RU	SU	SP	
DIOR	No. tests	5	5	5				
	Minimum	2.75	39	29				
	Average value	**2.78**	**111**	33				
	Maximum	2.80	199	38				
	Standard Deviation	0.03	61	3				
	Coefficient Variation	0.01	0.55	0.10				
Fresh MGWK	No. tests	10	10	7	3	4	3	10
	Minimum	2.64	137	32	34	31	33	30
	Average value	**2.68**	**221**	37	**42**	37	35	**34**
	Maximum	2.71	296	41	49	45	39	44
	Standard Deviation	0.02	48	3	8	6	3	4
	Coefficient Variation	0.01	0.22	0.09	0.18	0.17	0.09	0.13

From the laboratory test results, the following may be noted:

- Density determinations correspond to the UCS and triaxial tests. The average values for fresh rock samples of the four main rock types varies between 2.6 and 2.8 t/m^3 as indicated in Table 4.6 and Table 4.7. The average density for the saprolite from the triaxial testing varies between 1.8 and 2.0 t/m^3.

- The historical laboratory testing data base included a total of 159 UCS test results distributed among the four main rock types as indicated in Table 4.6 and the corresponding averages were used to characterize the intact rock strength. In general, the average UCS values for fresh rock are between 126 MPa and 166 MPa, with coefficients of variation of the order of 40%. These results indicate strong rocks, in particular as suggested by the maximum values with strengths greater than 200 MPa. Test results from the supplementary testing program indicated in Table 4.7 confirmed the strong character of the rock types tested, in particular for the MGWK unit with an average strength in excess of 200 MPa.
- Young’s modulus and Poisson ratio determinations were carried out on a few samples tested in uniaxial compression for the CAMB and MGWK units. Average modulus values of 79 GPa and 75 GPa were defined for these units, respectively.
- A total of 529 point load tests were carried out on samples of the four rock types studied, with the majority (65%) of the tests corresponding to the CAMB unit. Average values of the point load index (IS50) are between 5.8 MPa and 9.3 MPa. If the average values of UCS for each rock type are used to define a conversion factor from point load index (IS50) to UCS, values of the factor of 24, 16, 14 and 27 are defined for the CAMB, MGWK, DIOR and QFP units, respectively.
- The historic data base contains a total of 31 shear box test results, 26 of those carried out on saw cut surfaces in fresh rock samples of the CAMB and MGWK units. Average (base) friction angles defined for these units are 35^0 and 36^0, respectively. Results from the supplementary testing programme included 12 additional tests which indicated an average base friction angle of 33^0 for the DIOR unit and confirmed the existing value for the MGWK unit.
- In terms of strength characteristics along natural joints, the supplementary testing programme indicated peak friction angles of joints in metasandstone between 35^0 and 42^0 for roughness conditions from smoth planar to rough undulating, respectively. Similarly, the average residual friction angle determined for these joints was 34^0.
- The results of the triaxial testing on saprolites show a marked effect of the water content of the samples on the strength. The more recent tests on shallow samples from the boreholes drilled in March 2010 were carried out using rock mechanics

procedures as the samples were very hard as a result of the dry condition in which they were recovered. The photograph to the left in Figure 4.11 shows the rock like aspect of one of the samples after testing. Strength conditions represented by the Mohr-Coulomb parameters c = 2 MPa and $\varphi = 37^0$ were defined for the dry saprolite tested as shown in the graphs to the left of Figure 4.10.

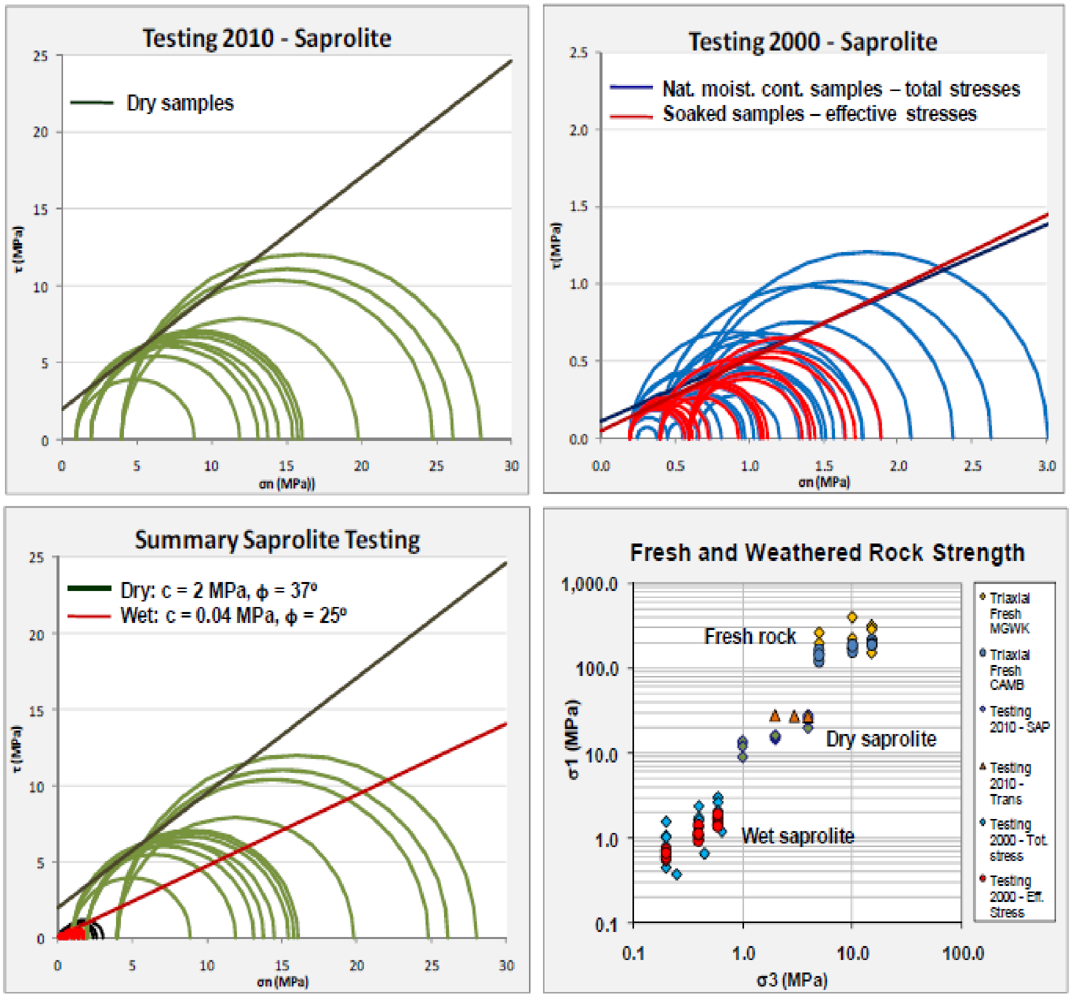

Figure 4.10 Results of historic (2000) and supplementary (2010) triaxial testing on saprolite and comparison with fresh rock strength (SRK, 2010)

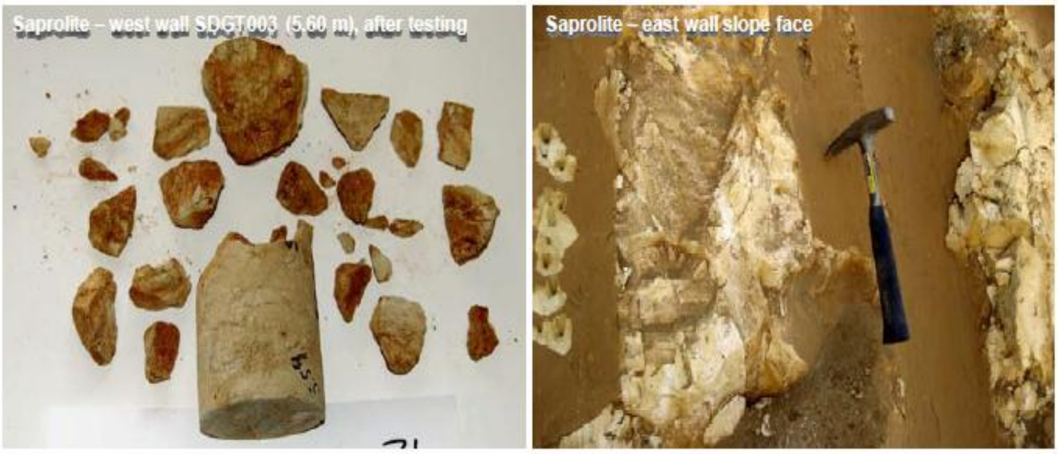

Figure 4.11 Dry hard saprolite from a core sample after testing (left) and moist soil-like saprolite at a slope face (right) (SRK, 2010)

- In contrast, the testing carried out in year 2000 was done on undisturbed wet samples using soil mechanics procedures to characterize the strength properties of the materials. Wet samples were tested either at their natural water content (7% to 27%) under total stress conditions or after being soaked in which case effective stress conditions were used during the test. The photograph to the left in Figure 4.11 shows the soil like aspect of the moist saprolite as observed in one of the slope faces of the east wall, which is probably closer to that of the samples tested in year 2000. In general, strength properties of the same order of magnitude were defined with the triaxial tests on wet samples as indicated in the upper right graph of Figure 4.10. Strength conditions corresponding to the Mohr-Coulomb parameters c = 40 kPa and $\varphi = 25^0$ defined with the tests on soaked samples were considered appropriate to represent the expected in situ strength conditions of the saprolites during the wet season, particularly considering their relatively low permeability characteristics and high thickness with which they occur in the pit area.
- A summary of all the results of the triaxial tests carried out on samples from fresh rock to wet saprolites is presented in the graph of $\sigma1$ versus $\sigma3$ included in the lower right corner of Figure 4.10 for comparative purposes. This graph illustrates the various orders of magnitude of the compressive strength of the materials according to their weathering (saprolite) and moisture conditions.

4.6 Groundwater Condition

The hydrogeological study of the area was carried out by SRK (2000) and subsequently by the mine, based on piezometer information and ground water measurements on site. Seepage mapping in the pit and observed performance of the slopes has confirmed the existence of a groundwater regime having a moderate effect on the pit excavations. The objective of the hydrogeologic programme is to define the strategies required to achieve dewatered slopes using wells and sub-horizontal drainage. In terms of the present study, a simple model has been considered for the stability analysis which is consistent with the observed groundwater regime.

CHAPTER FIVE

GEOTECHNICAL SLOPE MODEL

This chapter presents a description of the geotechnical model defined for the slope stability analysis. It includes the definition of the geometry, the location of the geotechnical units, the structural and strength characteristics of the rock mass and other geomechanical parameters associated with these units and the assumption of groundwater conditions.

5.1 Slope Geometry

The slope geometries for the analyses were derived from representative sections of the current and planned pit layouts as included in the latest geological model of the pit area. An East-West section (Section W4) (a) representative of the current west wall of the pit and a South-North section (Section S2) were used for analyses of calibration of the estimated rock mass strength parameters. The location of the sections used for the verification of the overall slope stability is indicated in Figure 5.1 for the current and planned pits. Also, the location of the main faults (F) in the west slope considered for the analysis of structurally controlled failures is indicated in this Figure 5.1.

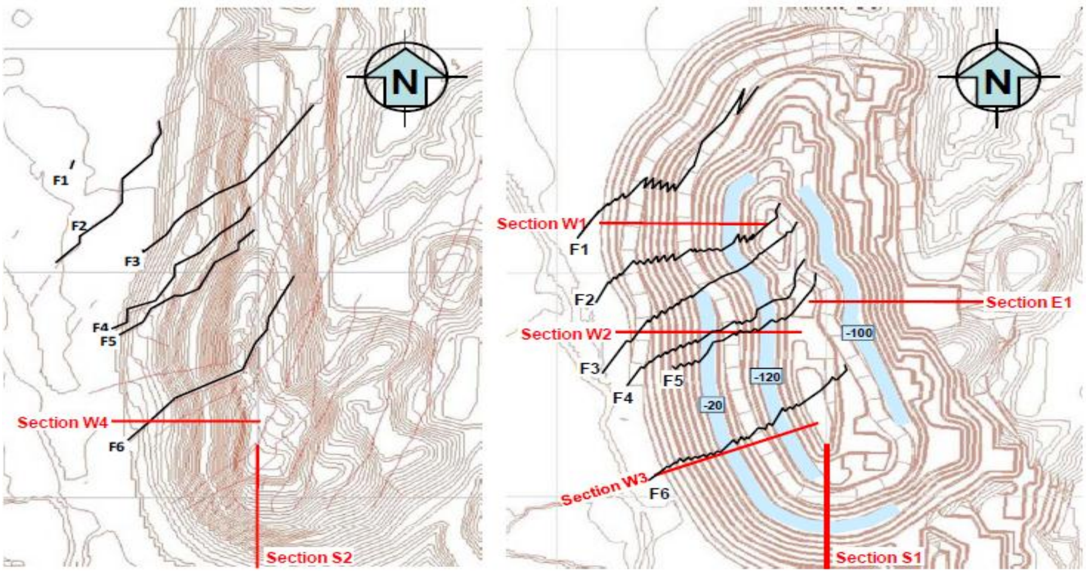

(a) (b)

Figure 5.1 (a) Current (left) and (b) planned (right) pit geometries with location of sections for stability analysis (SRK, 2000)

The planned pit layout shown in Figure 5.1 incorporates the recommended preliminary slope angles from the pre-feasibility level geotechnical investigation completed by (SRK, 2009). However, for the present study, this pit layout was used only as a reference and the slope geometries for analysis were derived from the geometrical design parameters summarized in Table 5.1, with variations of these parameters considered when required for the purpose of sensitivity analysis carried out to confirm the adequacy of the values. Three slope angle configurations were used for the analysis of the West slope corresponding to stack angles (toe to toe) of 60^0, 55^0 and 50^0. Similarly, stack angles of 60^0 and 55^0 were considered for the analysis of the East slope. The stack angle considered in the saprolite zones is 35^0.

Table 5.1 Slope geometry parameters (SRK, 2009)

Aspect	West Wall		East Wall	
	Saprolite & Weathered Rock	Hard Rock (MGWK)	Saprolite & Weathered Rock	Hard Rock (CAMB)
Batter angle (°)	70	75	70	75
Bench heigth (m)	10	20	10	20
Stack angle (°)	35	55	35	60
Bench width (m)	10.65	8.65	10.65	6.20
Geotechnical berm width (m)		30		30
Maximum stack heigth (m)		100		100

In general the geometrical design parameters include a bench height of 10m and bench face angle (batter angle) of 70º in saprolite and weathered rock and values of these parameters of 20m and 75^0, respectively, in fresh rock on the pit limit. Also, a ramp width of 40m and safety berm width of 30m to limit the height of the stacks to 100m was considered.

The general geometrical configurations of the west and east slopes used for the analysis of overall stability are illustrated in Figure 5.2. These configurations correspond to the current slope design with stack angles recommended from the previous evaluation carried out by SRK (2000), i.e. 55^0 in the west wall and 60^0 in the east wall. Overall slope angles along these sections are 47^0 (excluding the saprolite) and 52^0 for the west and east slopes, respectively.

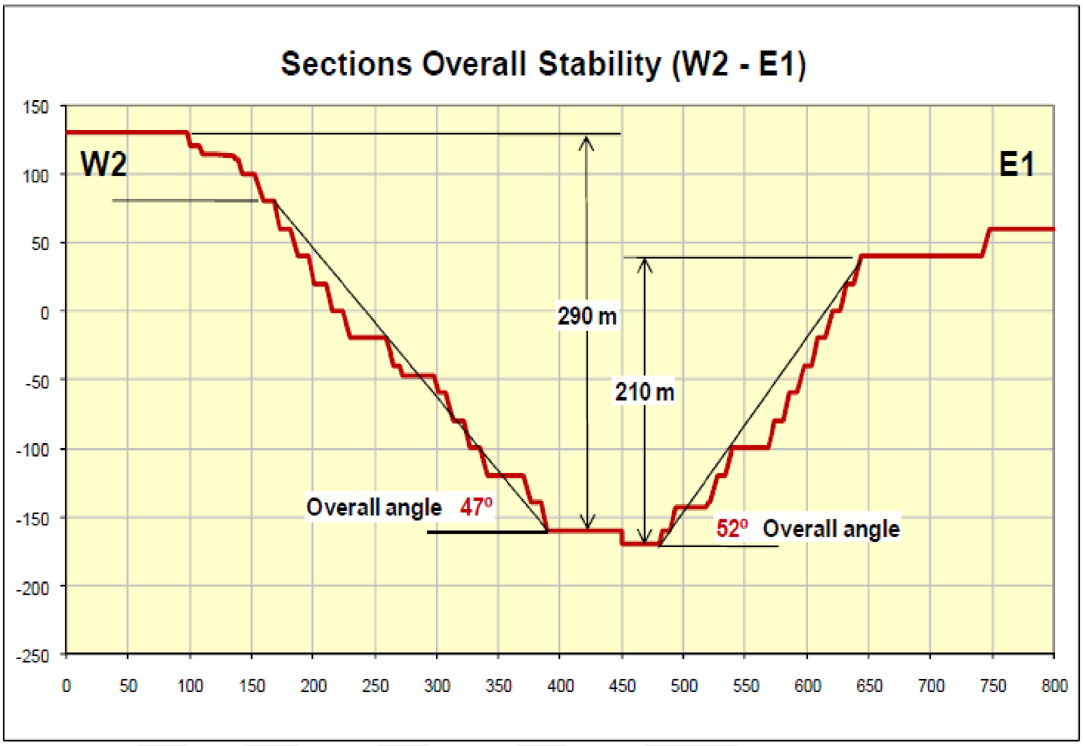

Figure 5.2 Slope geometry for sensitivity analysis of overall slope stability (SRK, 2000)

5.2 Geotechnical Units

The available geological model was used as the basis to define the boundaries of the geotechnical units for the slope stability analysis. Figure 5.3 shows the extent of the main geotechnical units exposed on the surface of the (a) current and (b) planned pits, based on the interpretation of the geological model. The reduction of the percentage of saprolite and weathered rock exposed on the surface of the slopes in the deep pit is evident in these projections.

An east-west cross section of the final pit, including the geometry of the current pit, the extent of the geotechnical units and the attitude of the main faults of relevance for the east wall stability, is shown in Figure 5.4. This section can be considered as typical of the deep sulphide pit and includes a modification in the extent of the weaker materials at the top of the west slope, which is a design condition considered necessary to prevent the occurrence of failures in these materials as experienced in the oxide pit. A close inspection of the exposures of the saprolite and weathered rock horizons revealed the transitional character of the contact of these units and suggested elevation

+80 m as a more adequate soft-unweathered rock boundary for the purpose of slope design.

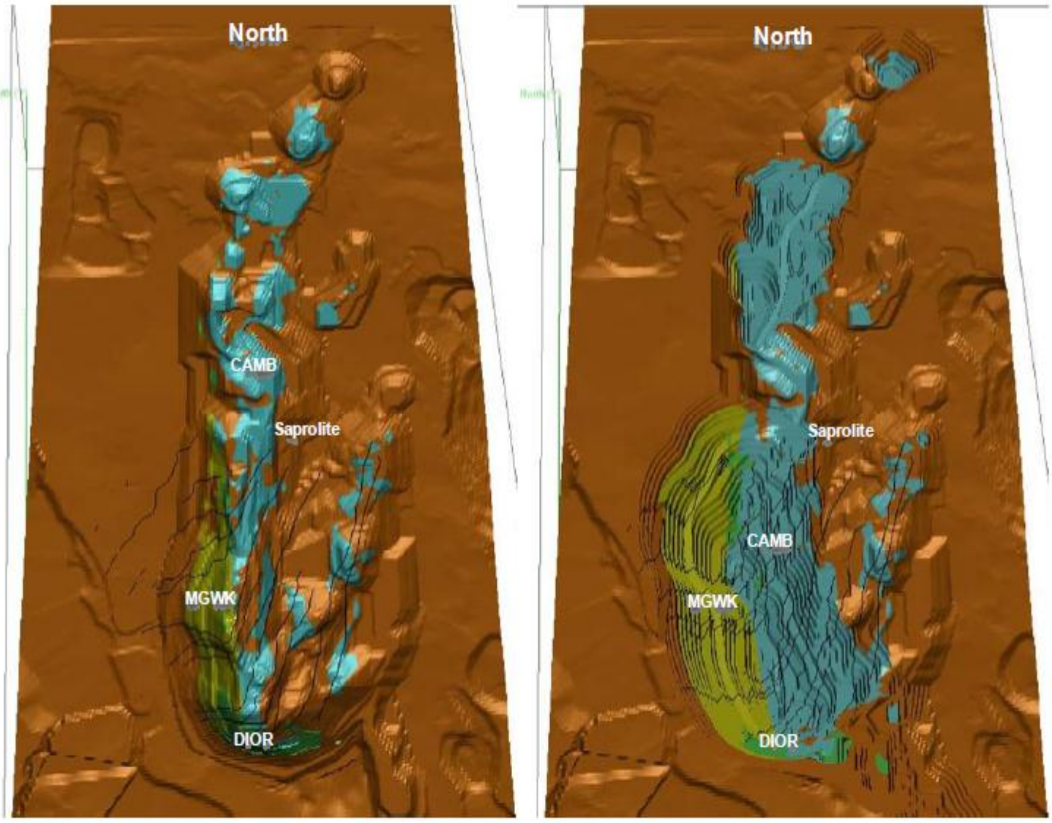

(a) (b)

Figure 5.3 Projection of the surface geology for the (a) current (left) and (b) planned (right) pits (SRK, 2009)

The current pit design considers 30m wide geotechnical berms at elevations -20 m and -120 m on the west slope and -100 m on the east slope, as shown in blue in the plan view of Figure 5.1. Overall slope angles (excluding the slope in saprolite at the top) are of the order of 49^0, with the current arrangement of geotechnical berms and ramps. The results of the stability analysis for the stack slopes will show the benefits of replacing the geotechnical berms by an additional ramp without compromising the overall angles.

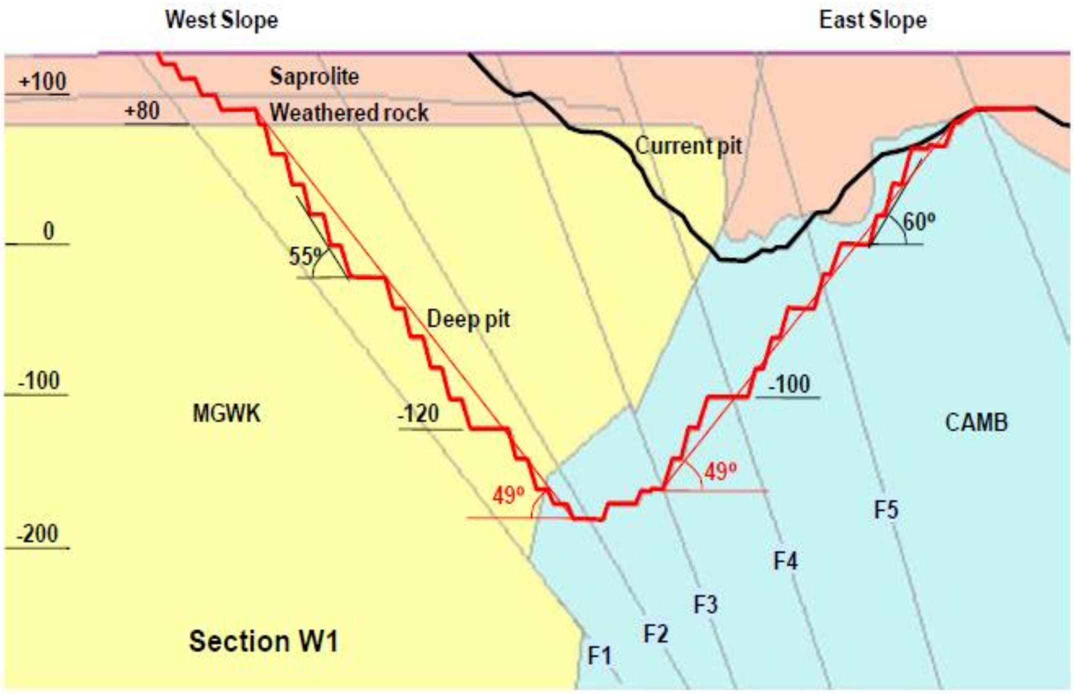

Figure 5.4 East-west cross section along section W1 with pit geometry and geology (SRK, 2009)

5.3 Structural Patterns

In terms of the orientation of structures, the data collected from oriented core from the three boreholes drilled and the existing surface mapping data were used to define main joint patterns and to identify potential failure modes controlled by structural features at different slope scales. Figure 5.5 shows the stereographic contour plots with the results of the analysis of orientation of joint sets for the (a) west (drill core data) and (b) east (surface mapping data) slopes. The three joint sets defined are J1 associated to the local faulting, striking NE and dipping SE; J2 with direction SE dipping steeply NE and J3 associated to the bedding with orientation NNW dipping WSW. The joint set orientations were defined in terms of average values and variability characteristics for the probabilistic analysis represented by angles of the cone of variability for one standard deviation.

In general there was good agreement between the results based on the new drill core data (1082 poles west slope) and those based on surface information (267 poles west slope central area and 366 poles east slope). For the stability analysis of the west slope it was considered more appropriate to use the orientations derived solely from boreholes due to the deeper location of this slope. For the east slope the available orientations from surface mapping were considered sufficient.

Some variability of the joint set orientations are expected along the pit length as suggested by the results of the surface mapping orientations; however, the use of the drill core data for the analysis of the west slope was considered appropriate as it corresponds to the central area of the pit, where the highest slope will be excavated and where joint sets J1 and J2 are more intensively represented.

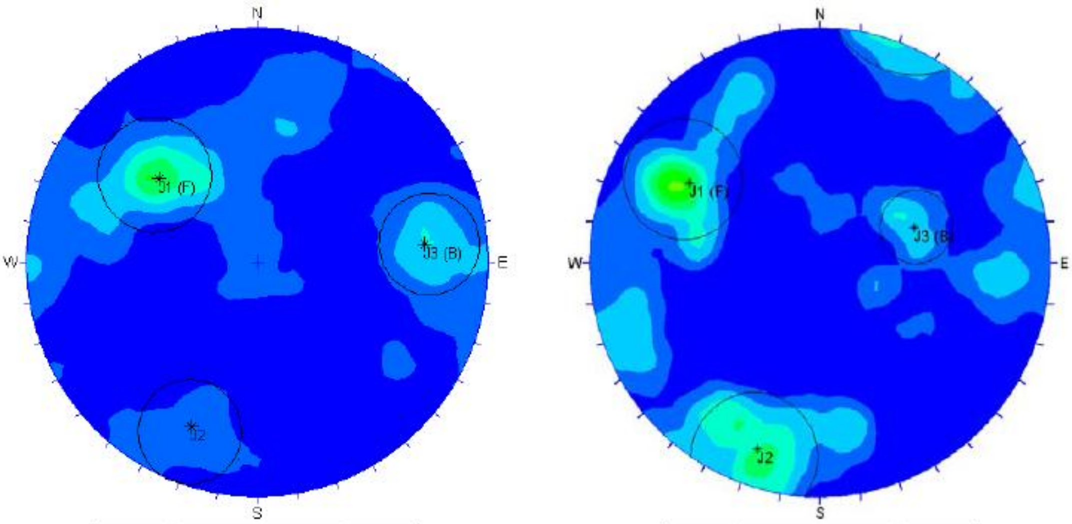

Set	Dip	D Dir	θ (°)
J1 (F)	58	130	21
J2	74	022	16
J3 (B)	72	264	16

θ = variability cone angle

West Wall – Drill Core Data
Equal Angle – Lower Hemisphere
1082 Poles

(a)

Set	Dip	D Dir	θ (°)
J1 (F)	67	121	20
J2	80	19	18
J3 (B)	47	250	15

θ = variability cone angle

East Wall – Surface Mapping Data
Equal Angle – Lower Hemisphere
366 Poles

(b)

Figure 5.5 Orientation of main joint sets for the (a) west (left) and (b) east (right) walls (SRK, 2009)

In terms of the joint sets characteristics, the joint condition descriptors from the drill core were used to supplement and confirm the existing information from surface mapping. Table 5.2 shows a summary of the properties of the main joint sets of relevance for the slope stability evaluation. This information suggests that the J1 set associated with the faults in the area is of major relevance for the stability of the slopes due to the high persistence and expected low strength of these structures. The J3 set associated with the bedding appears to be the less critical of the main sets due to its higher strength condition anticipated.

Table 5.2 Summary of joint set characteristics (SRK, 2009)

Joint Set No.	Structural Association	Wall	Dip (°)	Dip Direction (°)	Micro Roughness	Macro Roughness	Joint Alteration	Dip Continuity (m)	Strike Continuity (m)
J1 (F)	Faulting	W - E	40 - 90	090 - 160	Rough/Smooth Undulating	Undulating	Soft sheared chlorite	6 - >10	>10
J2		W - E	60 - 90	350 - 050	Smooth Planar	Undulating	Chlorite staining	1.5 - >10	>10
J3 (B)	Bedding	W	60 - 90	240 - 300	Smooth Planar	Undulating	Clean	0 - 10	>10
J3 (B)	Bedding	E	30 - 60	220 - 280	Rough Undulating	Undulating	Clean	0 - 2	<10

5.4 Rock Parameters for Design

The characterization of the geomechanical parameters for design include the estimation of the rock mass strength properties, the saprolite and weathered rock strength characteristics and the main joint set strength properties, using the available borehole log and laboratory testing data bases available.

5.4.1 Rock Mass Strength

The estimation of the rock mass strength parameters was based on the updated drill hole log database and on the existing laboratory testing results. The drill hole database includes 3,166 raw log data records that were converted to 4,026 records representing 10 meter rock intervals. Mohr-Coulomb parameters (c and φ) based on the Hoek-Brown criterion were estimated to represent the rock mass strengths. The methodology followed is illustrated in the diagram of Figure 5.6.

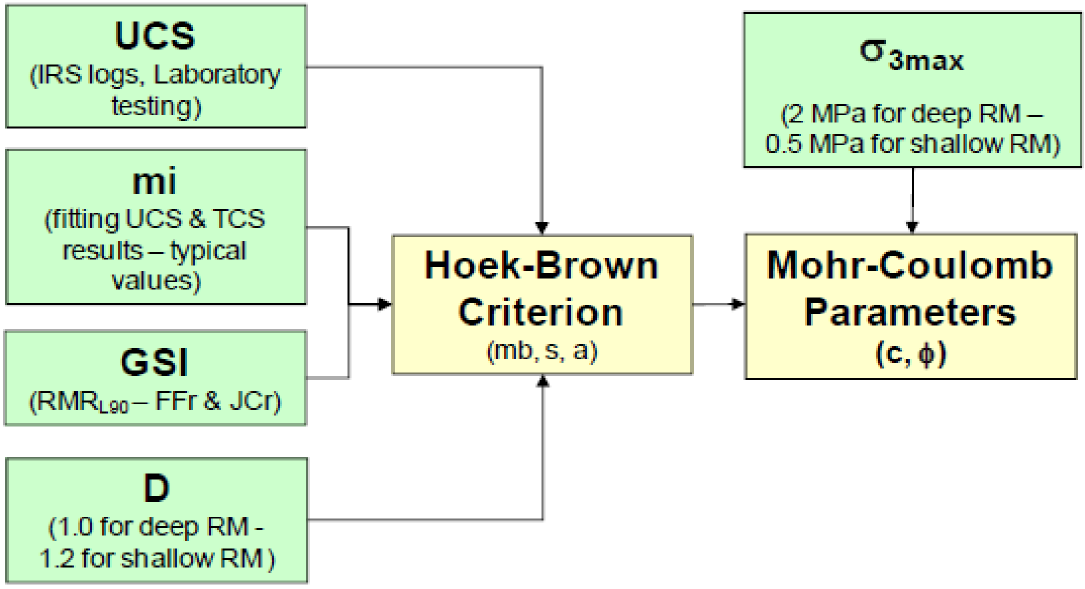

Figure 5.6 Methodology for the estimation of rock mass strength parameters (SRK, 2009)

The estimation of mi values was based on typical values published in literature for the various rock types and the results were verified by fitting Hoek-Brown failure envelopes with the results of UCS and triaxial testing. The estimation of the Geological Strength Index (GSI) from the Laubscher classification system was based on the translation of Laubsher's indexes Joint Condition rating (JCr) and Fracture Frequency rating (FFr) into Hoek's scales for Surface Condition and Structure of the GSI chart.

Two sets of strength parameters were estimated corresponding to deep (>30m, D=1 and σ3max=2.0 MPa) and shallow (<30m, D=1.2 and σ3max=0.5 MPa) rock mass conditions. A summary of the estimated rock mass strength parameters is presented in Table 5.3.

For comparison purposes Table 5.3 also includes the estimated strength of the saprolite (Sap) which is discussed in the following Section, and the parameters assigned to the weathered diorite (DIORw) and shear zone (SZ) required for the stability analysis of the south slope. The strength parameters for the DIORw and SZ units result from reducing the UCS value of the DIOR by 50% after calibration based on the stability evaluation of the current south slope.

Table 5.3 Summary of revised rock mass strength parameters (SRK, 2009)

No.	Code	Lithological / Geotechnical Unit	IRS (MPa)	UCS (MPa)	mi	RMR	GSI	Shallow RM (<30m)		Deep RM (>30m)	
								c (kPa)	Φ (°)	c (kPa)	Φ (°)
1	DIOR	Diorites	106	126	24	53	45	196	45.1	620	42.4
2	CAMB	Carbonated marbles	106	136	6	57	53	363	38.2	698	36.0
3	MGWK	Meta-sandstones	102	151	15	50	42	182	40.7	553	38.5
4	QFP	Quartz feldspar porphyries	144	167	19	54	48	261	47.6	721	44.7
5	DIOR w	Weathered diorite			24		45	147	39.5		
6	SZ	Shear zone			24		45	147	39.5		
7	Sap	Saprolite & weathered rock						40	25.0		

5.4.2 Saprolite and Weathered Rock Strength

Following the discussion on the results of the triaxial tests on saprolites, it was considered appropriate to assign the Mohr-Coulomb parameters c = 40 kPa and φ = 25^0 from the tests on wet samples, to the saprolites and weathered rock horizons. These parameters account for the presence of interstitial water within these soil-like materials with low permeability, which is a condition very likely to prevail particularly during the rainy season.

No differentiation was done in terms of the strength properties between the shallower saprolite levels and the deeper weathered rock of the transitional zone. This consideration is based on the observed historical performance of the slopes in the current pit which suggests that it is the weaker soft material present in the parent joints of the transitional zone that control the stability of the slopes, in spite of the apparent strong, rock like appearance of the material in these horizons.

5.4.3 Joint Strength Parameters

The estimation of joint strength properties was based on the (Barton-Bandis criterion, 1990) which enabled the estimation of equivalent Mohr-Coulomb parameters (c and φ) for a defined maximum level of normal stress. The methodology followed is illustrated in the diagram of Figure 5.7.

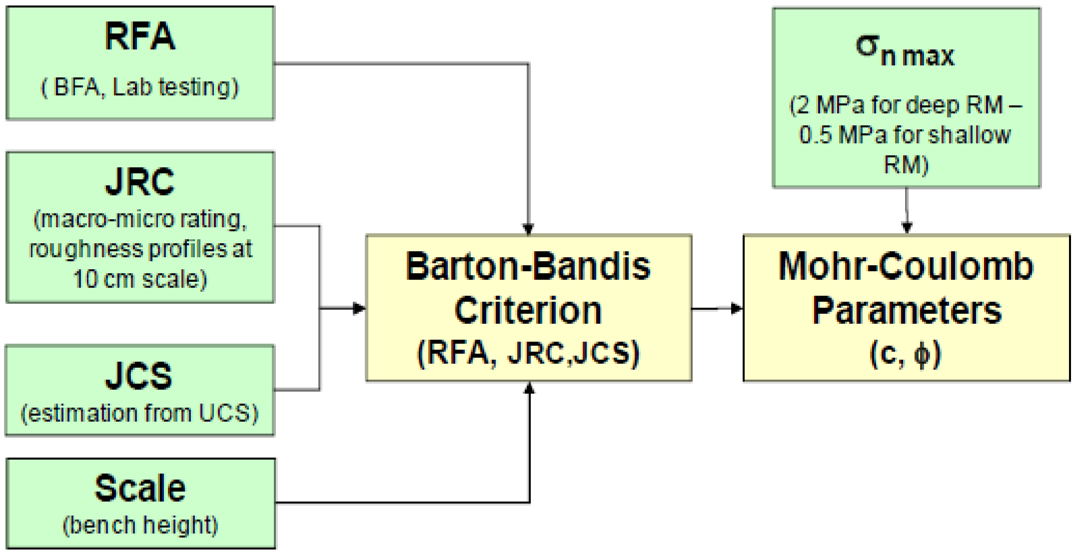

Figure 5.7 Methodology for the estimation of joint strength parameters (SRK, 2009)

Values of residual friction angle (RFA) were derived from the laboratory testing results for the three joint sets relevant for the stability analysis of the slopes. Representative values of JRC and JCS were estimated from borehole log data and a scale dimension consistent with inter-ramp slopes was assumed for the estimation of parameters representative of field conditions. Mohr-Coulomb parameters for joint strength were estimated assuming maximum normal stresses (σn max) of 0.5 and 2.0 MPa for shallow and deep rock mass conditions, respectively. Some adjustments to the parameters were made as indicated in the footnotes of Table 5.4 to account for field conditions not included in the estimation. For instance, the cohesion values for the joint set J3 associated to bedding were increased by a factor of 5 to account for the in situ welded condition of these joints. We believe that these cohesion values are still conservative for slope scales larger than two benches owing to the low persistence of the joints, but they are considered adequate for design purposes as they are not constraining the current design angles. A summary of the estimated joint strength parameters is presented in Table 5.4.

Table 5.4 Summary of estimated joint strength parameters (SRK, 2009)

No.	Geotechnical Unit Description	Code	Joint Set	UCS (MPa)	JCS (MPa)	RFA (º)	JRC log	Scale (m)	Joints Shallow RM (<30m)		Joints Deep RM (>30m)	
									c (kPa)	Φ (º)	c (kPa)	Φ (º)
1	Metagreywackes & Metasandstones	MGWK	J1 (F)	151	76	32	6	20	7	37	25	35
2	Metagreywackes & Metasandstones	MGWK	J2	151	151	34	3	20	5	39	18	37
3	Carbonated marbles	CAMB	J3 (B)	136	136	35	6	20	36	41	137	39

5.4.4 Summary of Strength Parameters for Design

A summary of the average strength parameters considered for the design of the slopes is shown in Figure 5.8. This graph indicates the relative variation of the strength properties in terms of Mohr-Coulomb parameters for the various rock conditions from residual on joint surfaces, through to natural joint planes, up to rock mass conditions.

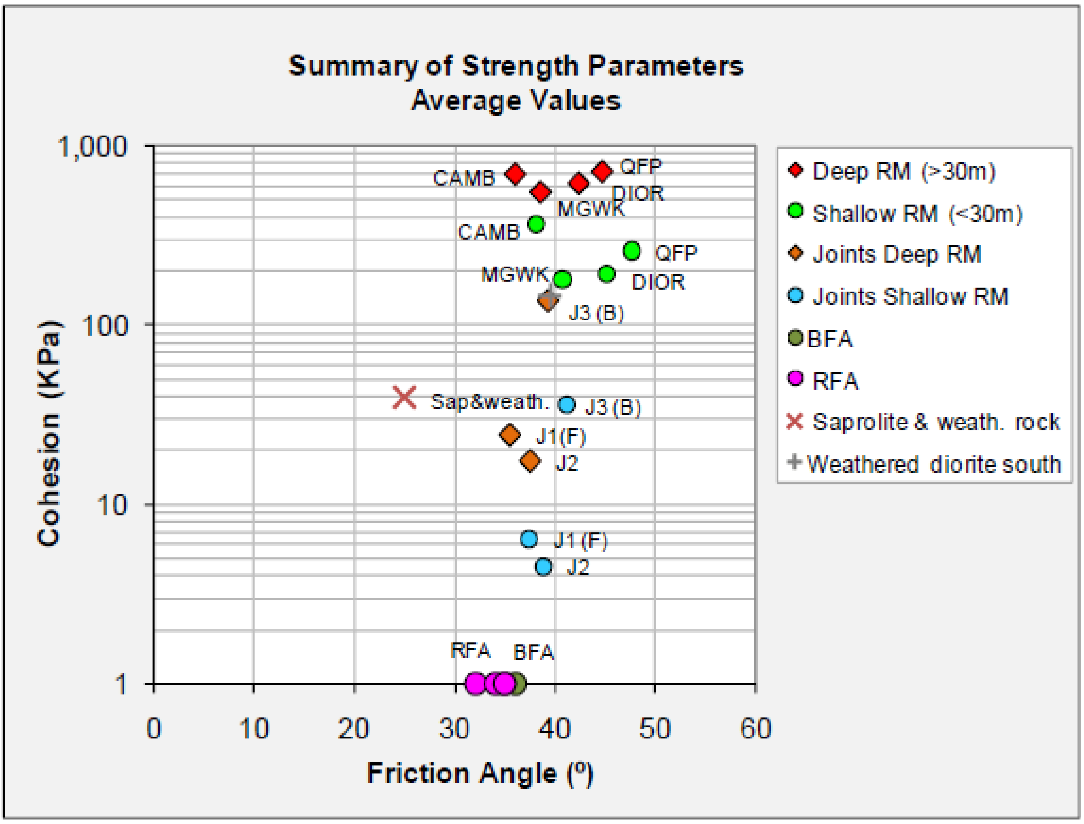

Figure 5.8 Summary of rock mass, joint and residual strength parameters for design (SRK, 2009)

In terms of the variability characteristics of the strength properties required for the estimation of the probability of failure of the slopes, coefficient of variations (CV) of 30% and 10% were considered for the estimation of standard deviations for the cohesions and friction angles, respectively. It is believed that these assumptions are consistent with the recorded variability of the rock strength factors included in the borehole and laboratory testing data bases, and also take into account the expected reduction in variability due to the larger scale of the geotechnical units in the sections for analysis.

5.5 Groundwater Conditions

A general review of the available reports on groundwater conditions at the Sadiola mine was carried out in order to verify the adequacy of the current assumptions used for the stability analysis of the future pit. The revised information suggests that the groundwater conditions for design depicted in Figure 5.9 are appropriate to represent the expected situation of the deep pit under routine dewatering practices. It is estimated that dryer slopes would be achievable with an ongoing dewatering programme including pumping wells and horizontal drain holes in areas with a high phreatic surface, should this be required.

The groundwater conditions used for slope design consider a depth of the water level of 30m (base of the saprolite) at a distance of one pit depth from the pit edge, a constant gradient from this location to a point 50m behind the slope face at half the height of the wet portion of the slope, and water surface reporting at the bottom of the pit. Water pressures are calculated as a function of the gradient of the water surface as indicated in Figure 5.9 to account for the effect of seepage through the slope.

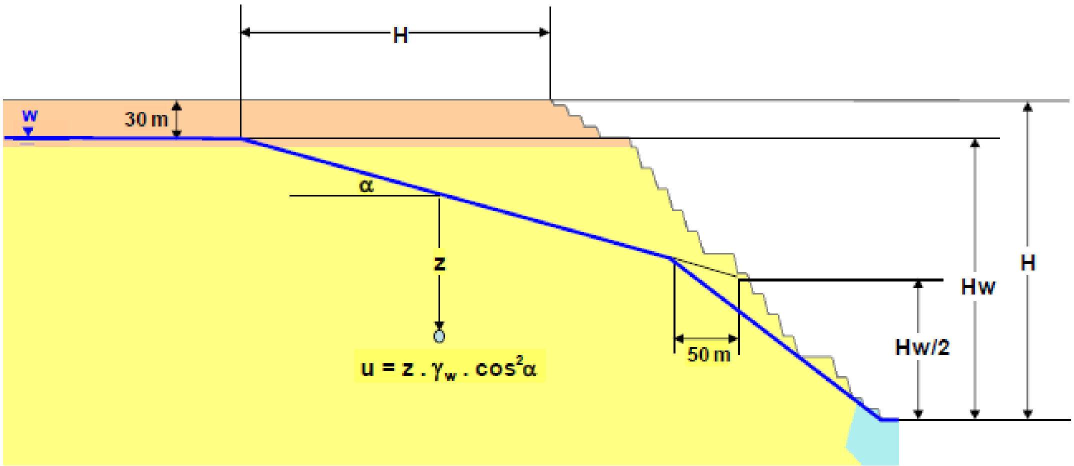

Figure 5.9 Groundwater conditions for stability analysis

CHAPTER SIX
SLOPE STABILITY EVALUATION

The slope stability evaluation was carried out for the west, east and south slopes, considering both, rock mass and structurally controlled failure mechanisms at the various scales of the slopes. In general, the analysis at bench and stack scale were carried out with the programs SWEDGE and OCPLANE from Rocscience for the analysis of wedge and planar failure mechanisms, respectively. The analysis of sensitivity of stability of the stack slopes, as well as the evaluation of the overall stability of the slopes was done through analysis with the program SLIDE from Rocscience based on the limit equilibrium method (LEM). The stability of the overall slopes was verified with stress deformation analysis with the program PHASE2 using a stress reduction technique on a finite element model (FEM).

6.1 West Slope

The stability analysis of the west slope include a general kinematic analysis using the main structural orientations defined with the latest geotechnical drilling, and stability analysis at bench, stack and overall scale, according to the relevant failure mechanisms in each case and using the updated material strength parameters as appropriate.

6.1.1 Kinematic Analysis

The results of the kinematic analysis to identify structurally controlled failure modes on the west slope indicate the possibility of wedge failures along joint sets J1 (F) and J2 and toppling events associated to the joint set J3 (B). Figure 6.1 shows the results of the kinematic analysis of the west slope for bench and stack (inter-ramp) slope scales.

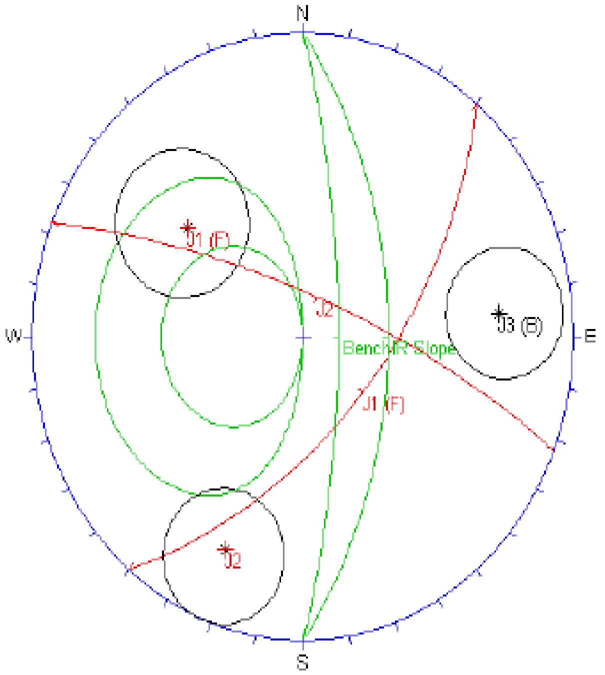

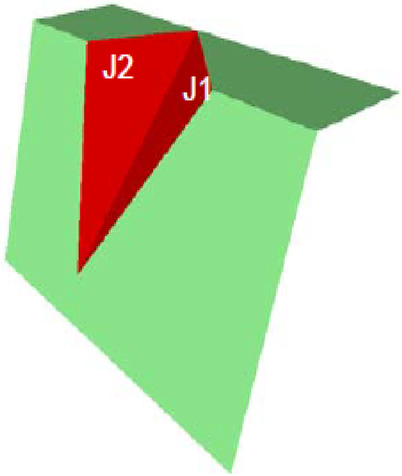

Set	Dip	D Dir	θ (°)
J1 (F)	58	130	21
J2	74	022	16
J3 (B)	72	264	16
Bench	75	090	
IR Slope	55	090	

Note:
θ = confidence cone angle

Figure 6.1 Kinematic analysis of west slope (SRK, 2009)

In terms of wedge failure, in general the analysis suggest the possibility of occurrence of relatively big wedges at bench scale and shallow wedges at stack scale. In terms of toppling failure the low persistence of the J3 (B) joint set suggests that this failure mode might be unlikely at scales larger than one bench. Moreover, the majority of the reported toppling failures in the west slope have occurred in the saprolite and weathered rock levels, and there are indications that the failure mechanism might consist of initial ravelling and sliding at the base of the unstable slope, followed by the toppling of blocks defined by the J3 set at the top of the slope.

A kinematic analysis was also carried out to assess the possibility of occurrence of wedges defined by one of the main faults identified in the pit area. Figure 6.2 shows the projected location of these faults on the west slope of the deep pit and the results of the kinematic analysis of wedges defined by the intersection of these structures with a joint of the J2 set. The faults are in general steep, resulting in a low likelihood of defining wedges at stack scale, except for fault F1 with an average dip of 52^{0} which could form a relatively shallow but high (4 bench) wedge indicated in the Figure.

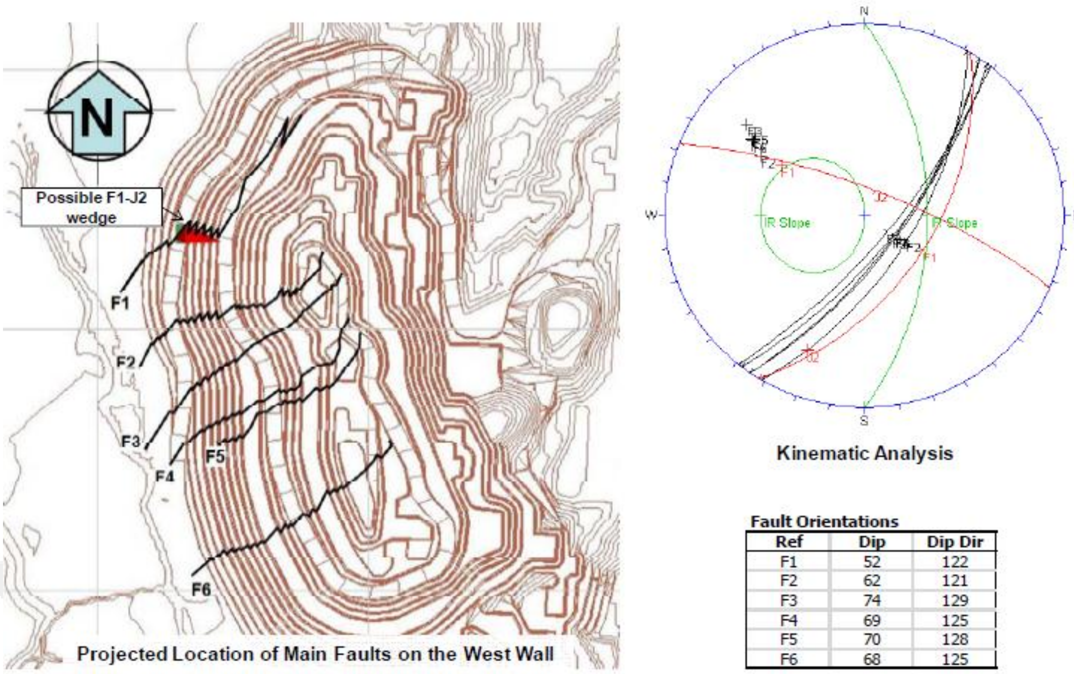

Figure 6.2 Kinematic analysis of fault related wedges in the west wall (SRK, 2009)

The results of the stability evaluation of this wedge are shown in Table 6.1. Factors of Safety (FoS) and Probability of Failure (PoF) values have been calculated for stack angles of 51^0, 53^0 and 55^0. The wedge for the 55^0 stack angle is similar to the wedge failure that occurred in 2008. The flattening of the slope results in the reduction of the PoF due to the reduction of its volume. A high PoF for this type of wedge would be acceptable if provisions to reduce the impact of these failures are included in the pit design.

Table 6.1 Stability analysis of wedge F1-J2 (SRK, 2009)

Stack Slope		Dip / Dip Dir Wedge Planes			Vol m3	FoS	PoF
Angle	Height	F1	J2	Intersec.			
55	80	52 / 122	74 / 022	48 / 093	6,152	1.00	28%
53	80				3,178	1.04	13%
51	80				1,097	1.15	4%

6.1.2 Bench Scale Stability

The stability of benches in terms of wedge failure was evaluated for various bench configurations in order to assess the implications of bench height and face angle on the stability conditions. The current pit benches in hard rock are 10 m high with a steep face; however, 20m high benches battered at 75^0 are currently being considered on the pit limits for the design of the deep pit. Table 6.2 and Figure 6.3 show the results of the wedge stability analysis at bench scale in terms of FoS and PoF values. PoF values refer to the bench rather than to the wedge and they account for the frequency of occurrence of the wedges which has been assumed at one every 100 m.

Table 6.2 Analysis of wedge failure at bench scale west slope (SRK, 2009)

Bench Height (m)	Batter Angle (°)	Bench Width (m)	FoS	Wedge Vol (m^3)	PoF wedge	LFB (m)	No. of Wedges/ 100m	PoO wedge	PoF
10	75	4.32	1.28	40	10%	6.9	1	7%	1%
15	75	6.48	1.15	135	21%	10.3	1	10%	2%
20	75	8.65	1.09	322	28%	13.8	1	14%	4%
10	90	7.00	1.12	114	37%	11.2	1	11%	4%
15	90	10.50	1.06	383	42%	16.8	1	17%	7%
20	90	14.00	1.03	909	45%	22.3	1	22%	10%

Higher benches provide wider berms which are beneficial for rock fall control, but also result in the reduction of the stability condition of potential unstable wedges. On the other hand, battered bench faces cause the reduction of wedge sizes improving the stability condition of the benches, but they take valuable space from the berms.

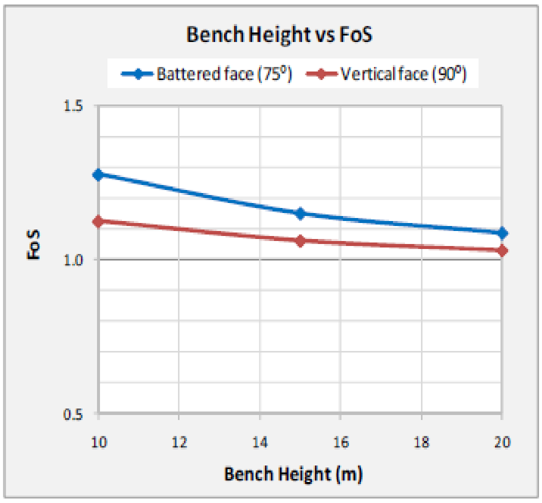

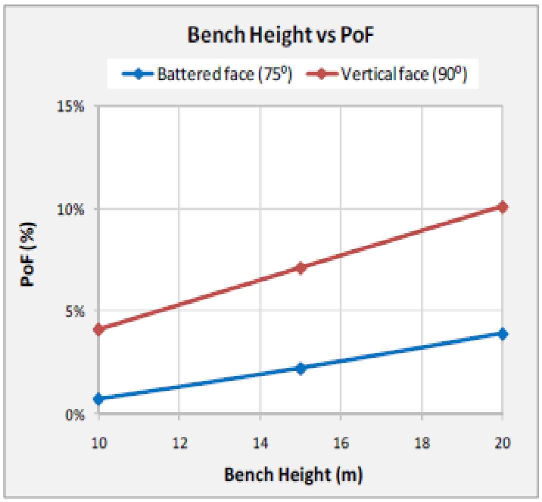

Figure 6.3 Results of wedge failure analysis at bench scale in the west wall (SRK, 2009)

The results of the stability analysis in Figure 6.3 show a moderate reduction in the stability condition with the increase of bench height from 10 m to 20 m. For the battered face case the FoS reduces from 1.28 to 1.09 and the PoF increases from 1% to 4%. This reduction in stability is of similar magnitude to the gain of stability by having a 75^0 bench face instead of a vertical face. In conclusion, the current design configuration does not impair the stability of the benches in terms of potential wedge failures, and adds the benefit of having wider berms for rock fall control.

6.1.3 Stack Slope Stability

Saprolite and weathered rock:

The current design of the pit considers the saprolite at elevation +100 m approximately and therefore the slope below this level is designed with a steep angle as it is assumed to be excavated in hard rock. However, the observed performance of these slopes suggests that the irregular transition from saprolite to weathered rock extends below this elevation affecting the stability of the slopes designed for harder rock conditions. To account for this situation a weathered-unweathered rock boundary at elevation +80 m has been added to the geotechnical model to update the slope design in these soft rock materials. With this modification, the average slope height in saprolite and weathered rock is 50 m or five 10 m high benches.

In order to assess the required slope design in these soft materials, a sensitivity analysis was carried out for slope heights ranging from 20 m (2 benches) to 50 m (5 benches), and for stack angles from 35° to 55°. Details of the slope configurations considered and the results of the analysis are shown in Figure 6.4. For this analysis the same strength properties were assumed for the saprolite and weathered rock horizons.

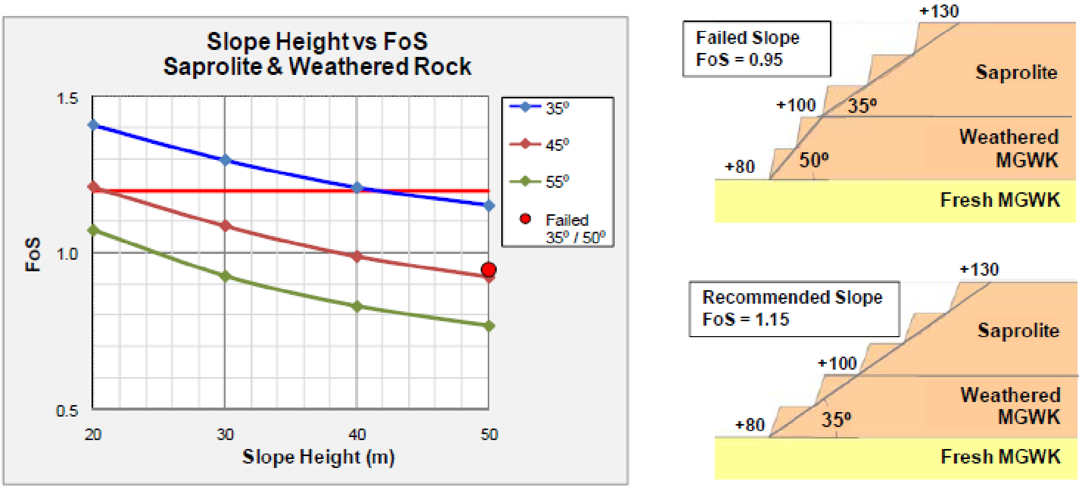

Figure 6.4 Results of the stability analysis on the saprolite and weathered rock (SRK, 2009)

The results of the analysis indicate that a 30m high slope in the saprolite at 35° is stable (FoS = 1.3), which is consistent with the observed performance of the slopes in saprolite in the current pit. The graph in Figure 6.4 also shows a marked reduction of the FoS with the increase of the slope angle, and the FoS reduces to 1.0 for a 30 m high slope at 50^0, which may correspond to the various failures reported between elevations +80 m and +100 m in the current pit. These failures may be typified by a slope configuration consisting of a 30^0 slope angle between elevations +130 m and +100 m and 50^0 angle between elevations +100 m and +80 m as sketched in Figure 6.4, which yields a FoS of 0.95. The recommended slope angle in this case is 35^0 (toe to toe) which results in a FoS of 1.15, considered acceptable given the actual transitional conditions of the saprolite not represented by the model.

Rock mass failure in unweathered rock:

To facilitate the assessment of stability of the stacks in the west slope in terms of rock mass failure, a sensitivity analysis was carried out for stack angles of 50^0, 55^0 and 60^0 (toe to toe), slope height of 100m (5 benches) and wet and dry conditions. Shallow rock mass strength parameters were used for this analysis and the corresponding results are shown in Figure 6.5.

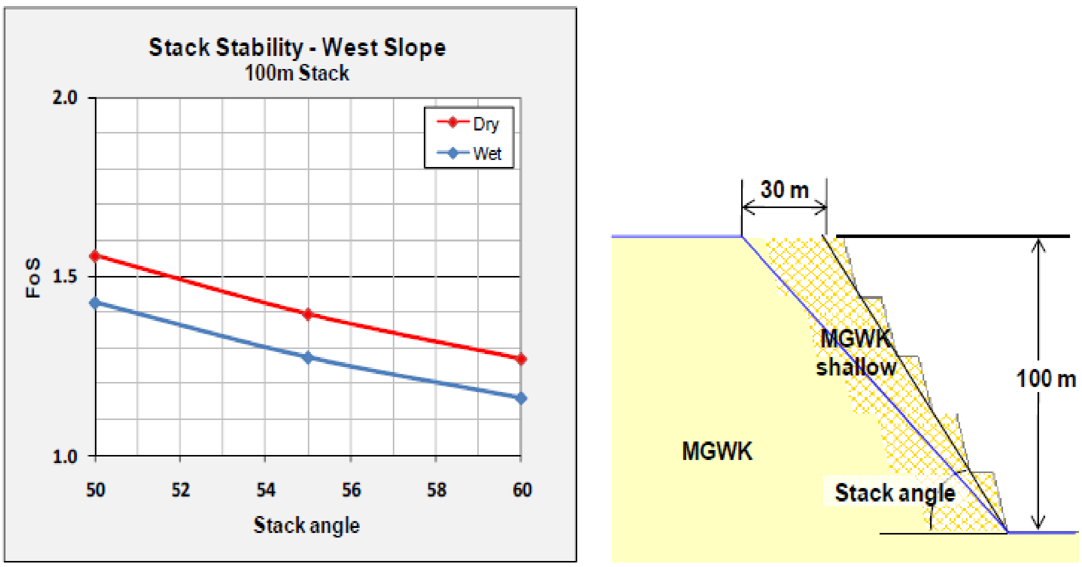

Figure 6.5 Results of analysis of sensitivity of stack stability in west slope (SRK, 2009)

The results of Figure 6.5 suggest that 55^0 could be considered the appropriate stack angle for the west slope under routine dewatering conditions. Although the results of the analysis indicate that steeper slopes might be acceptable in terms of rock mass failure, particularly for dryer slope conditions or lower slope heights, it is considered that the 55^0 stack angle constitutes the upper bound value for this slope in order to maintain acceptable berm widths required for rock fall mitigation.

Structurally controlled failure in unweathered rock:

The possibility of occurrence of wedge failures at stack (inter-ramp) scale in the west slope was confirmed by the results of the kinematic analysis. In order to assess the likelihood of these failures and its potential impact, a sensitivity analysis was carried out for stack heights ranging from 20 m to 100 m and stack angles between 52^0 and 55^0. The results of these stability analyses are summarized in Table 6.3 and Figure 6.6. In this case the PoF values calculated are the result of considering the variability of the orientation of the planes and their strength properties.

Table 6.3 Analysis of wedge failure at stack scale, west slope (SRK, 2009)

Height (m)	Slope angle 52°			Slope angle 55°		
	FoS	Volume (m^3)	PoF	FoS	Volume (m^3)	PoF
40	2.79	8	1%	1.30	180	3%
60	2.16	27	2%	1.16	607	5%
80	1.84	64	3%	1.10	1438	7%
100	1.65	125	4%	1.06	2809	8%

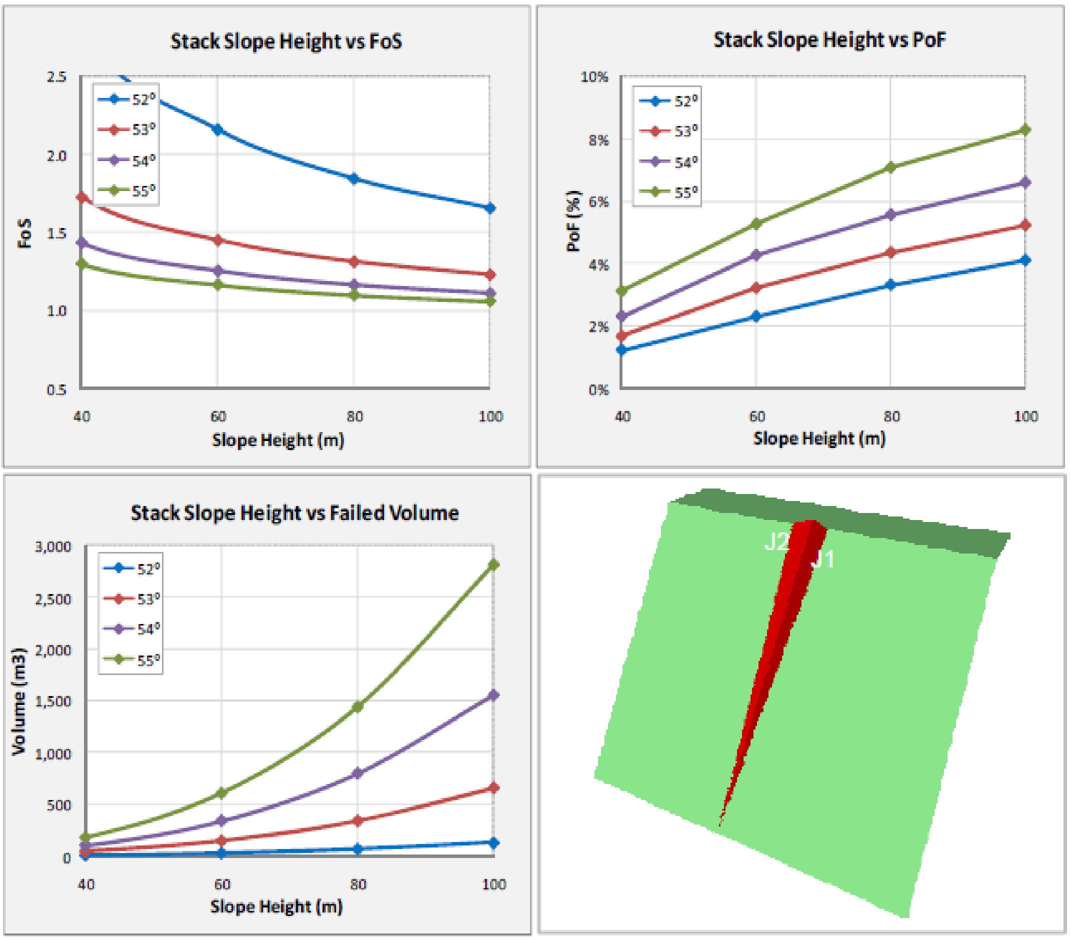

Figure 6.6 Results of wedge failure analysis at stack (inter-ramp) scale (SRK, 2009)

The results of the analysis indicate acceptable stability conditions for the 55^0 stack angle for slopes up to 60 m high (3 benches), but marginal stability for greater slope heights. PoF values larger than 5% for stacks of 3 or more benches represent a situation that may be a nuisance for the operation unless additional ramp access is provided in the pit design. The flattening of the stack slopes result in a marked reduction of the volume of the wedges as shown in Figure 6.6 with the consequent improvement of the stability conditions. The current layout of ramps and geotechnical berms in the design results in a large percentage of high stack slopes and a higher susceptibility to impacts from failures, which would suggest the need of a 53^0 stack angle to reach PoF values consistent with these design factors.

6.1.4 Overall Slope Stability

The overall slope stability was verified with limit equilibrium analysis on the sections W1, W2 and W3 as shown in Figure 4.1. A stability analysis was also carried out on section W4 of the current slope in order to benchmark the FoS values calculated for the final pit. In all cases, dry and best estimated wet conditions were considered. The results of these analyses are summarized in Table 6.4.

Table 6.4 Results of overall slope stability of the west wall (SRK, 2009)

Section	Pit	Slope Angle (º)	Slope Height (m)	FoS		PoF	
				Dry	Wet	Dry	Wet
W1	Deep	49	305	1.53	1.32	2%	6%
W2	Deep	48	291	1.62	1.41	1%	5%
W3	Deep	47	308	1.59	1.37	1%	5%
W4	Current	49	191	1.81	1.63	1%	1%

Factors of safety for wet conditions between 1.32 and 1.41 were obtained for the final west wall of the pit with slope heights of the order of 300 m and overall slope angles around 49^0. These values are consistent with the 1.63 value calculated for the 191 m high and 49^0 angle current slope. In terms of probability of failure, values less than 6% are obtained for the design sections under wet conditions, which correspond well with the 1% value calculated for the current slope. The results for dry conditions provide an indication of the available margins of stability to be gained with depressurisation strategies if required.

The results of the limit equilibrium analysis (LEM) with the program SLIDE were verified with stress deformation analysis (FEM) using the program PHASE2 assuming an elastic perfectly plastic behaviour of the rock mass. Stress reduction factors (SRF) are calculated with this methodology, which are equivalent to the factors of safety (FoS) resulting from the limit equilibrium analysis. A comparison of the results obtained with both methodologies is presented in Figure 6.7 for sections W1 (a) and W4 (b) considering wet slope conditions. The results of the analysis with both approaches show good correspondence in terms of the mechanism of failure and the factors of safety calculated.

In general, the results of the analysis suggest that the current overall design angles are adequate and result in acceptable stability conditions of the slopes. It is believed that the overall slope angles will not be affected by the suggested adjustments on the saprolite slope and on the configuration of ramps and geotechnical berms.

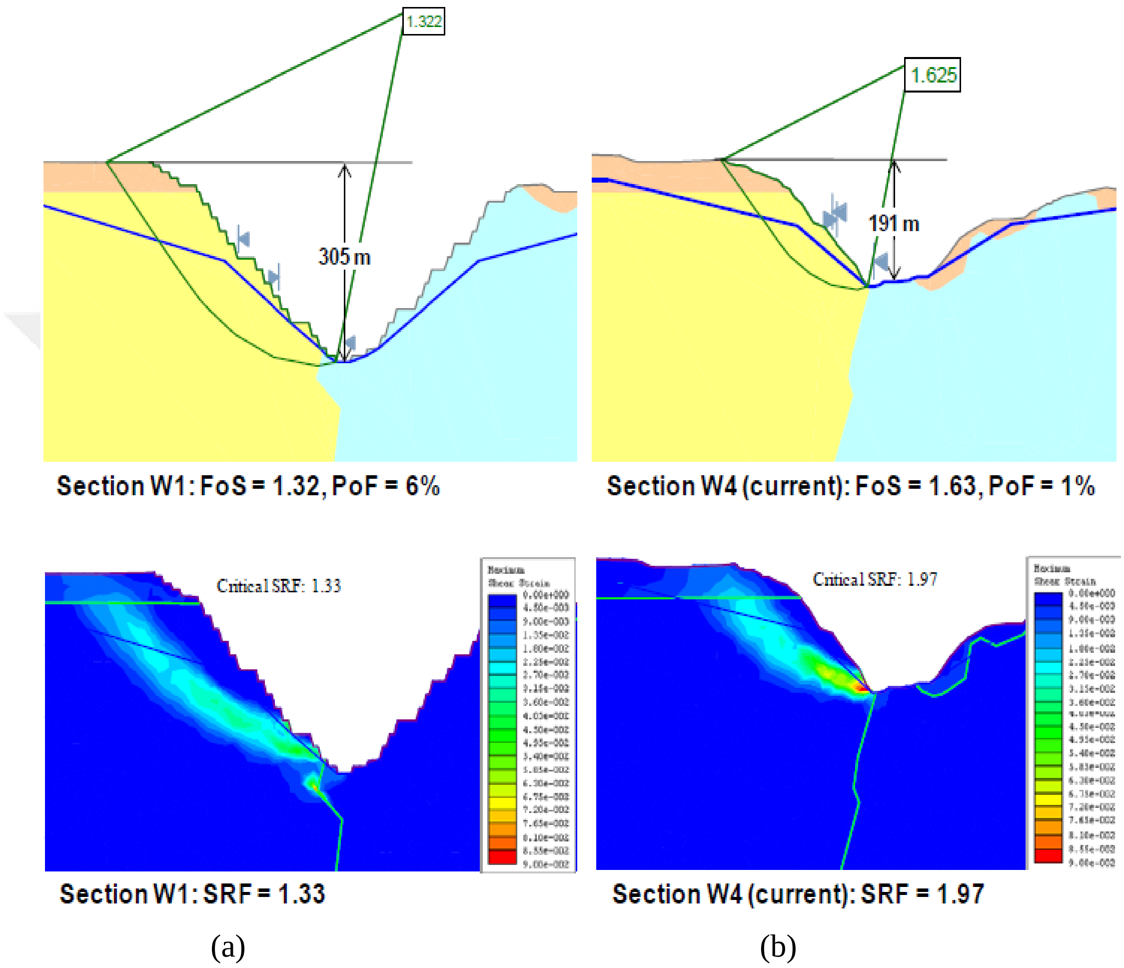

Figure 6.7 Comparison of LEM and FEM analysis of overall slope stability of west wall (SRK, 2009)

6.2 East Slope

The evaluation of the stability of the east slope includes a general kinematic analysis using the main structural orientations derived from surface mapping, and stability analysis at bench, stack and overall scale, according to the relevant failure mechanisms in each case and using the updated material strength properties as appropriate.

6.2.1 *Kinematic Analysis*

The results of the kinematic analysis for the east slope at bench and stack (inter-ramp) scales are shown in Figure 6.8. These results suggest the possibility of occurrence of planar failures along the joint set J3(B) with joint sets J1 and J2 acting as release surfaces through the development of tension cracks similar to those observed in the planar failure of 2006 (see photograph in Figure 5.4). Joints from sets J1 and J2 might also favor the occurrence of toppling events although no failures with this mechanism have been reported in the unweathered rock levels of the east slope.

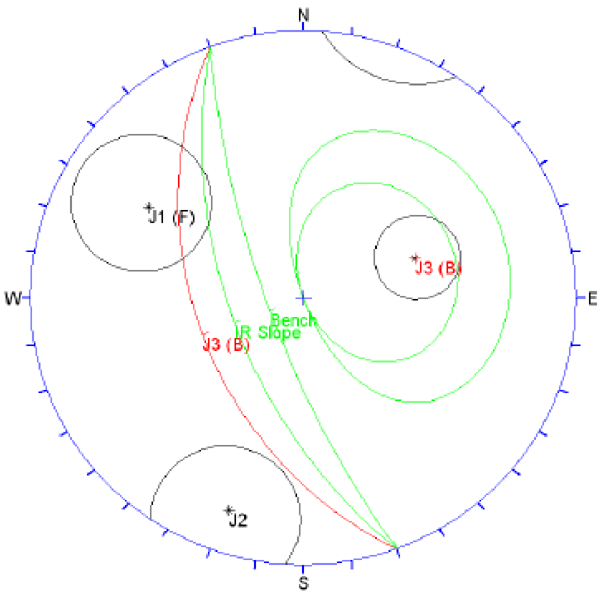

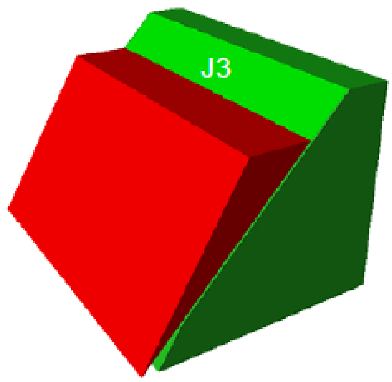

Set	Dip	D Dir	θ (°)
J1 (F)	67	121	20
J2	80	19	18
J3 (B)	47	250	15
Bench	75	250	
IR Slope	60	250	

Note:
θ = variability cone angle

Figure 6.8 Kinematic analysis of east slope (SRK, 2009)

6.2.2 *Bench Scale Stability*

A sensitivity analysis of bench stability for planar failure in the east slope was carried out to assess the effects that changes of bench height and face angle would have on stability conditions in the slope. Bench heights ranging from 10 m to 20 m and bench faces from vertical to battered at 75^0 were considered for this analysis. Table 6.5 and Figure 6.9 show the results of the stability analysis for planar failure at bench scale in terms of FoS and PoF values. Estimated strength properties corresponding to welded joint conditions were used for these analyses, which also implies that good blasting practices are assumed to be in place.

Table 6.5 Analysis of planar failure at bench scale east slope (SRK, 2009)

Bench Height (m)	Batter Angle (º)	Bench Width (m)	FoS	Vol (m^3/m)	PoF
10	75	3.09	2.42	7.2	0%
15	75	4.64	1.89	16.2	1%
20	75	6.19	1.62	28.8	3%
10	90	5.77	1.67	17.9	2%
15	90	8.66	1.39	40.2	7%
20	90	11.55	1.24	71.5	16%

The results of the analysis indicate in general, high FoS and low PoF values, in particular for the battered case condition. The results also show the strong positive effect that the inclined face has on the stability, balancing the reduction of stability caused by the increase in bench height. The stability conditions of the current bench design configuration with a height of 20 m battered at 75^0 are represented by a FoS of 1.62 and PoF of 3%, which can be considered acceptable. In conclusion, the current design configuration maintains acceptable stability conditions of the benches in terms of potential planar failures.

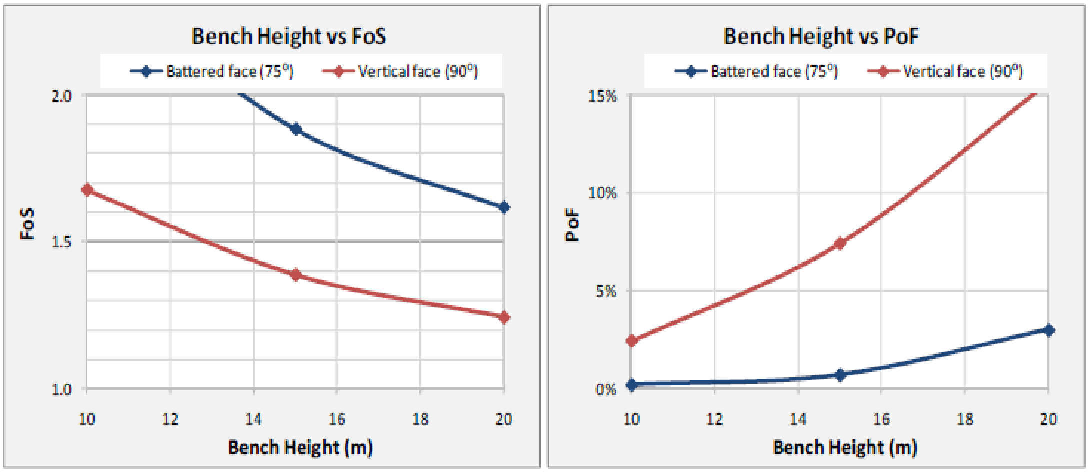

Figure 6.9 Results of planar failure analysis at bench scale in the east wall (SRK, 2009)

6.2.3 Stack Slope Stability

Rock mass failure:

The assessment of stack stability in terms of rock mass failure in the east slope was based on a sensitivity analysis for stack angles of 50^0, 55^0 and 60^0 (toe to toe), slope height of 100m (5 benches) and wet and dry conditions. Shallow rock mass strength parameters were used for this analysis and the corresponding results are shown in Figure 6.10. These results suggest that rock mass failure is not the critical failure mode in this slope and a practical upper bound stack angle of 60^0 with a maximum stack height of 100 m is considered the appropriate design value owing to the constrains imposed by the required berm widths for rock fall control.

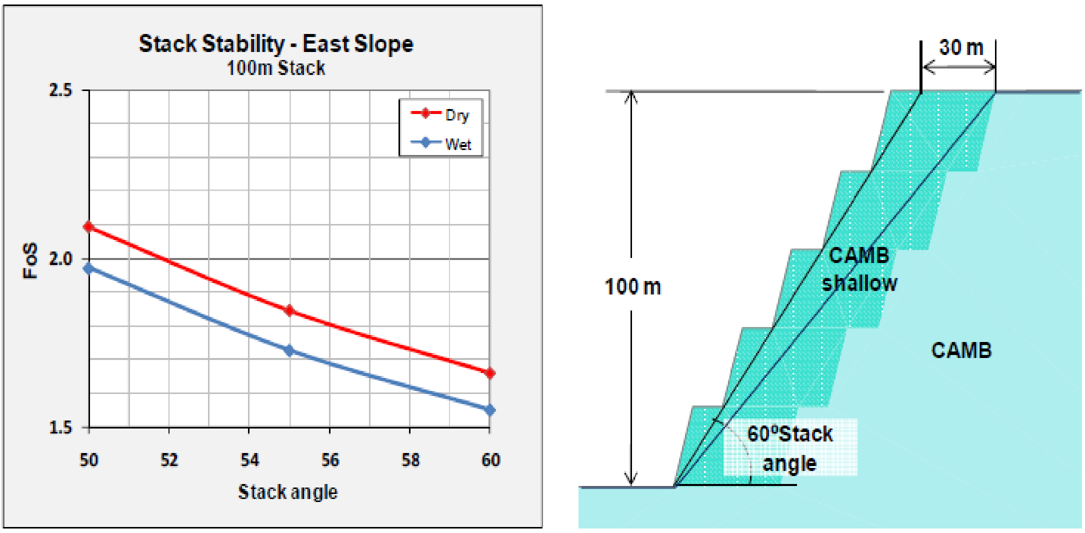

Figure 6.10 Results of analysis of sensitivity of stack stability in east slope (SRK, 2009)

Structurally controlled failure:

The likelihood of occurrence of planar failures at stack slope scale is anticipated to be low due to the low persistence and relatively high strength of the joints associated with the bedding in the east slope (joint set J3). This perception is consistent with the actual performance of the slopes in the current pit. In order to assess the likelihood of failures at stack scale controlled by the joint set J3, a sensitivity analysis was carried out for slope heights between 40 m and 100 m for two assumptions of strength along the planar failure surface associated to joint set J3. The strength assumptions considered correspond to cohesion values equivalent to one half (180 kPa) and one third (120 kPa) of the value estimated for the shallow rock mass conditions, keeping the same friction angle (39^0). The results of these stability analyses are shown in Table 6.6 and Figure 6.11.

Table 6.6 Analysis of planar failure at stack scale east slope (SRK, 2009)

Height (m)	Half of RM Strength			Third of RM Strength		
	FoS	Volume (m^3/m)	PoF	FoS	Volume (m^3/m)	PoF
40	2.51	284	0%	1.92	284	0%
60	1.92	639	0%	1.54	639	1%
80	1.63	1137	1%	1.34	1137	3%
100	1.46	1776	2%	1.22	1776	7%

The results of these analyses indicate acceptable stability conditions for the east stack slopes in terms of planar driven failure modes, even for the conservative assumption of strength, with a FoS of 1.22 and a PoF of 7%.

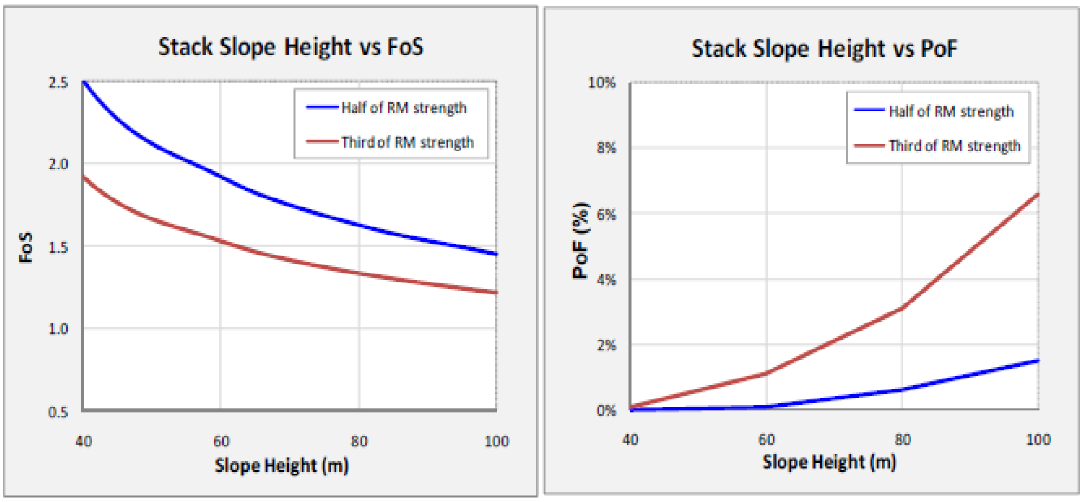

Figure 6.11 Results of planar failure analysis at stack scale (SRK, 2009)

6.2.4 Overall Slope Stability

The overall stability of the east slope was verified with a limit equilibrium analysis on section E1 indicated in Figure 5.1. The analysis considered dry and best estimate wet conditions with the results shown in Figure 6.12. A factor of safety of 1.50 and probability of failure of 4% were obtained for the 210 m high slope with an overall angle of 52^0 under wet conditions. This analysis might be considered as an extension of the analysis at stack scale where a fraction of the rock mass strength was assigned to the planar failure surface. In this case the larger volume involved in a potential slide event implies the development of a deeper composite slip surface along which the full rock mass strength estimated for this unit is available. This result indicates acceptable stability conditions for the currently designed slope and no further adjustments are anticipated.

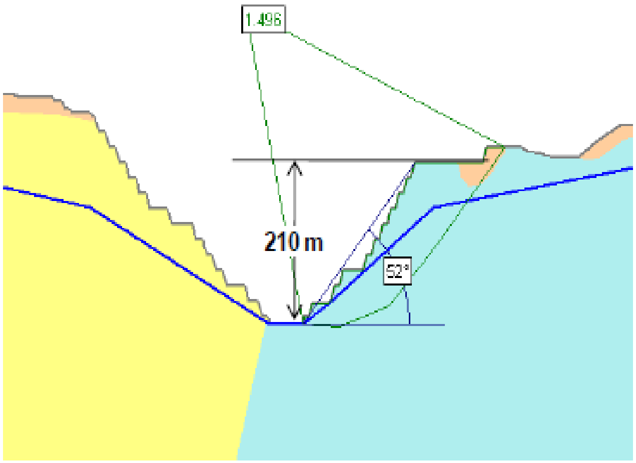

Section E1: FoS = 1.50, PoF = 4%

East Slope - Overall Stability

Section	E1
Slope Angle (º)	52
Slope Height (m)	210
FoS dry	1.69
FoS wet	1.50
PoF dry	1%
PoF wet	4%

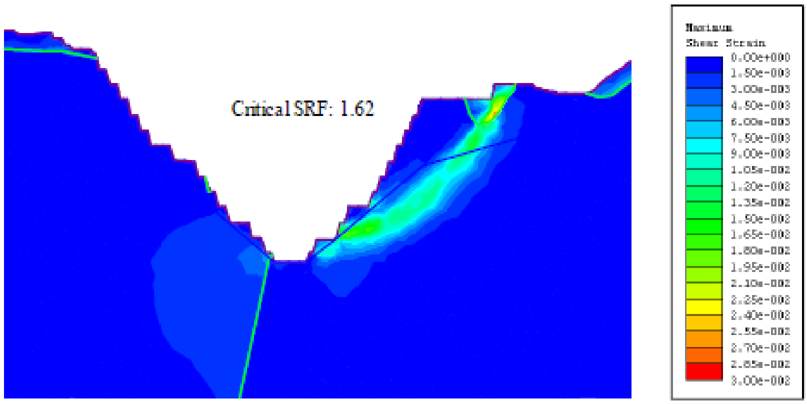

Figure 6.12 Comparison of LEM and FEM analysis of overall slope stability of east wall (SRK, 2009)

6.3 South Slope

The stability assessment of the south slope focuses on the calibration of the strength parameters of the weathered diorite in this area through the analysis of the current slope and the use of these results for the evaluation of the planned slope at stack and overall scales. No major issues were identified in terms of structurally controlled failures at bench scale.

6.3.1 Kinematic Analysis

A kinematic assessment of the south slope was carried out in order to verify the potential for structural controls on the stability of this slope. The main joint set orientations defined for the entire pit area were used for this analysis, as no specific data exists for the diorite unit in the south slope. The result of this analysis is presented in Figure 6.13, which indicates that no major structural controls are anticipated in this slope, other than shallow wedges at bench scale associated to the joint sets J2 and J3. This result is consistent with the observed conditions of the current slope where rock is exposed. However, a larger proportion of hard rock exposure is expected in the deep pit with possible occurrence of local variations in the orientations of the main joint sets which might define occasional wedges and blocks at bench scale.

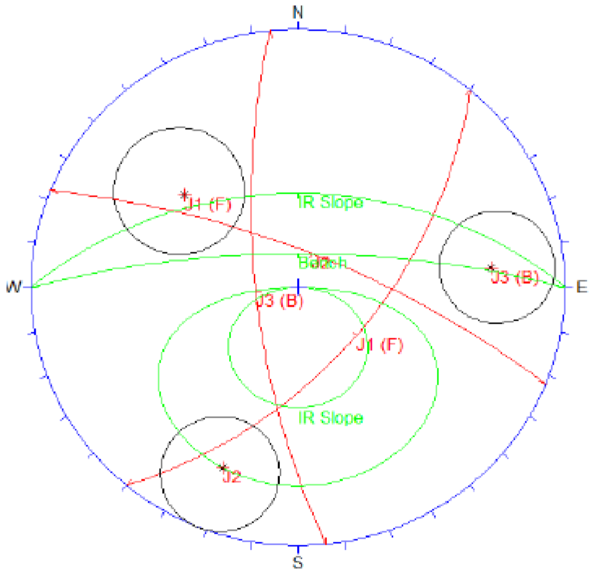

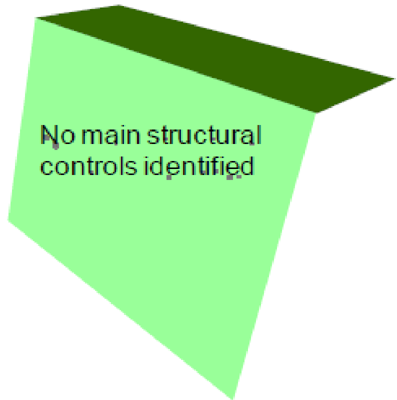

Set	Dip	D Dir	θ (°)
J1 (F)	67	121	20
J2	80	19	18
J3 (B)	47	250	15
Bench	75	0	
IR Slope	50	0	

Note:
θ = variability cone angle

Figure 6.13 Kinematic analysis of south slope (SRK, 2009)

6.3.2 Bench Scale Stability

The current south slope is developed mostly in saprolite and soft rock and the bench configuration corresponds to 10 m high benches mined in 3.3m steps. However, it is anticipated that the expected conditions of the weathered diorite in the planned slope will enable the development of the current bench design configuration consisting of 20m high benches battered at 75^0. The berm width will be 11.4 m which is consistent with the 50^0 recommended stack angle.

Bench scale stability will be determined by the actual local conditions at site, which cannot be defined more precisely with the level of available data, as this area is geotechnically complex due to the concurrence of geological features of difficult definition like the contact zone, diorite intrusions, shear zones and so forth. The verification of the stability condition of the current 20m high bench design using the calibrated strength parameters for the weathered diorite (c= 147 kPa, $\varphi = 40^0$) yield a factor of safety of 1.92 for dry conditions.

6.3.3 Stack Slope Stability

The evaluation of the stability of the stack slope in the south wall considers a rock mass failure mechanism and was based on a sensitivity analysis for stack angles between 40^0 and 60^0 (toe to toe), slope height of 100m (5 benches) and wet and dry conditions. Rock mass strength parameters of the diorite, downgraded to account for the weathering and sheared conditions observed in this area were used for this analysis. The calibration of the strength parameters was based on stability analysis of the current slope as described in the following Section. The results of the sensitivity analysis are shown in Figure 6.14 and they suggest a stack angle of 50^0 with a maximum stack height of 100m as the appropriate design values for this slope.

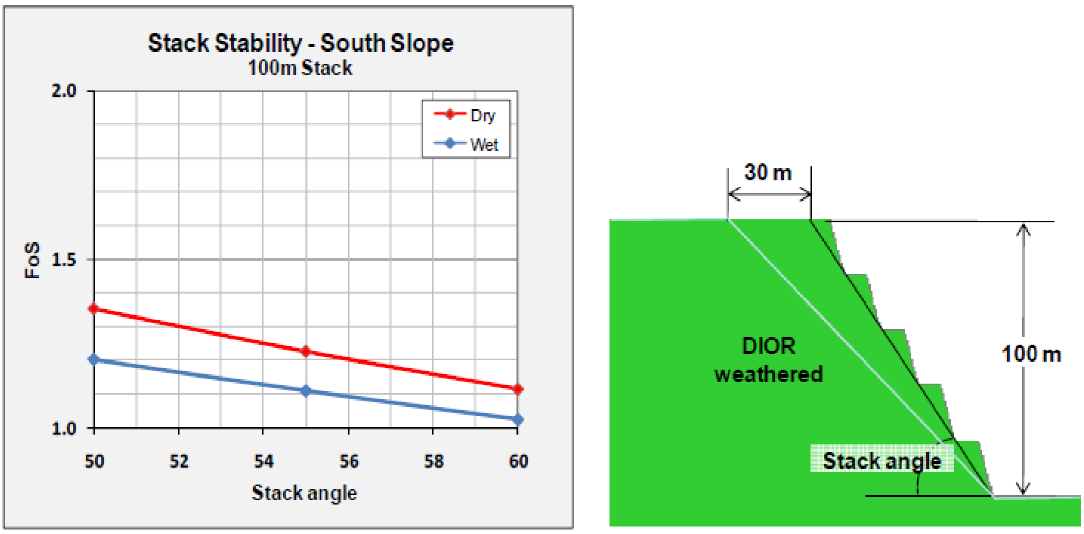

Figure 6.14 Results of analysis of sensitivity of stack stability in south slope (SRK, 2009)

6.3.4 Overall Slope Stability

The overall slope stability was verified with limit equilibrium analysis on the sections S1 and S2 as shown in Figure 5.1. The stability analysis of section S2 on the current slope was intended to calibrate the strength parameters of the weathered diorite, which were then used for the evaluation of the planned slope of the deep pit. In all cases, dry and best estimate wet conditions were considered for the analysis. The results of the stability evaluation of the south slope are summarized in Table 6.7, Figure 6.15 and Figure 6.16.

Table 6.7 Results of stability analysis of south slope (SRK, 2009)

Section	Pit	Slope	Slope Angle (°)	Slope Height (m)	FoS		PoF	
					Dry	Wet	Dry	Wet
S1	Deep	Overall	42	310	1.40	1.22	1%	6%
S1	Deep	Stack1	43	50	0.87	0.87	81%	81%
S1	Deep	Stack2	46	190	1.17	1.13	16%	22%
S1	Deep	Stack3	34	90	3.15	2.70	0%	0%
S2	Current	Overall	34	202	1.42	1.21	2%	9%
S2	Current	Stack1	33	40	1.20	1.20	15%	15%
S2	Current	Stack2	42	110	1.31	1.31	6%	6%
S2	Current	Stack3	34	83	2.31	1.77	0%	0%

The analysis was carried out for the overall slope and for three stacks to cover the various slope angles and geotechnical units along the profile. The critical slip surfaces for the current slope are shown in Figure 6.15. The corresponding FoS values for wet conditions are of 1.21 (a) for the overall slope, 1.20 (b) for the top 40 m in saprolite, 1.31 (c) for the steeper upper half of the slope mostly in weathered diorite and 1.77 (d) for the flatter lower half of the slope in weathered diorite with a shear zone at the toe. The strength parameters initially estimated from the borehole logs and laboratory testing data for the diorite were downgraded to account for the local weathered conditions observed on the slope. Values of c = 147 kPa and $\varphi = 40^0$ resulting from reducing the UCS value by 50% are thought to represent adequately the in situ conditions of the diorite in the south slope according to the stability conditions obtained with these parameters as shown in Figure 6.15.

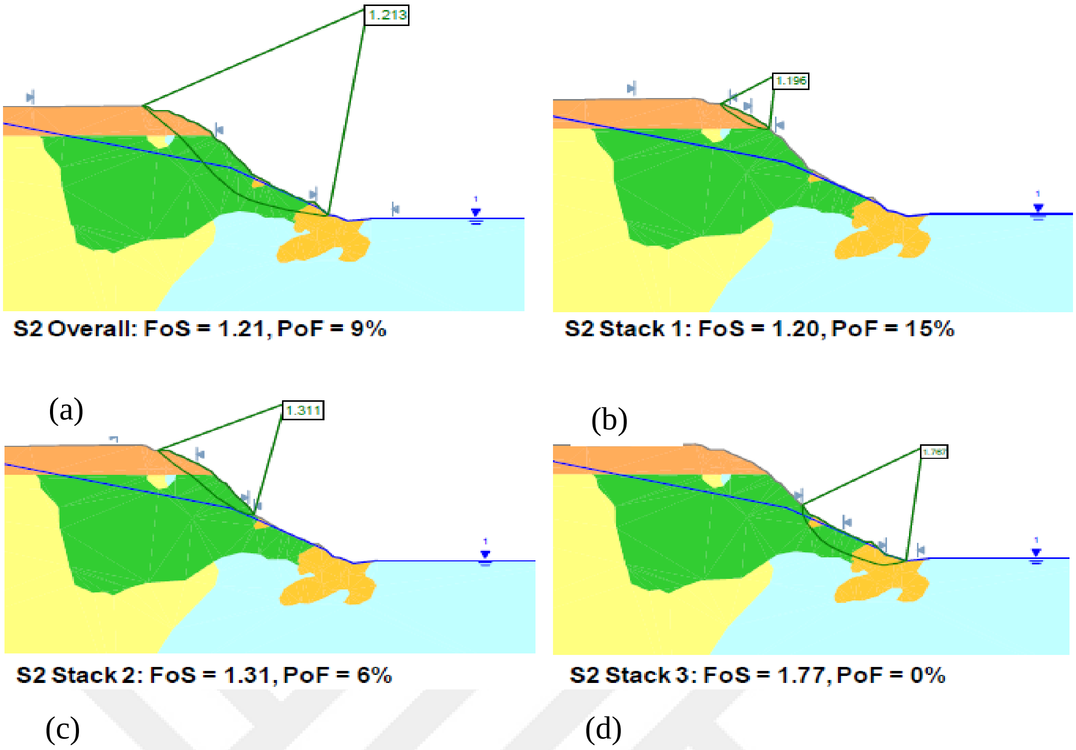

Figure 6.15 Results of stability analysis of current south slope for calibration of strength (SRK, 2009)

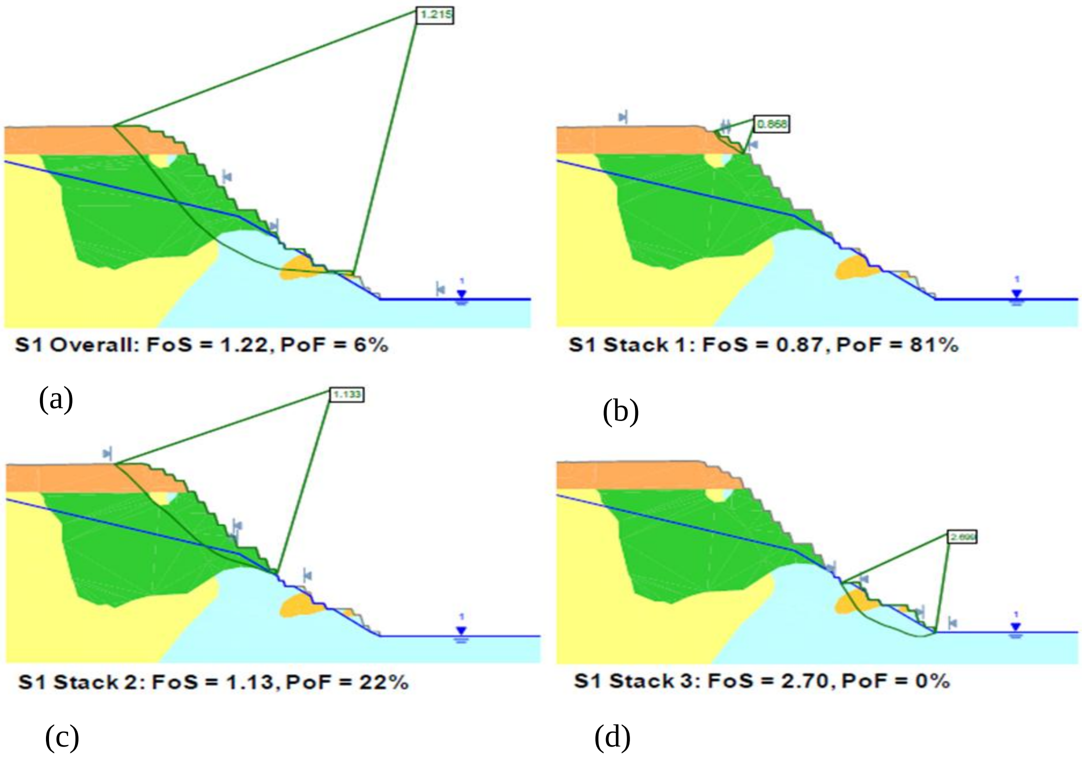

Figure 6.16 Results of stability analysis of south slope of deep pit (SRK, 2009)

The critical slip surfaces defined for the various zones of the slope of the planned pit are indicated in Figure 6.16. For wet conditions they correspond to FoS values of 1.22 (a) for the overall slope, 0.87 (b) for the saprolite at the top of the slope, 1.13 (c) for the steeper upper half of the slope in weathered diorite and 2.7 (d) for the flatter lower half of the slope in marble with shear zones. Although the stability conditions of the overall slope seem adequate, there is a marked imbalance between those conditions in the upper and lower halves of the slope, which suggest the need of adjustments at stack scale to have an acceptable design.

The recommended adjustments in the south slope configuration include:

- First, modify the saprolite slope to conform to the configuration for the saprolite of the west slope, with 10 m high benches and a 35^0 stack angle (toe to toe).
- Second, flatten the stack slope in weathered diorite from the current 55^0 to 50^0, in accordance with the results of the sensitivity analysis for the stack slope.
- Third, steepen the stack slope in the marble and shear zones of the lower third of the slope from the current 46^0 to 50^0, to take advantage of the small stack height in this area and the expected improvement of rock mass conditions with depth.

In spite of the uncertainty in the local geotechnical conditions in this area, in particular at the bottom of the planned pit, it is believed that the recommended adjustments would result in a balanced design with low impact on the overall slope angle of the current design. In general, the current 43^0 overall angle would flatten 3^0 which corresponds to a 35m push back of the slope crest.

CHAPTER SEVEN
SLOPE DESIGN RECOMMENDATIONS

Based on the results of the slope stability evaluation described in Chapter 6, the following specific design recommendations have been derived in terms of bench and stack slope configurations. No specific adjustments in the overall slope angles are required and it is anticipated that these angles will not be affected by the implementation of the recommended adjustments in the stack configurations.

7.1 Bench Configuration

The sensitivity analysis carried out for bench heights between 10m and 20m and bench face angles from vertical to 75^0 battered, indicate that the current design configuration that combines a higher bench with a battered face results in acceptable stability conditions in terms of wedge and planar failure modes. However, in terms of rock fall control the desired configuration is that which provides the wider berms. There are different criteria commonly used to verify the adequacy of the width of berms as catching elements for rock fall control. These criteria relate the minimum berm width required to mitigate rock fall events with the height of the bench (H) and are based on empirical data. In general, the vertical bench configurations exceed the required catch berm criteria for rock fall control, but the battered configurations just meet these criteria for bench heights of 20 m. The graph to the right (a) of Figure 7.1 shows that according to the Modified Richie criterion, vertical benches in general do not constrain the current design stack angles for the west and east slopes regardless of the bench height; however, the angle is constrained for battered benches less than 20m high.

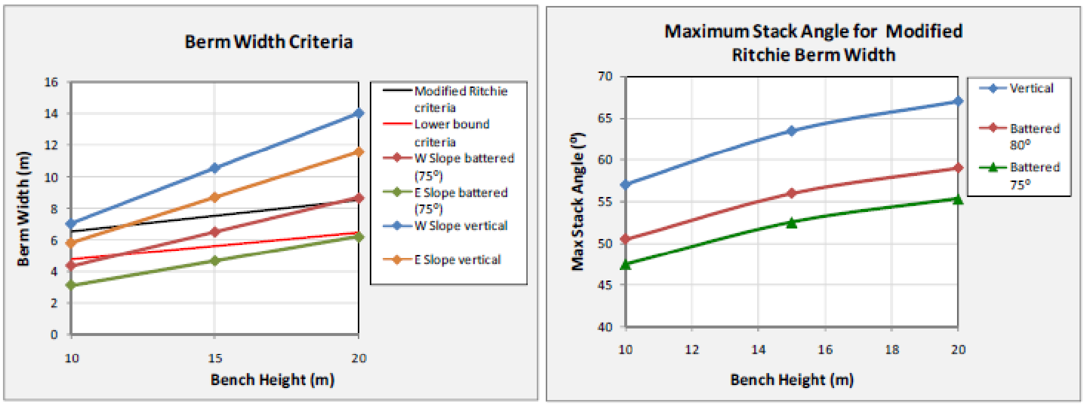

(a) (b)

Figure 7.1 Catch berm criteria for rock fall control (SRK, 2009)

The Modified Richie criterion for berm width is considered a conservative rule in some cases and might be appropriate for the west slope where historic performance of the slope has shown this form of instability to be a relevant factor to consider in the design. The lower bound criterion appears to be sufficient for the east slope where rock mass conditions and observed performance of the slope suggest rock fall events to be a less critical issue.

Based on the various analysis carried out to assess bench stability and performance, it is considered that the current bench configuration for design provides a good balance between the benefits of having higher benches (wider berms for rock fall control) and the benefits of having battered faces (improved stability for structurally controlled failures). Figure 7.2 shows a summary of the recommended bench configurations with their relevant stability controls calculated.

Adequate performance of the berms for rock fall control requires in addition, a good reliability of the design berm width, which means that very good blasting quality is required to ensure that the prescribed berm width will be achieved in a high percentage of the berms length. This is particularly critical in the east wall, where the minimum berm width required for rock fall control has already been taken to the limit.

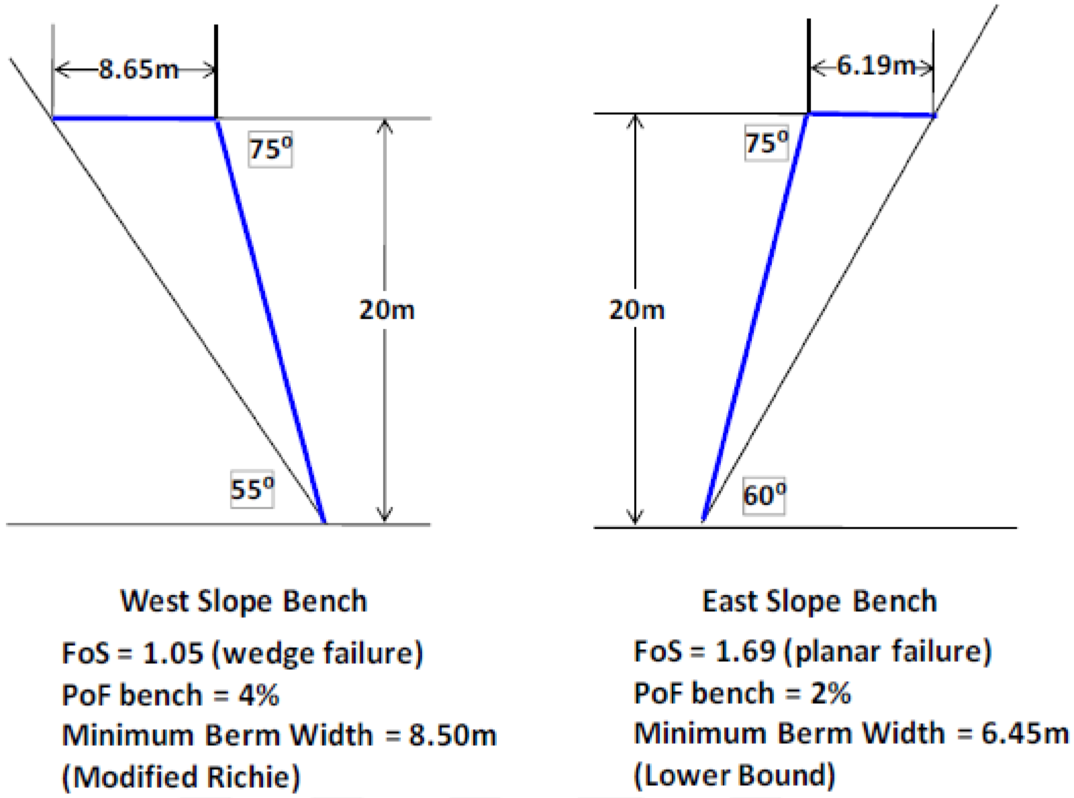

Figure 7.2 Recommended bench configurations and their stability controls (SRK, 2009)

7.2 Stack Slopes in Saprolite and Weathered Rock

Based on the analysis of stability of the saprolite and weathered rock in the west slope, the recommendation in this area is to extend the saprolite slope design from elevation + 100 m down to elevation +80 m into the weathered rock transition. The slope should have 10 m high benches with a 35^0 stack angle (toe to toe). The recommended configuration is also valid for the saprolite slopes in other areas of the pit, and in particular in the south slope, where the current design angle would result in a high risk of instability.

7.3 Stack Slopes in Unweathered Rock

The results of the stability analysis at stack scale in the west slope indicate acceptable stability conditions (PoF < 5%) in terms of wedge failure for stack heigths up to 60 m high (3 benches), but for higher slopes the increased likelihood of failures might be unacceptable for a pit with a single ramp access. In this case the results suggest the need for flattening the slope to 53^0 to achieve acceptable stability conditions for stack heights up to 100m.

A more efficient alternative to maintain the levels of risk within acceptable levels without modifying the slope angle, consists of modifying the current layout of ramps and geotechnical berms so as to have a double ramp system, eliminating the need for the geotechnical berm and without alteration of the overall angle. This recommendation is illustrated conceptually in Figure 7.3 where the (a) current (left) and (b) recommended (right) layouts of ramps and geotechnical berms are sketched.

The benefits of the double ramp system illustrated in the sketch to the right in Figure 7.3 are twofold: first, the double ramp system reduces the impact of potential failures of the stack slopes and consequently the acceptability criterion of PoF values for design might be increased to say 10%; second, the additional ramp would break the continuity of the stack slope in the southern half of the pit in a more convenient way, reducing the proportion of higher slopes as compared with the situation in the current layout.

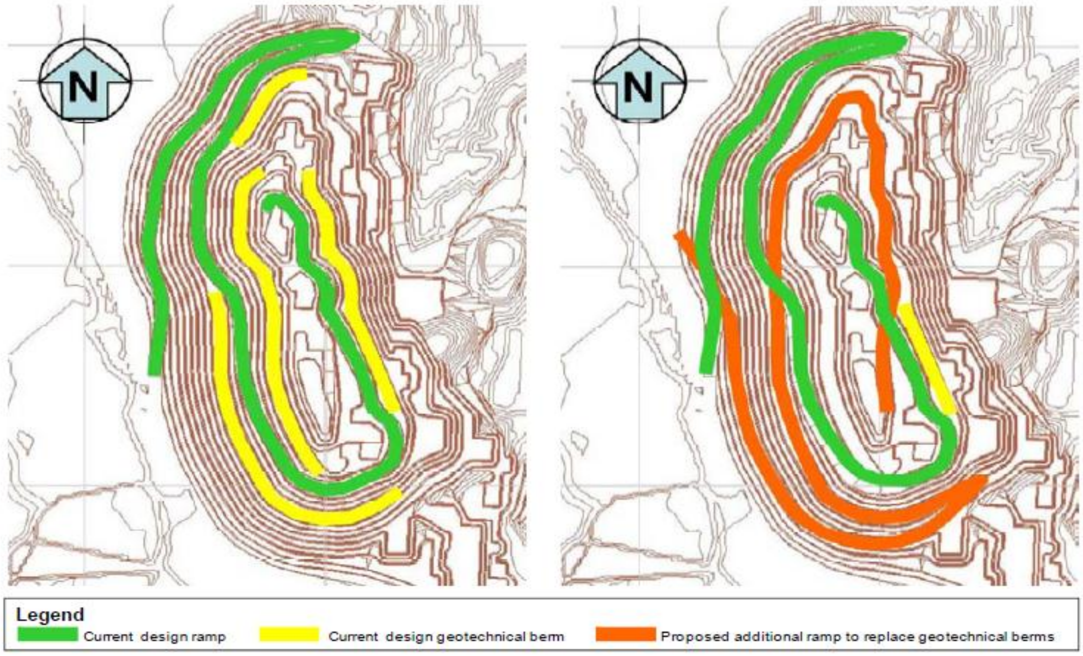

(a) (b)

Figure 7.3 Current (left) and recommended (right) design layouts of ramps and geotechnical berms (SRK, 2009)

In terms of the stack slopes in the south wall, the recommendations derived from the stability evaluation of this slope described in Chapter 6 include the implementation of a 50^0 stack angle (toe to toe) for the entire slope, which means flattening the slope from the current 55^0 above elevation -90 m and steepening the stacks from the current 46^0 below this level. Depending on the ramp configuration adopted for the design, these modifications might result in a 4^0 overall flattening of the slope.

7.4 Overall Slopes

No special modifications to the overall slopes are deemed necessary based on the results of the stability analysis, other than those resulting from the implementation of the recommended adjustments in the stack slopes.

7.5 Summary of Recommended Slope Configurations

Figure 7.4 shows a plan of the deep pit with the recommended stack slope angles (toe to toe) and the extent of the slope domains where these recommendations apply. The boundary of the slope domains is approximate and has been delineated on the basis of the trend orientation of the slopes and the character of the geotechnical units exposed in these areas.

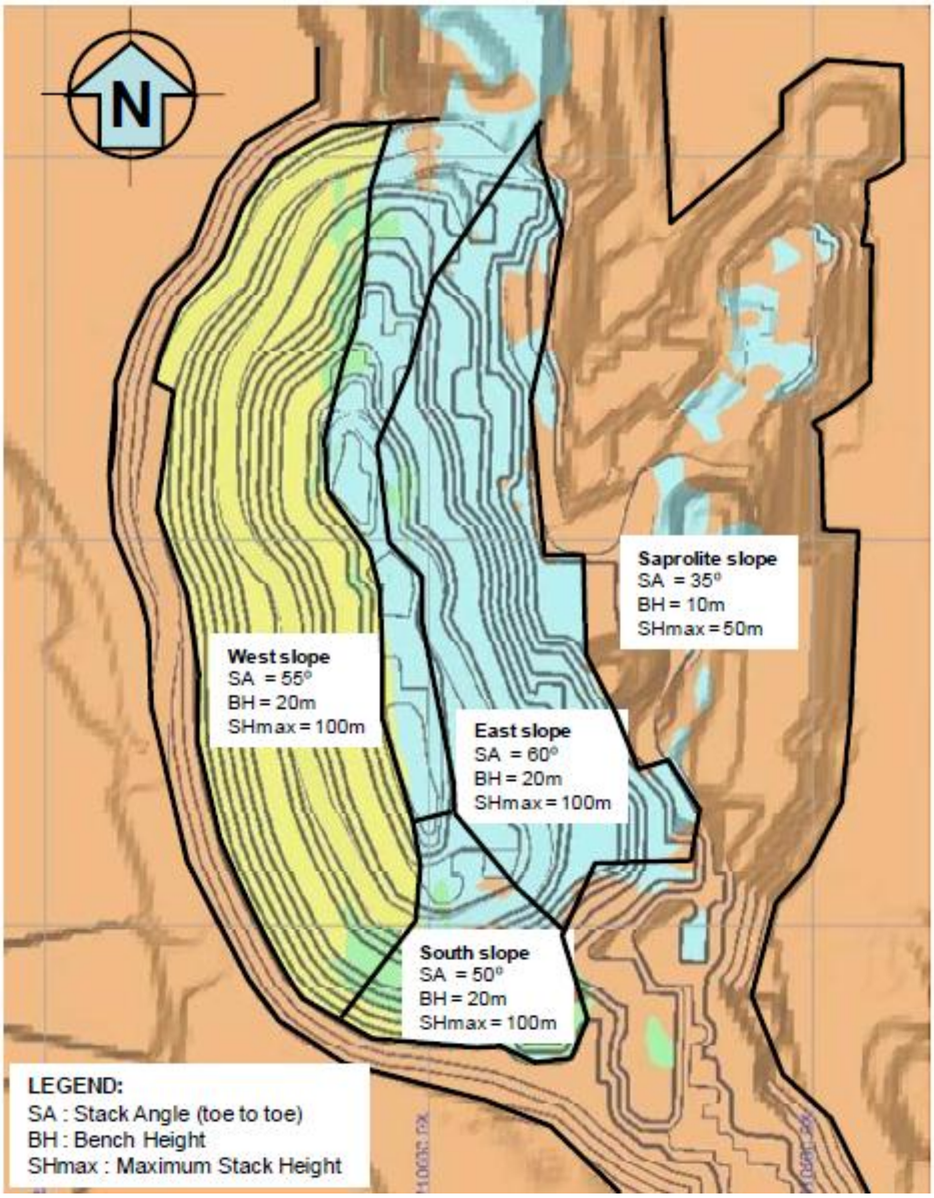

Figure 7.4 Plan showing recommended pit slope angles (SRK, 2009)

Typical slope profiles with details of the recommended bench and stack slope configurations are shown in Figure 7.5, Figure 7.6 and Figure 7.7, for the west, east and south slopes, respectively. They also include details of the slopes in saprolite at the top of the walls. The location of the ramps in these profiles is arbitrary, although the number of ramps is consistent with the recommended pit layout to reflect the characteristic overall slope angles of the sections.

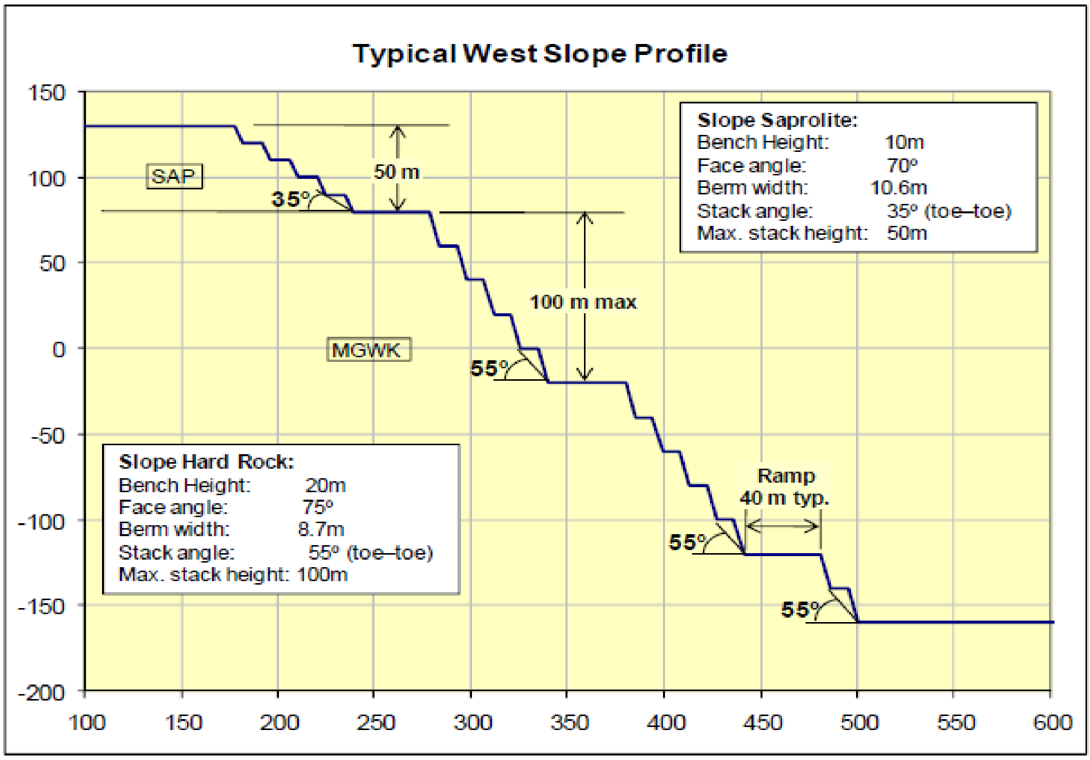

Figure 7.5 Typical west slope profile with recommended slope angles (SRK, 2009)

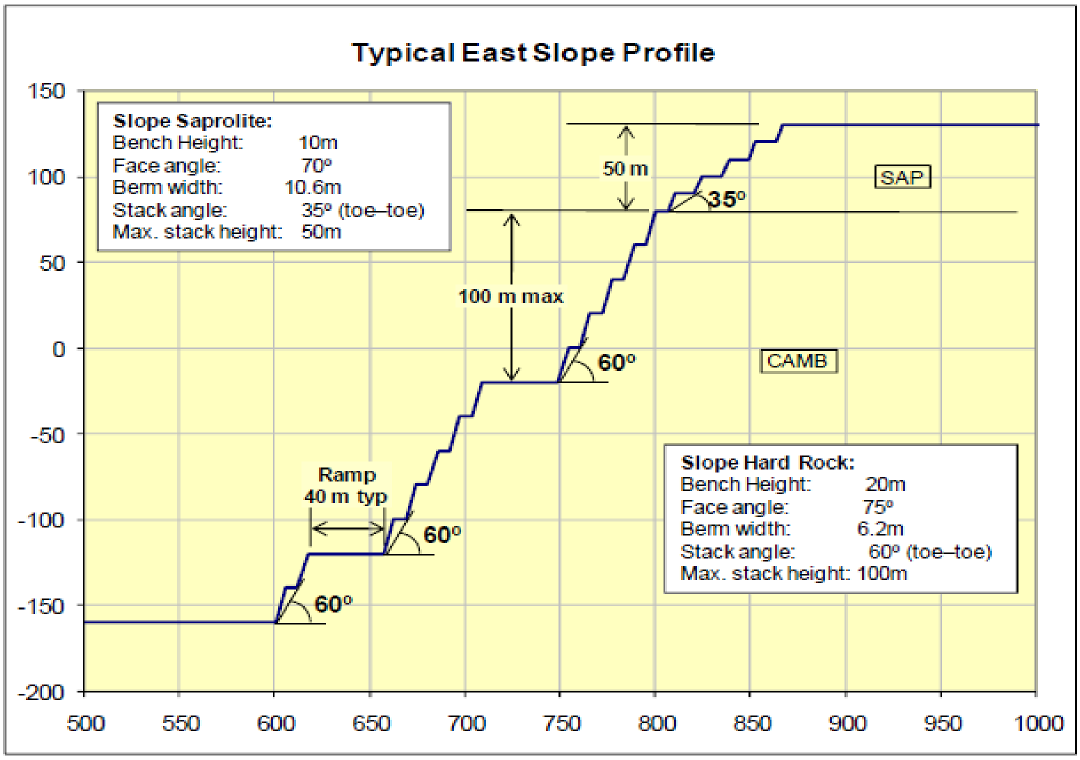

Figure 7.6 Typical east slope profile with recommended slope angles (SRK, 2009)

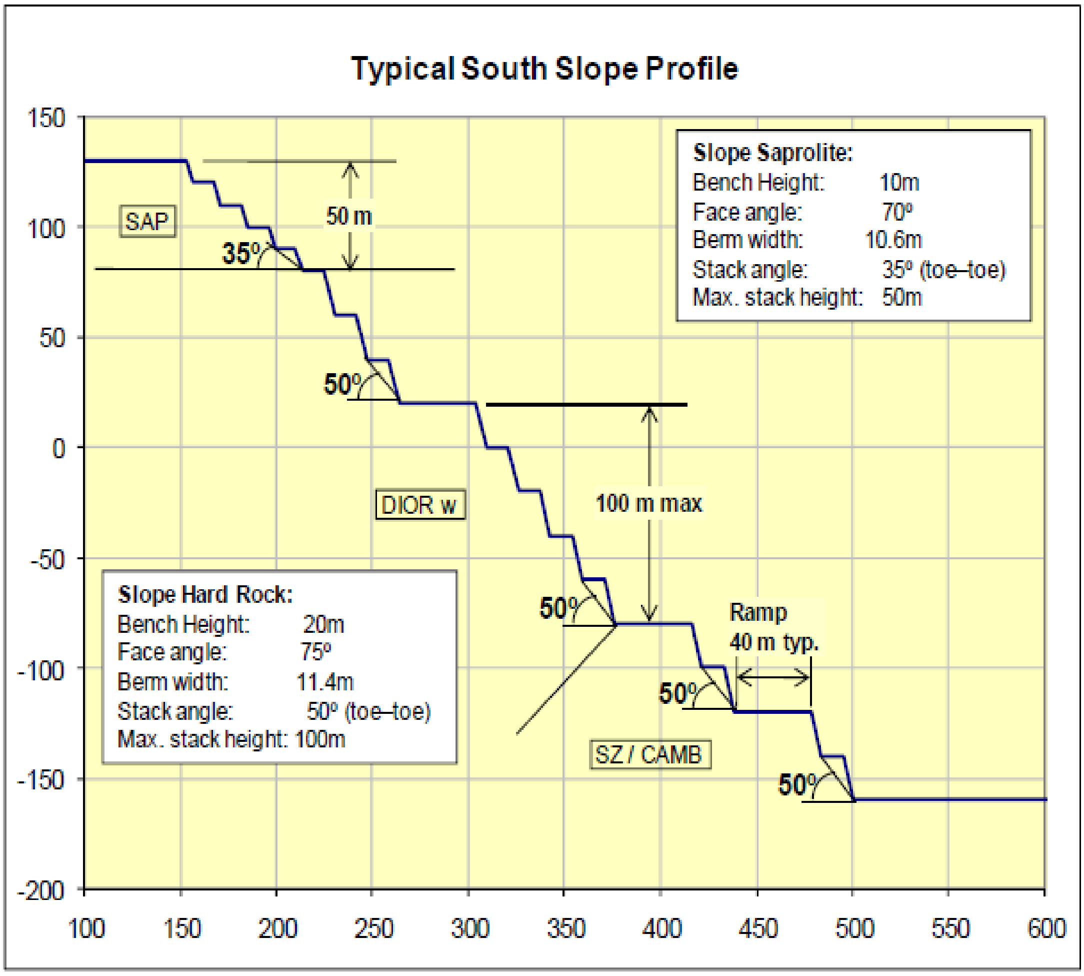

Figure 7.7 Typical south slope profile with recommended slope angles (SRK, 2009)

CHAPTER EIGHT

CALCULATION OF THE SLOPE STABILITY OF SADIOLA OPEN PIT GOLD MINE (FARABAKOUTA EAST) IN MALI

8.1 Methods of Study

The calculation of the slope stability involves determination of the safety factor of the benches. For that, it is first necessary to determine the physico-mechanical properties of the rocks in the laboratory, then in the rock mass. Once the physico-mechanical properties and the geometrical outline in open pit have been determined, the safety factor is calculated (Bishop and Fellenius method).

8.2 Determination of the Mechanical Properties of Rocks

8.2.1 Compressive Strength

The compressive strength is defined by the following relationship:

$$R_c = \frac{F_{max}}{S} \tag{8.1}$$

Where, R_c compressive strength (kgf/cm^2), F_{max} the breaking load (kgf), S area to which the load is applied (cm^2).

The compressive test was carried out at the Sadiola Open Pit Gold Mine Laboratory on two test pieces of marble rock taken from each bench (bench 3 and bench 6) of Farabakouta East Pit. The results obtained are given in Table 8.1.

Table 8.1 Compressive strength of marble samples (Sadiola Open Pit Gold Mine Laboratory)

Bench N°	**Lithology**	**Sample N°**	**Resistance R_c (Kgf/cm^2)**
B-3	Marble	M-1	1256.7
	Marble	M-2	1259.3
	M. Mean	—	**1258**
B-6	Marble	M-1	1071.4
	Marble	M-2	1068.6
	M. Mean	—	**1070**

According to Table 8.1, the compressive strength of marble is very strong (Brown 1981).

8.2.2 Tensile Strength

The tensile strength is defined by the following relationship:

$$R_t = \frac{T_{max}}{S} \qquad (8.2)$$

Where, R_t tensile strength (kgf/cm^2), T_{max} the maximum tensile force (kgf), S surface of the test piece on which the tensile force is applied (cm^2).

The tensile strength values from Sadiola Open Pit Gold Mine Laboratory are given in Table 8.2.

Table 8.2 Tensile strength of marble samples (Sadiola Open Pit Gold Mine Laboratory)

Bench N°	**Lithology**	**Sample N°**	**Resistance R_t (Kgf/cm^2)**
B-3	Marble	M-1	125.67
	Marble	M-2	125.93
	M. Mean	__	**125.8**
B-6	Marble	M-1	107.14
	Marble	M-2	106.86
	M. Mean	__	**107**

8.2.3 Cohesion and Internal Friction Angle of a Sample

To determine the cohesion and the internal friction angle of the samples, Benyounes (1989). We used the following two relations:

$$C_{sam} = \frac{R_c.R_t}{2.\sqrt{R_c.R_t - 3R_t^2}} \quad (8.3)$$

$$\Phi_{sam} = \arcsin\left(\frac{R_c - 4.R_t}{R_c - 2.R_t}\right) \quad (8.4)$$

Where, C_{sam} cohesion of a sample (kgf/cm^2), Φ_{sam} friction angle of a sample (°), R_c compressive strength (kgf/cm^2) and R_t tensile strength (kgf/cm^2).

The values obtained for (C_{sam}) and (Φ_{sam}) are given in Table 8.3.

Table 8.3 Estimated (C_{sam}) and (Φ_{sam}) values for marble

Sample N°	**(M-1, M-2) (bench 3)**	**(M-1, M-2) (bench 6)**
C_{sam} (Kgf/cm^2)	237.7	202.2
Φ_{sam} (°)	48.59	48.59

8.2.4 Discontinuity Spacing

The discontinuities such as fractures and joints in rock mass affect their mechanical properties and their slope stability. They are the most important factors that characterize rocks and soils. They allow to choose the method of exploitation, to solve the problem of the stability of the edges of the quarry, the bench.

Discontinuity spacing is equal to the average distance between the cracks:

$$n = \frac{L}{N} \tag{8.5}$$

Where, L length of the studied part of the rock mass (m), N number of cracks on the measured part.

Table 8.4 gives the classification of the discontinuities according to the values of n (Bieniawski, 1989).

Table 8.4 Classification of discontinuities according to discontinuity spacing (Bieniawski, 1989)

Class	**Average interval between discontinuities n (cm)**	**Density of discontinuities**
n 1	> 200	Very weak
n 2	60 to 200	Weak
n 3	20 to 60	Average
n 4	6 to 20	Strong
n 5	< 6	Very strong

We made measurements of the cracking on the benches 3 and 6. We used a square frame of 1 m of sides (figure 8.1). The average number of cracks over the length of 1 m is around 7, giving a n value of 0.14 m (14 cm). According to Table 8.4. It can be said that the density of discontinuities in the Farabakouta east (FE) pit is strong.

Figure 8.1 Photo showing the use of a square frame of 1 m of sides to measure the number of cracks on the benches (Personal archive, 2017)

8.3 Determination of the Mechanical Characteristics of the Rock Mass

Let C_m and Φ_m be the cohesion and internal friction angle of the rocks in the rock mass.

To determine the mechanical properties C_m and Φ_m of the rock mass, several corrective parameters must be taken into account, which are mainly:

- The structural weakening coefficient of the rock mass λ.
- The coefficient of decrease of the value of the internal friction angle λ_Φ.

The values of C_m and Φ_m are determined by the following formulas, Benyounes (1989):

$$C_m = \lambda . C_{sam} \tag{8.6}$$

$$\Phi_m = \lambda_\Phi . \Phi_{sam} \tag{8.7}$$

Where, C_m cohesion of a rock mass (kg/cm^2), Φ_m internal friction angle of a rock mass (°), C_{sam} cohesion of a sample (kgf/cm^2), Φ_{sam} friction angle of a sample (°), λ and λ_Φ corrective coefficients (without units).

8.3.1 Coefficient of Structural Weakening of the Rock Mass

The coefficient of structural weakening of the rock mass (λ) is calculated using the formula:

$$\lambda = \frac{1}{1+a.ln\frac{H}{h}} \tag{8.8}$$

Where, a coefficient depending on the resistance of the rocks and the properties of discontinuities, H the average height of the bench (m), h the average spacing between the discontinuities (m).

The values of coefficient "a" as a function of uniaxial compressive strength are given in Table 8.5.

Table 8.5 Coefficient "a" as a function of uniaxial compressive strength R_c

a	0	0.5	2	3	4	7	10
R_c (Kg/cm^2)	0-1.5	1.5-9	10-49	50-99	100-199	200-300	> 300

The values of the structural weakening coefficient found for the two benches are given in Table 8.6, taking into account the following parameters:

- a = 10 ($R_c > 300$ kg/cm^2)
- H = 15 m (height of benches 3 and 6)
- h = 0.14 m

Table 8.6 Structural weakening coefficient values for both benches (3 and 6)

Bench	3	6
λ	0.021	0.021

8.3.2 The Coefficient of Decrease of the Value of the Internal Friction Angle

The value of the decrease coefficient of the internal friction angle is taken equal to 0.8 ($\lambda_\Phi = 0.8$).

8.3.3 Determination of the Cohesion of the Rock Mass

The cohesion of the rock formation in the massif is given by the following relation:

$$C_m = \lambda . C_{sam} \tag{8.9}$$

Where, C_m cohesion of a rock mass (kgf/cm^2), C_{sam} cohesion of a sample (kgf/cm^2), λ structural coefficient of weakening.

The values of the cohesion of the rock mass calculated are given in Table 8.7.

8.3.4 Determination of the Internal Friction Angle of the Rock Mass

The internal friction angle of the rock mass is given by the relation:

$$\Phi_m = \lambda_{\Phi} . \Phi_{sam} \tag{8.10}$$

Where, Φ_m internal friction angle of a rock mass (°), Φ_{sam} internal friction angle of a sample (°), λ_{Φ} decrease coefficient of the internal friction angle (0.8).

The values of the internal friction angle of the rock mass calculated are given in Table 8.7.

Table 8.7 Cohesion Cm and internal friction angle Φm of the rock mass in benches 3 and 6

Rock Massifs	**Bench 3**	**Bench 6**
C_m (kgf/cm^2)	4.99	4.24
Φ_m (°)	38.87	38.87

8.4 Calculation of Slope Stability of Farabakouta East (FE) Pit

8.4.1 Calculation Method

For the calculation of the safety factor, we used the methods of (Fellenius, 1936) (8.11) and (simplified Bishop, 1954) (8.12). The factor of safety (Fs) is given by the following formulas:

$$F_s = \frac{\sum_{n=1}^{m}\left(C_m \frac{b_n}{cos\alpha_n} + W_n.cos\alpha_n.tan\Phi_m\right)}{\sum_{n=1}^{m} W_n.sin\alpha_n} \tag{8.11}$$

$$F_s = \frac{\sum_{n=1}^{m}(C_m.b_n + W_n.tan\Phi_m)}{m_\alpha.\sum_{n=1}^{m} W_n.sin\alpha_n} \tag{8.12}$$

$$m_\alpha = cos\alpha_n\left(1 + \frac{tan\alpha_n.tan\Phi_m}{F_s}\right) \tag{8.13}$$

Where, in these formulas, C_m cohesion of the rock mass, b_n width of the slice, W_n weight of the slice, Φ_m internal friction angle of rock mass, α_n inclination of the slice.

8.4.2 Calculation of the Safety Coefficient

The calculation of the slope stability was carried out on the two benches 3 and 6. For the calculation of the safety factor using the two methods; Fellenius and simplified Bishop, by the physico-mechanical datas of the rock mass are required.

γ = 25 kN/m^3
C_m = 499 kN/m^2 for bench 3 and 424 kN/m^2 for bench 6
Φ_m = 38.87°
H = 15 m
α = 85°

We also determined the failure circle centers by producing grid (Figure 8.2). The gridline parameters are grouped in Table 8.8.

Table 8.8 Gridline parameters for calculating factor of safety (Fs)

X_0	**Y_0**	**Number of lines**	**ΔY (m)**	**Number of columns**	**ΔX (m)**
-3	1	5	3	5	5

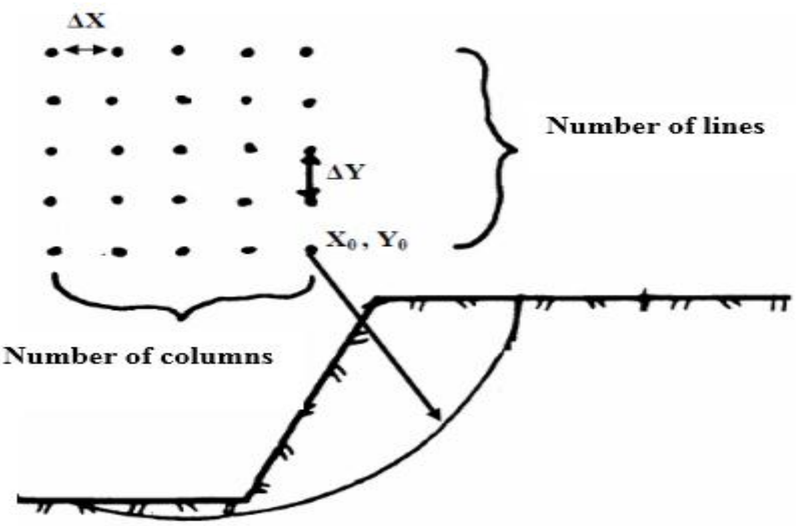

Figure 8.2 Gridline elements for determining the sliding circle for benches 3 and 6

The safety factor (Fs) was calculated by using an application on EXCELL which makes it possible to determine Fs using the methods of BISHOP and FELLENIUS. It is sufficient to introduce the physico-mechanical parameters of the rock mass and the coordinates X, Y and the radius of the circle R as well as the geometric parameters of the bench: height of the bench and angle of slope. An example of a spreadsheet is shown in Figure 8.3. The calculation results for the two benches are given in Tables 8.9 and 8.10.

Failure Surface		**Slope**		
			x	y
X center	-13		-12,5	-10,0
Y center	7	Bottom	-10,0	-10,0
Radius	17,5	Top	0,0	0,0
			2,5	0,0
nslices	15			
X left	3,5			
X right	-10,0	Rise	10	
b (slice width)	-0,90	Run	10	

Soil Properties	
gamma	25
c'	499
phi	38,8
ru	0

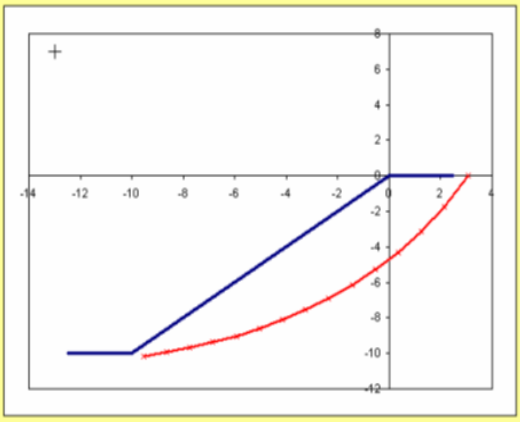

Slice #	X center	Y center	Y surface	alpha(rad)	alpha(deg)	h	hSinα	Secα	W	WSinα	Tanα	Sum 1	c' * l	(Wcosa - ul) * tanf
1	3,05	0,03	0,00	1,16	66,51	-0,03	-0,02	2,51	0,57	0,52	2,30	-461,03	-1126,81	0,18
2	2,15	-1,76	0,00	1,05	59,96	1,76	1,52	2,00	-39,59	-34,27	1,73	-461,15	-897,23	-15,93
3	1,25	-3,16	0,00	0,95	54,52	3,16	2,57	1,72	-71,06	-57,86	1,40	-464,18	-773,69	-33,16
4	0,35	-4,31	0,00	0,87	49,72	4,31	3,29	1,55	-97,09	-74,06	1,18	-468,80	-694,59	-50,47
5	-0,55	-5,30	-0,55	0,79	45,35	4,75	3,38	1,42	-106,84	-76,01	1,01	-465,84	-639,05	-60,37
6	-1,45	-6,15	-1,45	0,72	41,30	4,70	3,10	1,33	-105,69	-69,75	0,88	-458,53	-597,79	-63,84
7	-2,35	-6,89	-2,35	0,65	37,49	4,54	2,76	1,26	-102,07	-62,11	0,77	-452,15	-565,97	-65,12
8	-3,25	-7,53	-3,25	0,59	33,86	4,28	2,39	1,20	-96,35	-53,68	0,67	-446,45	-540,81	-64,33
9	-4,15	-8,10	-4,15	0,53	30,38	3,95	2,00	1,16	-88,81	-44,91	0,59	-441,29	-520,57	-61,60
10	-5,05	-8,59	-5,05	0,47	27,02	3,54	1,61	1,12	-79,65	-36,18	0,51	-436,55	-504,12	-57,05
11	-5,95	-9,02	-5,95	0,41	23,76	3,07	1,24	1,09	-69,01	-27,80	0,44	-432,14	-490,68	-50,78
12	-6,85	-9,38	-6,85	0,36	20,57	2,53	0,89	1,07	-57,01	-20,03	0,38	-428,01	-479,70	-42,91
13	-7,75	-9,69	-7,75	0,30	17,46	1,94	0,58	1,05	-43,74	-13,12	0,31	-424,10	-470,78	-33,55
14	-8,65	-9,95	-8,65	0,25	14,39	1,30	0,32	1,03	-29,27	-7,27	0,26	-420,36	-463,65	-22,79
15	-9,55	-10,16	-9,55	0,20	11,37	0,61	0,12	1,02	-13,65	-2,69	0,20	-416,78	-458,09	-10,76
										-579,25		-6677,37	-9223,56	-632,48

Bishop's Method

Enter F	1,21
Computed F	11,53

Increase F

Fellenius Method

F 17,02

Figure 8.3 Example of a sheet of the EXCELL application that we used for the calculation of the factor of safety

The extreme values of the safety factor obtained for the two benches are follows:

Bench n° 3

3.90 <Fs <6.85 Bishop

6.62 <Fs <12.72 Fellenius

Bench n° 6

3.46 <Fs <6.11 Bishop

5.76 <Fs <10.86 Fellenius

From the results obtained, it can be seen that the safety coefficient is relatively high for the two benches. The benches of the quarry are therefore very stable.

Table 8.9 Fs value for bench 3

X (m)	Y(m)	Fs BISHOP	Fs FELL		X (m)	Y(m)	Fs BISHOP	Fs FELL
- 3	1	5.23	10.86		- 3	10	6.18	8.30
- 8	1	4.33	9.70		- 8	10	5.06	7.20
- 13	1	3.90	10		- 13	10	4.44	6.72
- 18	1	4	11.14		- 18	10	4.28	6.9
- 23	1	4.07	12.72		- 23	10	4.18	7.17
- 3	4	5.54	8.21		- 3	13	6.55	8.63
- 8	4	4.55	7.32		- 8	13	5.36	7.43
- 13	4	4.20	7.41		- 13	13	4.86	7.09
- 18	4	4.14	8.04		- 18	13	4.32	6.62
- 23	4	3.98	8.31		- 23	13	4.40	7.17
- 3	7	5.89	8.24		- 3	16	6.85	8.87
- 8	7	4.81	7.17		- 8	16	5.63	7.64
- 13	7	4.34	7		- 13	16	5.04	7.15
- 18	7	4.02	6.90		- 18	16	4.59	6.78
- 23	7	4.04	7.48		- 23	16	4.29	6.64

Table 8.10 Fs value for bench 6

X (m)	Y(m)	Fs BISHOP	Fs FELL		X (m)	Y(m)	Fs BISHOP	Fs FELL
- 3	1	4.66	9.43		- 3	10	5.51	7.31
- 8	1	3.84	8.38		- 8	10	4.50	6.31
- 13	1	3.46	8.60		- 13	10	3.94	5.86
- 18	1	3.53	9.54		- 18	10	3.79	5.98
- 23	1	3.60	10.86		- 23	10	3.7	6.19
- 3	4	4.93	7.20		- 3	13	5.83	7.61
- 8	4	4.04	6.38		- 8	13	4.77	6.52
- 13	4	3.72	6.41		- 13	13	4.30	6.19
- 18	4	3.65	6.91		- 18	13	3.83	5.76
- 23	4	3.52	7.13		- 23	13	3.89	6.20
- 3	7	5.25	7.24		- 3	16	6.11	7.82
- 8	7	4.27	6.27		- 8	16	5.01	6.71
- 13	7	3.84	6.08		- 13	16	4.47	6.25
- 18	7	3.56	5.97		- 18	16	4.06	5.90
- 23	7	3.57	6.44		- 23	16	3.80	5.76

8.4.3 Influence of the Bench Height (H) on the Safety Coefficient (Fs)

For the study of the influence of the bench height on the safety coefficient (Fs), we have fixed all the other parameters, and varied only the bench height from 5 m to 30 m, by step of 5 m. The results of the calculation of the coefficient (Fs) as a function of the bench height (H) are given in Tables 8.11 to 8.15.

Table 8.11 Variation of Fs as a function of the bench height H for α = 45°

Bench	Bench height (m)	R (m)	Fs BISHOP	Fs FELLENIUS
3	5	15.5	28.42	47.75
	10	17.5	11.52	17.02
	15	22	7.68	10.55
	20	27	6.33	8.40
	25	32	5.97	7.63
	30	38	5.01	6.58
6	5	15.5	24.30	40.69
	10	17.5	9.97	14.62
	15	22	6.75	9.17
	20	27	5.64	7.39
	25	32	5.37	6.77
	30	38	4.53	5.85

Table 8.12 Variation of Fs as a function of the bench height H for α = 55°

Bench	Bench height (m)	R (m)	Fs BISHOP	Fs FELLENIUS
3	5	15.5	25.51	44.66
	10	18	10.18	15.94
	15	22	6.67	9.75
	20	27	5.37	7.54
	25	32	4.87	6.71
	30	38	4.47	6.01
6	5	15.5	21.82	38.05
	10	18	8.81	13.68
	15	22	5.85	8.46
	20	27	4.78	6.67
	25	32	4.38	5.93
	30	38	4.06	5.36

Table 8.13 Variation of Fs as a function of the bench height H for α = 65°

Bench	**Bench height (m)**	**R (m)**	**Fs BISHOP**	**Fs FELLENIUS**
3	5	16	20.20	36.36
	10	19	8.03	13.10
	15	23	5.58	8.81
	20	27	4.70	6.85
	25	32	4.12	5.85
	30	37	3.82	5.35
6	5	16	17.30	30.99
	10	19	7.03	11.26
	15	23	4.91	7.39
	20	27	4.18	6
	25	32	3.71	5.17
	30	37	3.47	4.75

Table 8.14 Variation of Fs as a function of the bench height H for α = 75°

Bench	**Bench height (m)**	**R (m)**	**Fs BISHOP**	**Fs FELLENIUS**
3	5	16.8	13.18	24.08
	10	20	6.63	10.99
	15	24	4.79	7.48
	20	28	4.05	6.08
	25	33	3.56	5.22
	30	38	3.28	4.69
6	5	16.8	11.34	20.55
	10	20	5.79	9.45
	15	24	4.23	6.49
	20	28	3.62	5.32
	25	33	3.22	4.61
	30	38	2.99	4.17

Table 8.15 Variation of Fs as a function of the bench height H for α = 85°

Bench	**Bench height (m)**	**R (m)**	**Fs BISHOP**	**Fs FELLENIUS**
3	5	17.5	9.99	18.34
	10	21	5.66	9.63
	15	25	4.21	6.73
	20	29	3.56	5.44
	25	34	3.16	4.72
	30	39	2.88	4.24
6	5	17.5	8.62	15.67
	10	21	4.96	8.30
	15	25	3.73	5.85
	20	29	3.19	4.77
	25	34	2.86	4.17
	30	39	2.63	3.77

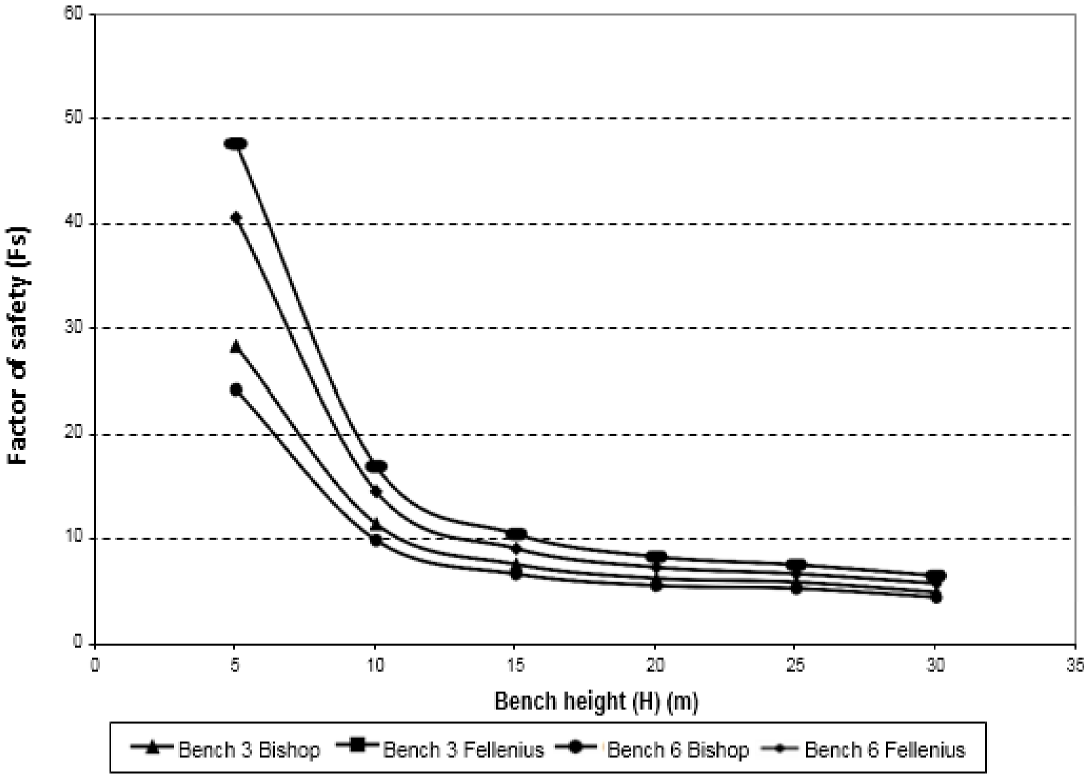

Figure 8.4 Variation of the factor of safety (Fs) as a function of H for α = 45°

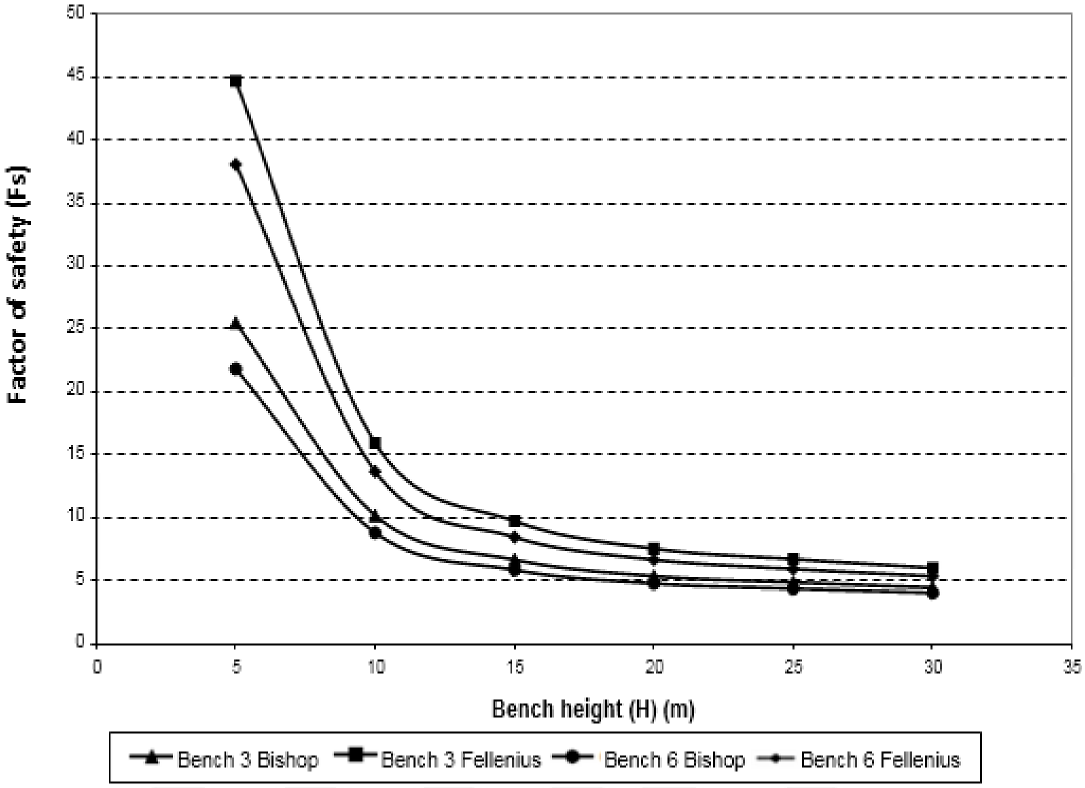

Figure 8.5 Variation of the factor of safety (Fs) as a function of H for α = 55°

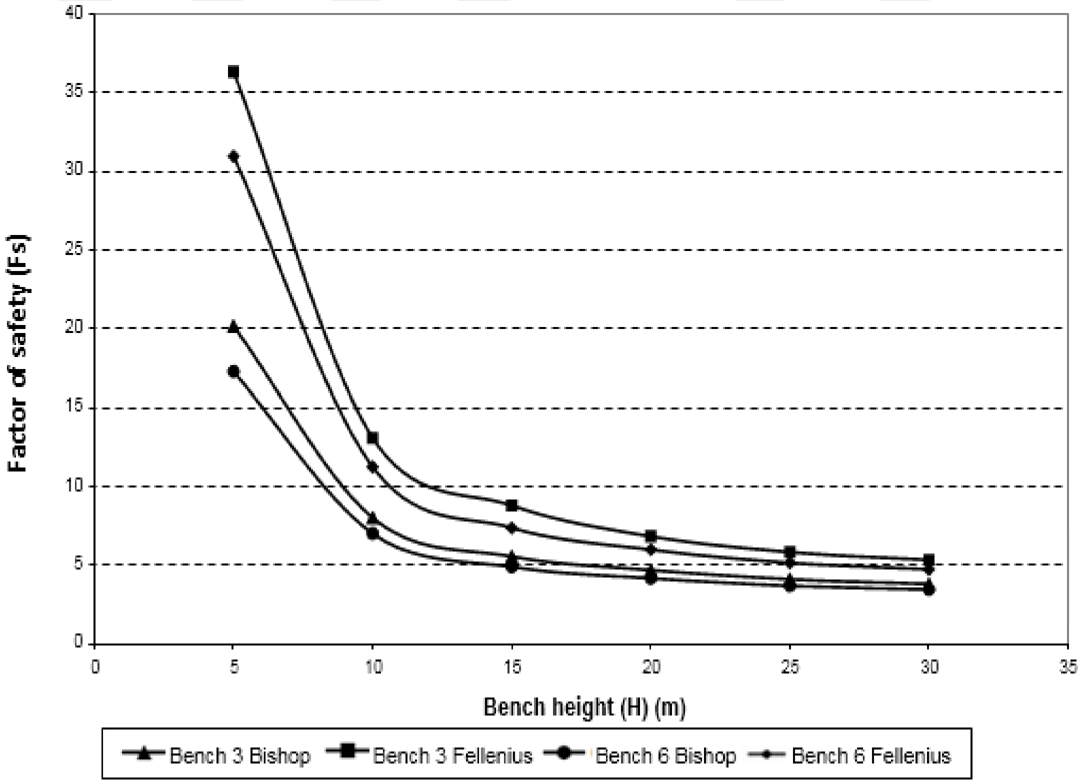

Figure 8.6 Variation of the factor of safety (Fs) as a function of H for α = 65°

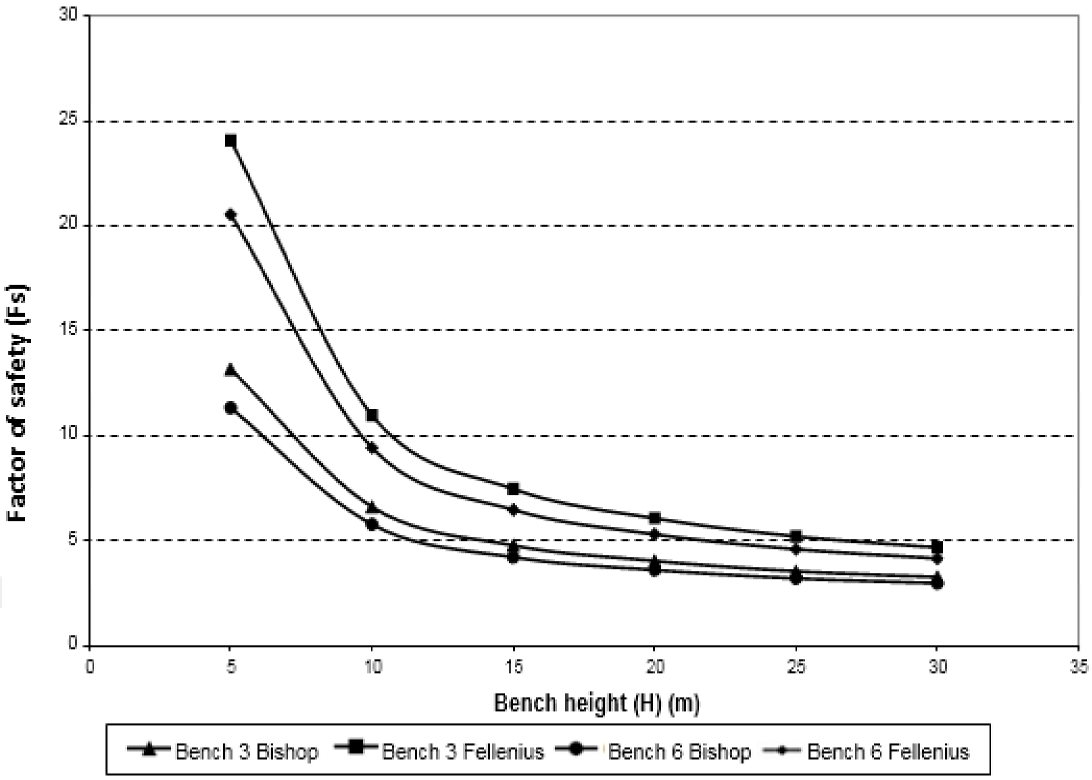

Figure 8.7 Variation of the factor of safety (Fs) as a function of H for α = 75°

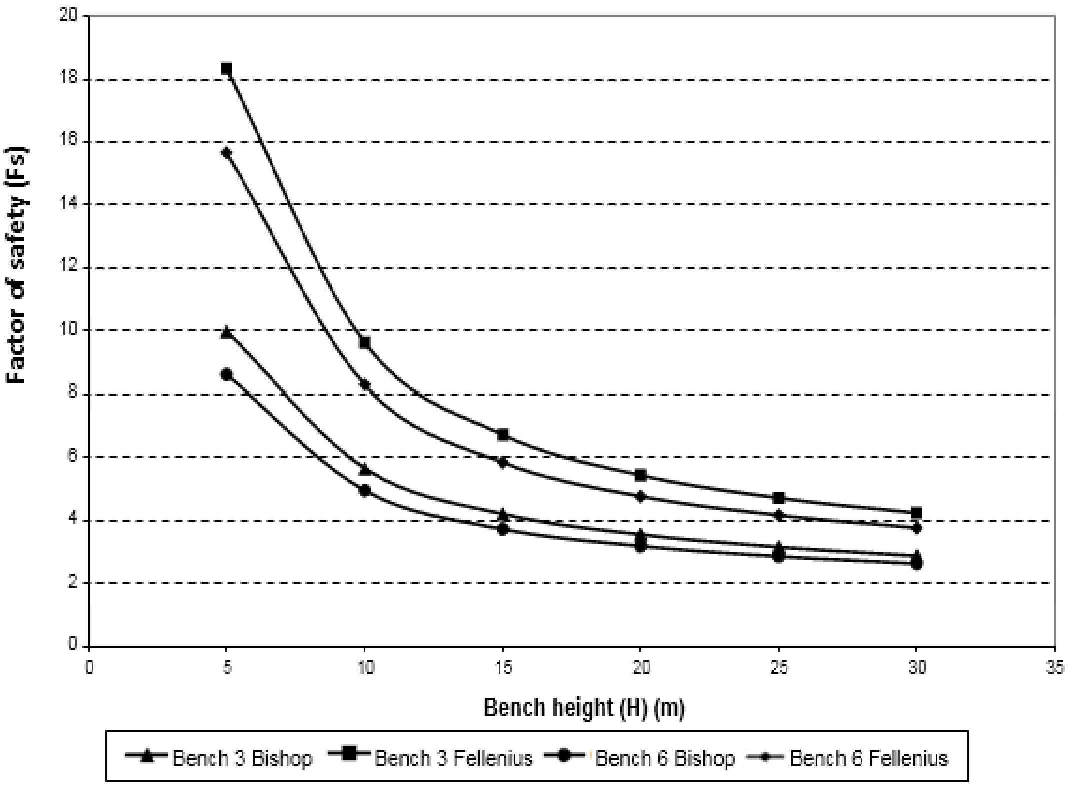

Figure 8.8 Variation of the factor of safety (Fs) as a function of H for α = 85°

8.4.4 Influence of the Slope Angle on the Safety Coefficient (Fs)

In this case, the slope angle (α) is varied from 45° to 85° with a step of 10°, the other parameters remaining invariant. The results obtained for the safety coefficient are given in Tables 8.16 to 8.21.

Table 8.16 Variation of Fs as a function of the slope angle α for H = 5 m

Bench	**Slope angle (α)**	**R (m)**	**Fs BISHOP**	**Fs FELLENIUS**
3	45	15	27.67	46.17
	55	15.5	24.79	43.08
	65	16	20.20	36.36
	75	16.8	13.18	24.08
	85	17.5	10.30	19.10
6	45	15	23.67	39.35
	55	15.5	21.20	36.69
	65	16	17.30	30.99
	75	16.8	11.34	20.55
	85	17.5	8.89	16.32

Table 8.17 Variation of Fs as a function of the slope angle α for H = 10 m

Bench	Slope angle (α)	R (m)	Fs BISHOP	Fs FELLENIUS
3	45	17.5	11.52	17.02
	55	18	10.18	15.94
	65	19	8.09	13.10
	75	20	6.63	10.99
	85	21	5.66	9.63
6	45	17.5	9.97	14.62
	55	18	8.81	13.68
	65	19	7.03	11.26
	75	20	5.79	9.45
	85	21	4.96	8.30

Table 8.18 Variation of Fs as a function of the slope angle α for H = 15 m

Bench	Slope angle (α)	R (m)	Fs BISHOP	Fs FELLENIUS
3	45	22	7.62	10.40
	55	22	6.67	9.75
	65	23	5.53	8.36
	75	24	4.79	7.48
	85	25	4.21	6.73
6	45	22	6.70	9.05
	55	22	5.85	8.46
	65	23	4.87	7.26
	75	24	4.23	6.49
	85	25	3.73	5.85

Table 8.19 Variation of Fs as a function of the slope angle α for H = 20 m

Bench	Slope angle (α)	R (m)	Fs BISHOP	Fs FELLENIUS
3	45	28	6.33	8.40
	55	27	5.34	7.43
	65	27.5	4.57	6.64
	75	28.5	3.98	6
	85	29.5	3.54	5.5
6	45	28	5.64	7.39
	55	27	4.76	6.52
	65	27.5	4.08	5.82
	75	28.5	3.56	5.26
	85	29.5	3.18	4.82

Table 8.20 Variation of Fs as a function of the slope angle α for H = 25 m

Bench	Slope angle (α)	R (m)	Fs BISHOP	Fs FELLENIUS
3	45	37	5.85	7.32
	55	32	4.87	6.71
	65	32	4.12	5.85
	75	33	3.56	5.22
	85	34	3.16	4.72
6	45	37	5.28	6.52
	55	32	4.38	5.93
	65	32	3.71	5.17
	75	33	3.22	4.61
	85	34	2.86	4.17

Table 8.21 Variation of Fs as a function of the slope angle α for H = 30 m

Bench	**Slope angle (α)**	**R (m)**	**Fs BISHOP**	**Fs FELLENIUS**
	45	42	5.66	6.93
	55	38	4.47	6.01
	65	37	3.81	5.34
3	75	37.5	3.33	4.85
	85	38.5	2.93	4.32
	45	42	5.14	6.21
	55	38	4.06	5.36
	65	37	3.46	4.75
6	75	37.5	3.03	4.31
	85	38.5	2.68	3.84

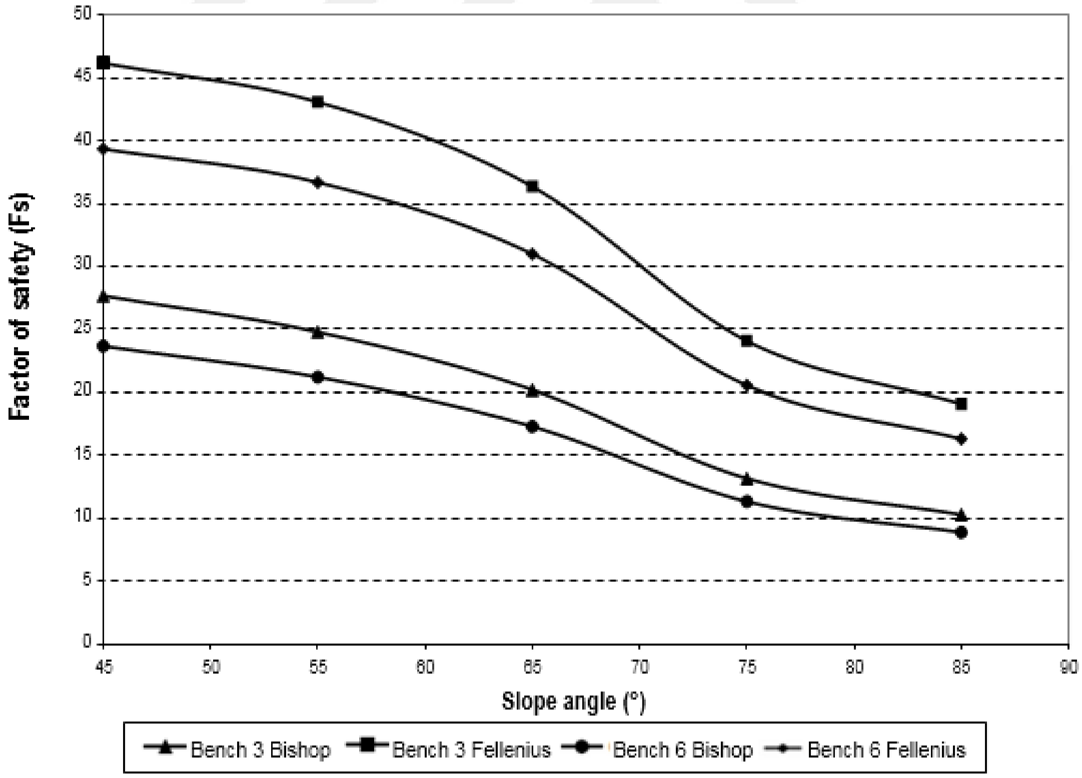

Figure 8.9 Variation of the coefficient Fs as a function of α for H = 5 m

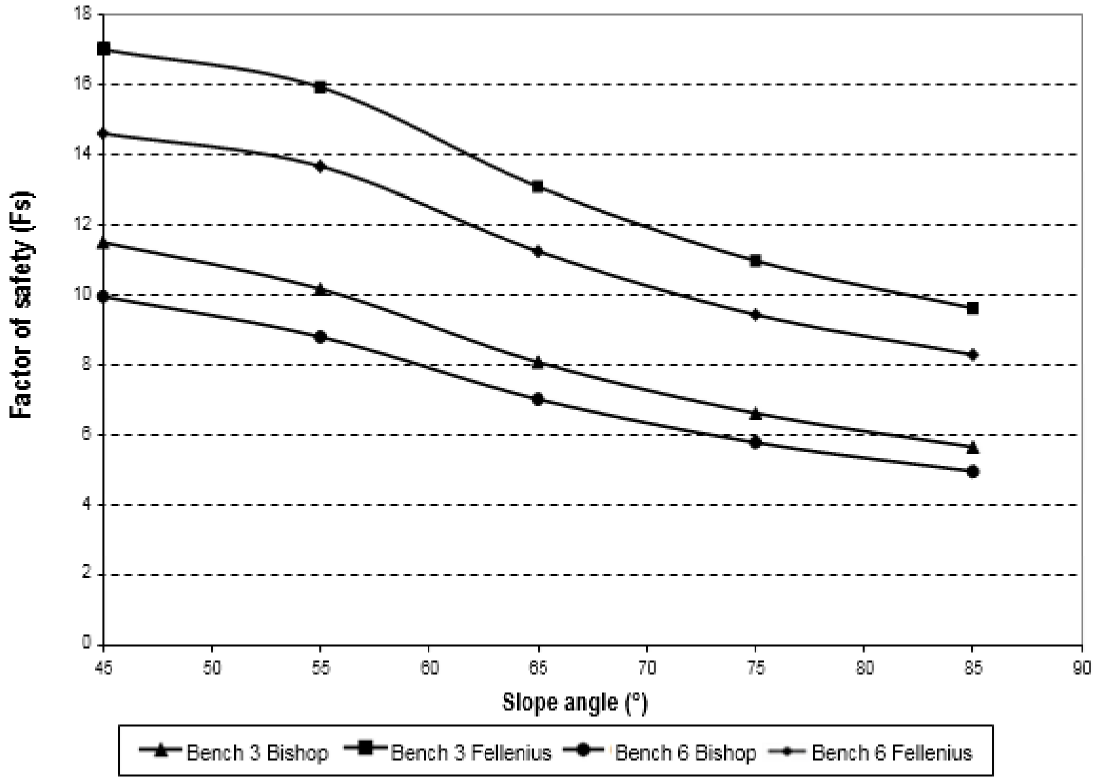

Figure 8.10 Variation of the coefficient Fs as a function of α for H = 10 m

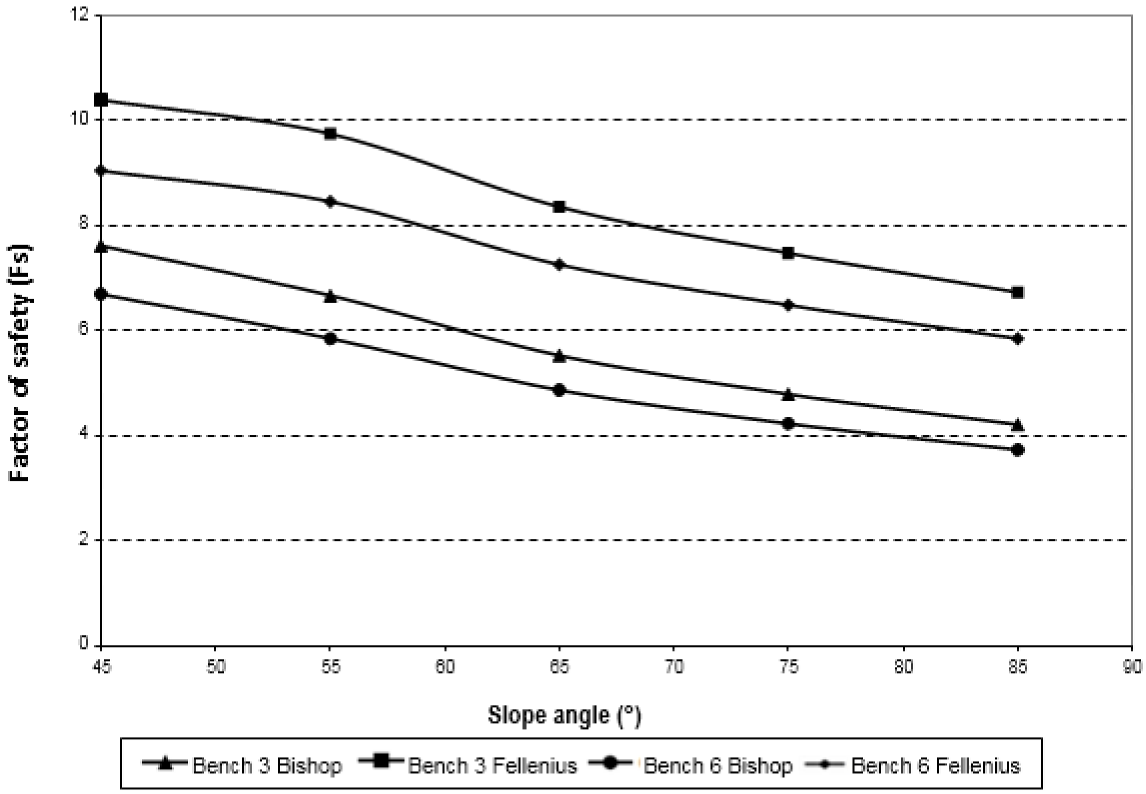

Figure 8.11 Variation of the coefficient Fs as a function of α for H = 15 m

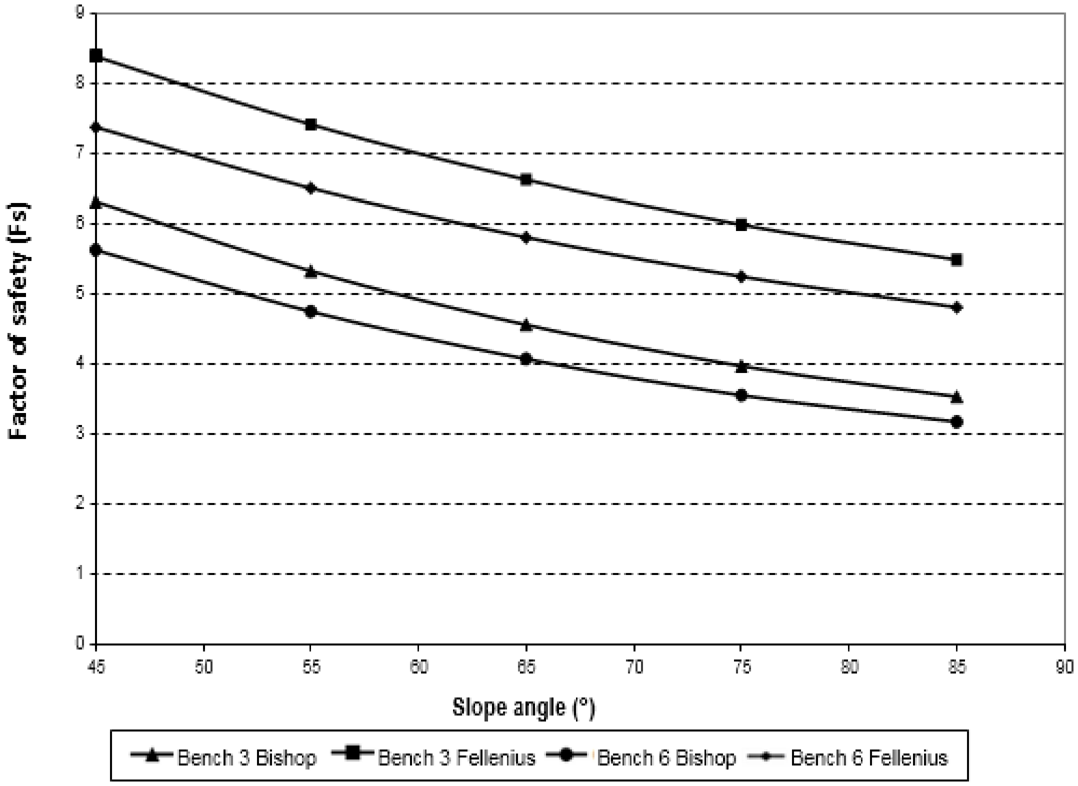

Figure 8.12 Variation of the coefficient Fs as a function of α for H = 20 m

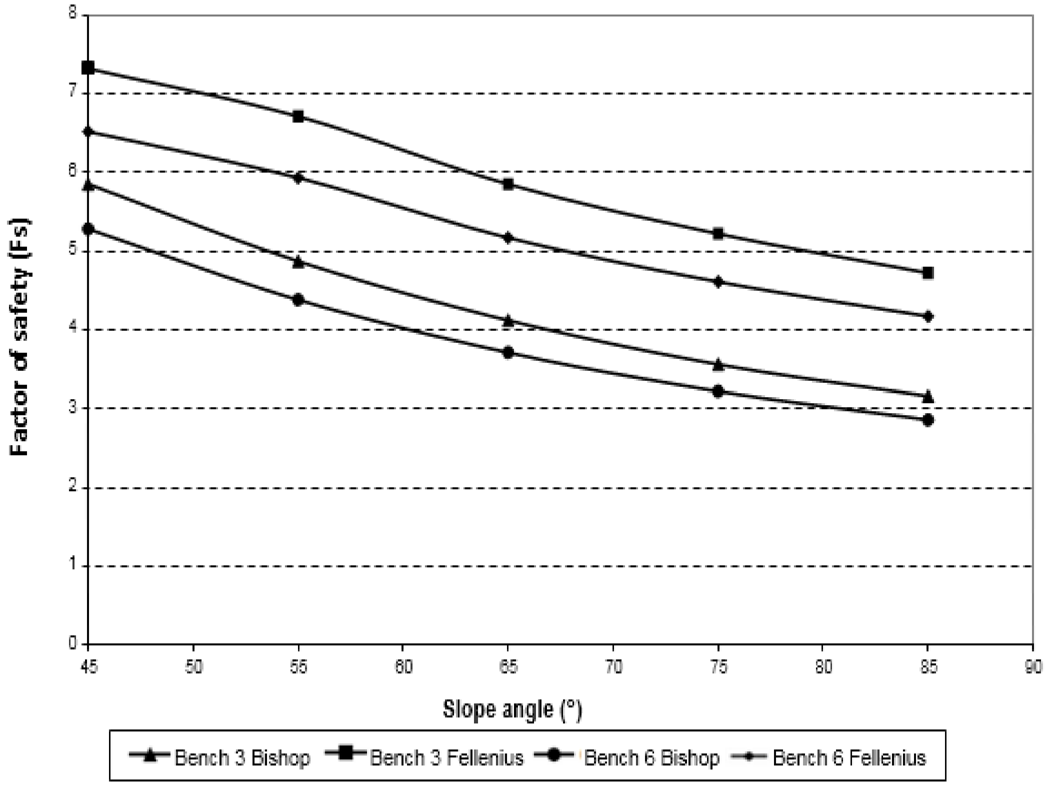

Figure 8.13 Variation of the coefficient Fs as a function of α for H = 25 m

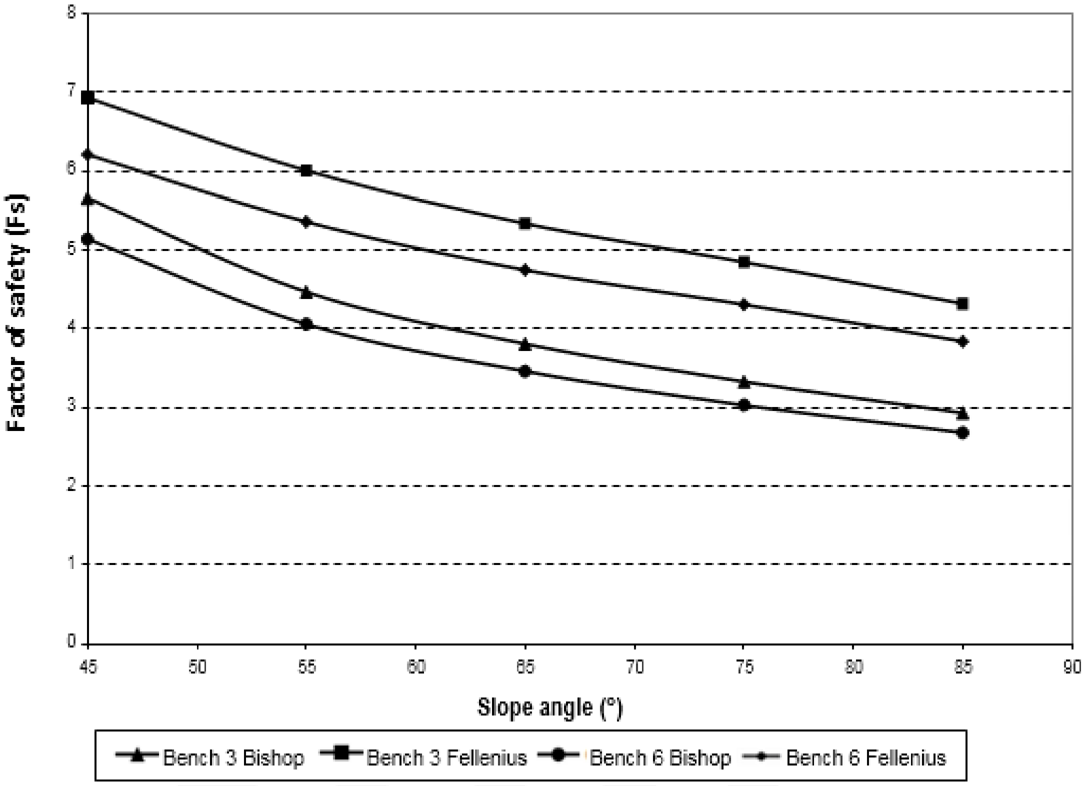

Figure 8.14 Variation of the coefficient Fs as a function of α for H = 30 m

8.4.5 Influence of Cohesion on the Factor of Safety (Fs)

In this case, the parameters (H, α, Φ ...) are fixed and the cohesion is only varied from 50 to 500 kN/m^2 with a step of 50 kN/m^2. The variation of the safety factor Fs is then obtained as a function of the cohesion C. The results obtained are given in Tables 8.22 to 8.26.

Table 8.22 Variation of the Fs as a function of the cohesion (C) for α = 45° (H = 15 m)

Benches	**Cohesion C**	**R (m)**	**Fs BISHOP**	**Fs FELLENIUS**
3 and 6	50	22	2.10	2.33
	100	22	2.72	3.24
	150	22	3.35	4.16
	200	22	3.97	5.07
	250	22	4.59	5.99
	300	22	5.21	6.90
	350	22	5.83	7.82
	400	22	6.45	8.73
	450	22	7.07	9.65
	500	22	7.69	10.56

Table 8.23 Variation of the Fs as a function of the cohesion (C) for α = 55° (H = 15 m)

Benches	**Cohesion C**	**R (m)**	**Fs BISHOP**	**Fs FELLENIUS**
3 and 6	50	22.5	1.78	1.98
	100	22.5	2.29	2.78
	150	22.5	2.80	3.59
	200	22.5	3.30	4.40
	250	22.5	3.81	5.21
	300	22.5	4.32	6.01
	350	22.5	4.83	6.82
	400	22.5	5.34	7.63
	450	22.5	5.84	8.43
	500	22.5	6.35	9.24

Table 8.24 Variation of the Fs as a function of the cohesion (C) for α = 65° (H = 15 m)

Benches	**Cohesion C**	**R (m)**	**Fs BISHOP**	**Fs FELLENIUS**
3 and 6	50	23	1.59	1.75
	100	23	2.09	2.49
	150	23	2.47	3.23
	200	23	2.91	3.96
	250	23	3.35	4.70
	300	23	3.78	5.43
	350	23	4.22	6.17
	400	23	4.66	6.91
	450	23	5.10	7.64
	500	23	5.54	8.38

Table 8.25 Variation of the Fs as a function of the cohesion (C) for α = 75° (H = 15 m)

Benches	**Cohesion C**	**R (m)**	**Fs BISHOP**	**Fs FELLENIUS**
3 and 6	50	24	1.46	1.59
	100	24	1.83	2.24
	150	24	2.20	2.90
	200	24	2.57	3.56
	250	24	2.94	4.21
	300	24	3.32	4.87
	350	24	3.69	5.52
	400	24	4.06	6.18
	450	24	4.43	6.84
	500	24	4.80	7.49

Table 8.26 Variation of the Fs as a function of the cohesion (C) for α = 85° (H = 15 m)

Benches	Cohesion C	R (m)	Fs BISHOP	Fs FELLENIUS
	50	25	1.37	1.46
	100	25	1.69	2.05
	150	25	2.00	2.64
	200	25	2.32	3.22
3 and 6	250	25	2.63	3.81
	300	25	2.95	4.40
	350	25	3.27	4.98
	400	25	3.58	5.57
	450	25	3.90	6.16
	500	25	4.21	6.75

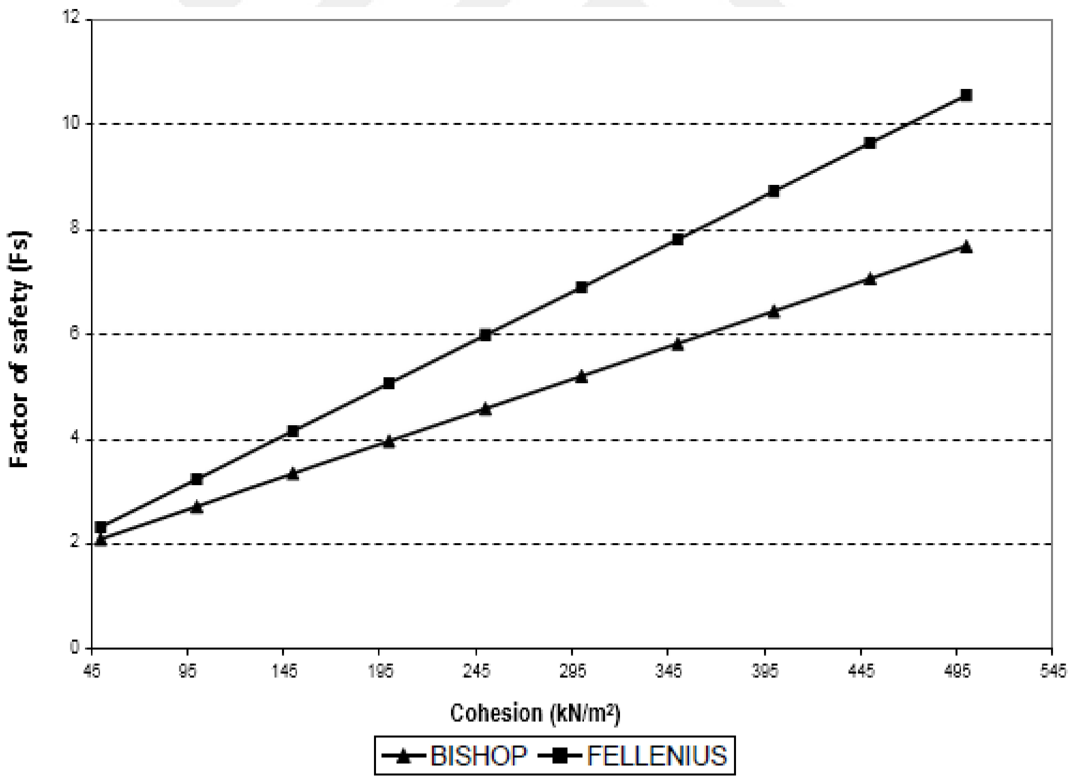

Figure 8.15 Variation of the Fs as a function of the cohesion (C) for α = 45°

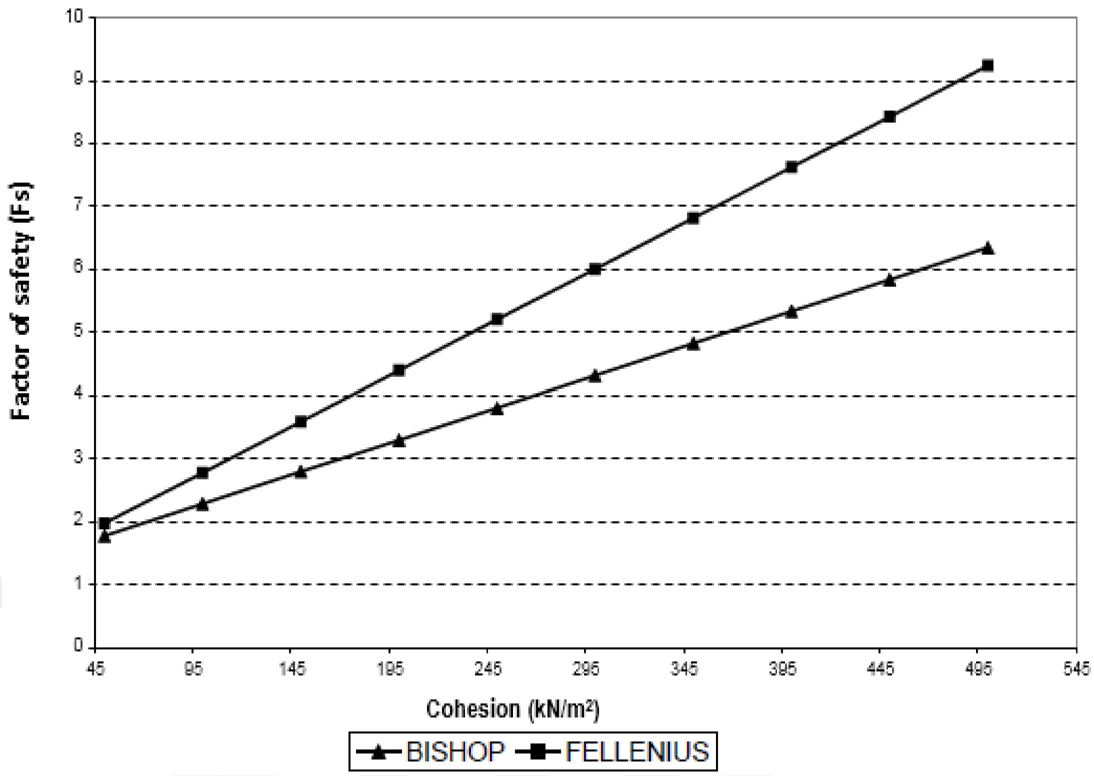

Figure 8.16 Variation of the Fs as a function of the cohesion (C) for α = 55°

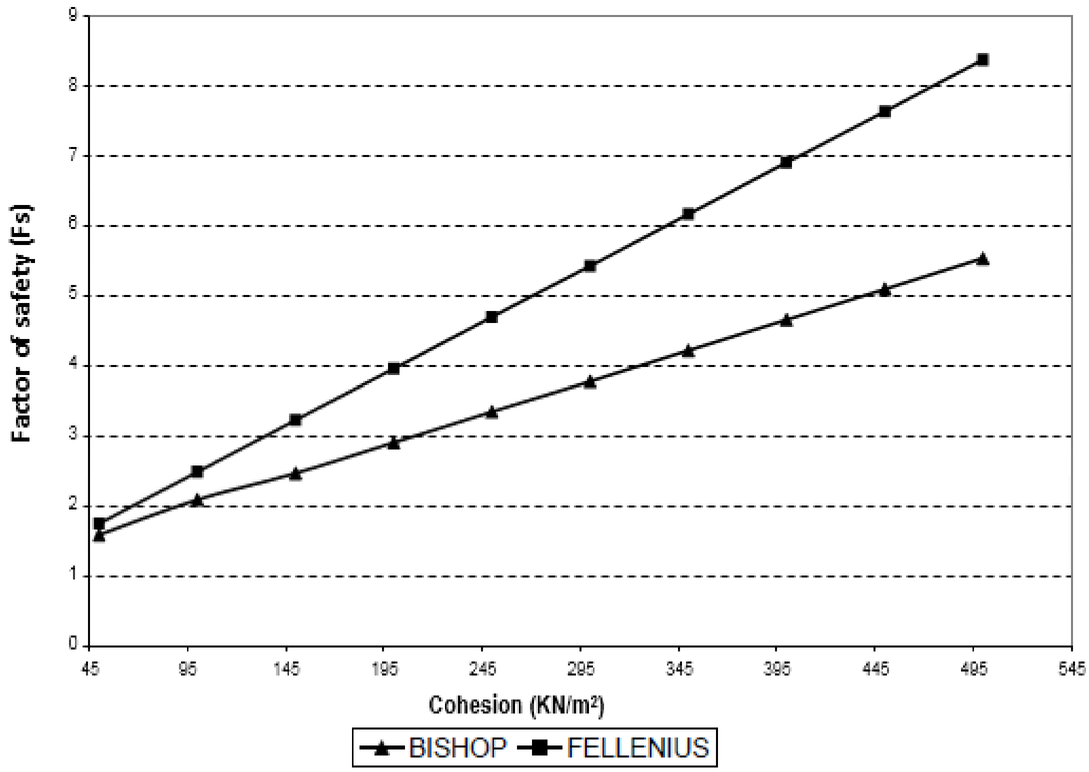

Figure 8.17 Variation of the Fs as a function of the cohesion (C) for α = 65°

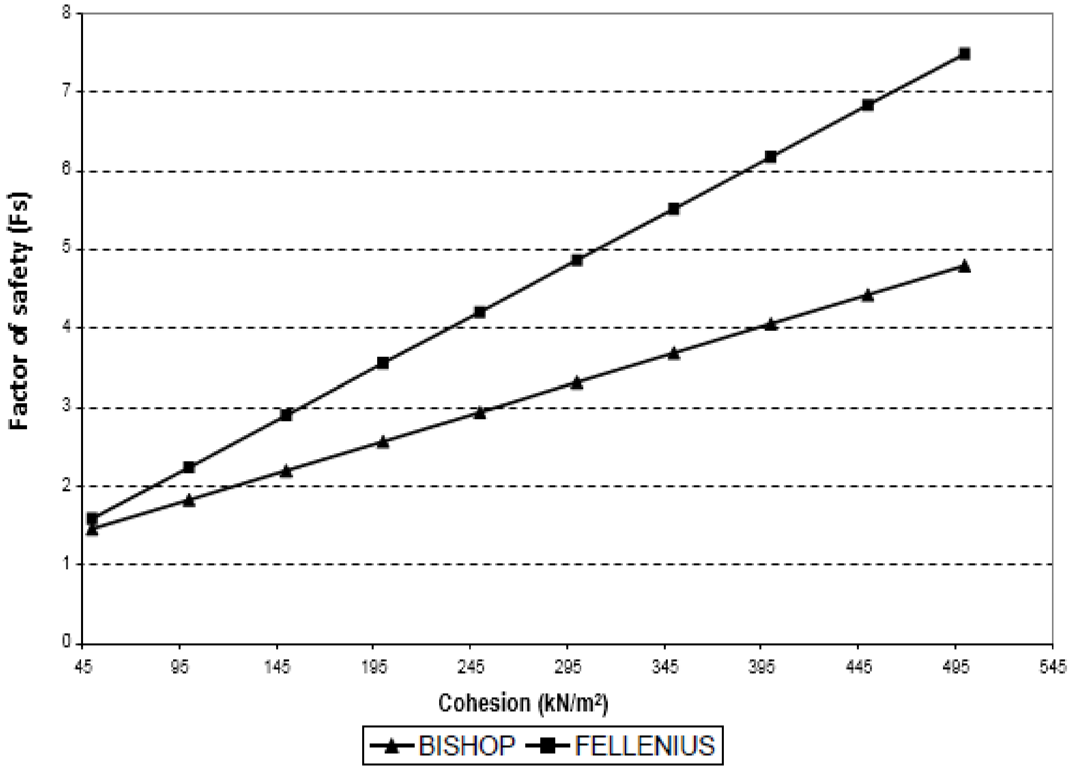

Figure 8.18 Variation of the Fs as a function of the cohesion (C) for α = 75°

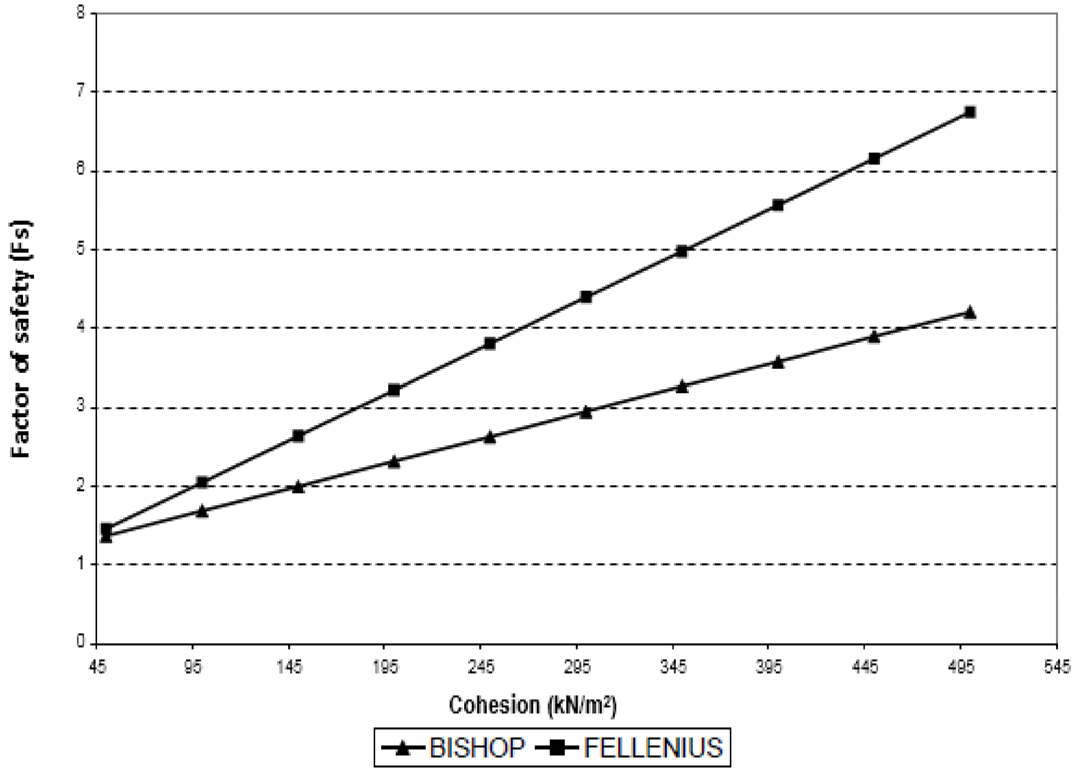

Figure 8.19 Variation of the Fs as a function of the cohesion (C) for α = 85°

8.4.6 Influence of the Internal Friction Angle on the Safety Coefficient (Fs)

We calculated the safety coefficient (Fs) as a function of the variation of the internal friction angle (Φ) from 5° to 45°, under the conditions of the pit: H = 15 m and α = 85°. The calculation results for benches 3 and 6 are given in Tables 8.27 and 8.28.

Table 8.27 Variation of the Fs as a function of the internal friction angle Φ for the bench 3 (α = 85° and H = 15 m)

Φ (°)	5	15	25	35	45
R (m)	25	25	25	25	25
Fs BISHOP	4.11	4.28	4.54	4.90	5.45
Fs FELLENIUS	5.96	6.15	6.37	6.62	6.94

Table 8.28 Variation of the Fs as a function of the internal friction angle Φ for the bench 6 (α = 85° and H = 15 m)

Φ (°)	5	15	25	35	45
R (m)	25	25	25	25	25
Fs BISHOP	3.67	3.78	3.96	4.23	4.66
Fs FELLENIUS	5.07	5.27	5.49	5.74	6.06

8.4.7 Calculation of the Critical Height H

For the calculation of the critical height of the benches, taking into account the angle of the slope of the quarry (85 °), the method of the Hoek chart was used (Figure 8.20). This method, established by Hoek, is sometimes used to calculate the safety coefficient Fs. To determine Fs, it is sufficient to know the function of the slope angle (X) and the function of the bench height (Y). The point of intersection of the latter allows us to determine the corresponding safety coefficient.

The functions X and Y are defined by the following formulas:

$$X = i - 1.2\Phi \quad (8.14)$$

$$Y = \frac{\gamma.H}{C} \quad (8.15)$$

Where, i slope angle, Φ internal friction angle, γ rock mass density, H Bench height, C cohesion of the rock.

The critical height of the bench can be determined by setting the other parameters and taking a critical safety factor (1.2).

For that, one calculates X, then we determine the point of intersection between the value of X and the value of Fs = 1.2. The value of Y corresponding is determined on a chart and H is thus determined.

For Fs = 1.2, i = 85°, Φ = 38.8°, γ = 25 kN/m^3, C = 499 kN/m^2 (bench 3) and 424 kN/m^2 (bench 6) shown in Tables 29 and 30.

Table 8.29 Critical height of bench 3 of the Farabakouta East (FE) Pit (for Fs = 1.2 and Fs = 1.4)

FOS	**X**	**Y**	**H (m)**
1.2	38.44	6	120
1.4	38.44	5	100

Table 8.30 Critical height of bench 6 of the Farabakouta East (FE) Pit (for Fs = 1.2 and Fs = 1.4)

FOS	**X**	**Y**	**H (m)**
1.2	38.44	6	102
1.4	38.44	5	85

From the results obtained, it can be seen that the critical height H is very high. Thus, the height of 15 m chosen for the benches of the quarry largely ensures the stability of the benches. Provided you take into account the cracks and tectonic accidents that cross the quarry (especially faults).

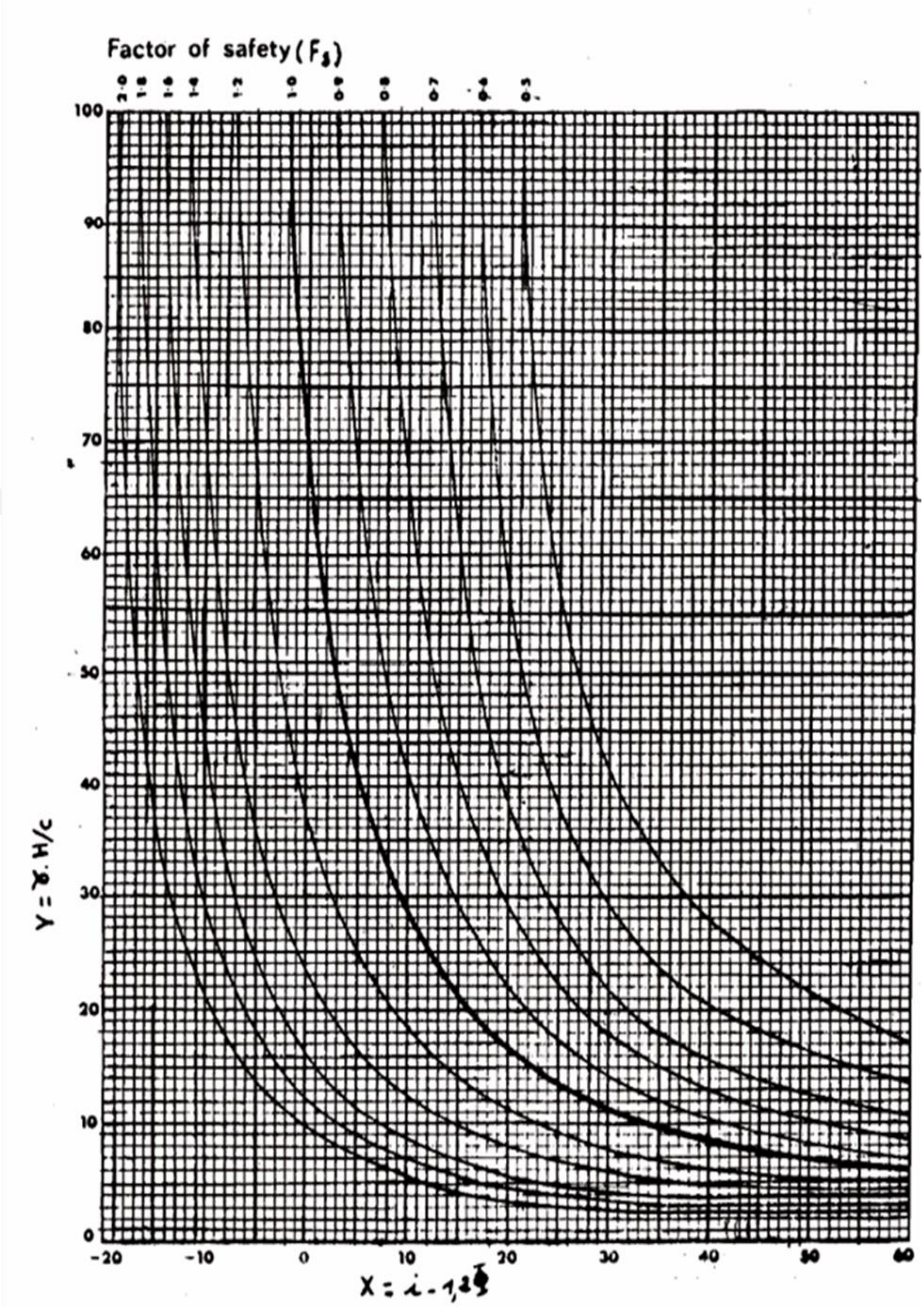

Figure 8.20 Abacus of Hoek (Hoek et al, 2002)

8.5 Results Interpretation

The first result that can be drawn from this study is that the slopes of the Sadiola gold mine are very stable, given the mechanical properties of marble (high compressive strength, high cohesion, etc.).

The Figures 8.4 to 8.8 show that the factor of safety decreases as the bench height increases. The values of the factor of safety are in all cases over 2, so the slopes are stable for H varying between 5 and 30 m.

The variation of the safety factor (Fs) decreases when the slope angle (α) increases (Figures 8.9 to 8.14). In all cases, the results obtained show that the slopes are stable for H varying between 5 m and 30 m. The lowest value of Fs is 2.68 obtained by Bishop's method for $\alpha = 85°$ and $H = 30$ m (bench 6). This value is much higher than the minimum allowed safety factor (1.2).

The safety factor increases with increasing cohesion value (Figures 8.15. to 8.19). For $\alpha = 85°$ and $C = 50$ kN/m^2, the value of the safety coefficient is close to the critical value allowed. We have seen that the value of C is generally very high for the Farabakouta East (FE) pit, but this value can decrease locally, especially in very cracked or faulted places because C depends on the coefficient of structural weakening.

The safety factor increases with the increase in the value of the internal friction angle. The slopes are stable for Φ varying between 5° and 45° while cohesion is between 50 kN/m^2 and 500 kN/m^2

CHAPTER NINE

CONCLUSIONS AND RECOMMENDATIONS

The study of slope stability in quarries requires several steps, the main ones being:

- To study the geological and mining conditions of the quarry;
- To study the physico-mechanical properties of the rocks of the quarry by carrying out measurements in the laboratory;
- To calculate the mechanical properties of rocks in the rock mass. The study of the rock mass cracking is one of the main parameters to be taken into account in this part.
- To calculate the factor of safety which will indicate us the state of stability of the terrains. If Fs <1.2, the rock mass is not stable. In this part of the study, it is necessary to study the variations of Fs as a function of the geometrical parameters and the mechanical properties of the terrains: bench height H, slope angle α, cohesion of the mass and internal friction angle.
- Finally, calculate the critical benches height according to the geometrical parameters and mechanical of the quarry.

To carry out a stability study of the slopes by following all the steps mentioned above, we took the Sadiola Open pit gold mine (Farabakouta East Pit) as an example.

The results of this study indicate that the compressive strength of marble is very high.

Measurements of the number of fissures in the rock mass have shown that the density of cracking is high.

For the calculation of stability, the methods of FELLENIUS and Simplified BISHOP were used. The BISHOP method gives values of Fs lower than those given by the Fellenius method. It is therefore recommended to use this method for calculating slope stability, especially in the case of unstable slopes or at the stability limit.

The estimation of slope stability using the calculation of the safety coefficient Fs, and the variations of Fs as a function of H, α, C_m and Φ_m show that the benches of the Farabakouta East (FE) pit are very stable.

The critical height of the bench was then calculated by the Hoek abacus (Hoek et al, 2002). This critical height turns out to be very high (100 m).

We recommend doing extensive studies in benches that are very cracked and where faults cross the gold deposit.

The recommendations derived from the present study were described in Chapter 7. In summary these recommendations suggest:

- Confirm the bench configurations used in the current design (Figure 7.2) consisting of 20 m high benches with 75^0 battered faces on the pit limits.
- Extend the saprolite slope design, consisting of 10 m high benches stacked at 35^0 toe to toe, from elevation +100 m down to elevation +80 m as sketched in Figure 6.4.
- Replace the geotechnical berms on the west slope with an additional access ramp as sketched in Figure 6.3, keeping the same stack (55^0 toe to toe) and overall ($\approx 49^0$) slope angles.
- Adjust the stack angles of the south slope implementing 35^0 (toe to toe) in the saprolite slope and 50^0 (toe to toe) in the rest of the slope with a maximum stack height of 100 m.

A plan with the recommended slope configurations is shown in Figure 7.4 and typical profiles are presented in Figure 7.5, Figure 7.6 and Figure 7.7**,** for the west, east and south slopes, respectively.

REFERENCES

Abouchami, W., Boher, M., Michard, A., and Albarede, F., 1990. A major 2.1 Ga event of mafic magmatism in West Africa: an early stage of crustal accretion. *Journal of Geophysical Research 95*, 17605-17629.

Barton, N., and Bandis, S. (1990). *Review of Predictive Capabilities of JRC-JCS Model in Engineering Practice*. Rock Joints, Proc. Int. Symp. on Rock Joints.

Bassot, J.-P. 1966. *Etude géologique du Senegal oriental et de ses conflns guin & maliens. MbrrL Bur. Rech. Mb-u, Parts, 40*, 1-322.

Bassott, J.P. (1987). The calc-alkaline volcano-plutonic complex of Dalema (Eastern Senegal) River: Discussion of its geodynamic significance in the context of Eburnean orogeny (lower Proterozoic). *Journal of African Earth Sciences 6*, 505-519.

Bassot, J.P., and Caen-Vachette, M., 1984. *Données géochronologiques et géochimiques nouvelles sur les granitoïdes de l'Est du Sénégal : Implications sur l'histoire géologique du Birimien de cette région ; in Klerkx, J., Michot, J., (eds.), African Geology : Belgium, Tervuren*, 196-209.

Benyounes K. (1989). Contribution à l'étude des glissements dans le terrain tendre – mine de fer – Ouenza. *Mémoire de PFE. ENP*. Alger. 128.

Bieniawski, Z. T. (1989). *Engineering Rock Mass Classifications*. John Wiley, Rotterdam.

Béziat, D., Bourges, F., Debat, P., Lompo, M., Martin, F., and Tollon, F., 2000. Palaeoproterozoic ultramafic-mafic assemblage volcanic rocks of the Boromo greenstone belt: fractionates originating from island arc in the West African Craton. *Precambrian Research 101*, 25-47.

Bishop, A.W. (1954). *The Use of the Slip Circle in the Stability Analysis of Slopes, Geotechnique 5*, 7 - 17.

Boher, M., Abouchami, W., Michard, A., Albarede, F., and Arndt, N.T. (1992). Crustal growth in West Africa at 2.1 Ga. *Journal of Geophysics Research 97*, 345-369.

Boshoff, F., Hanssen, E., Hill, J.V., Jones, D., Kaisin J., Traore, S., and Voet, H.w., 1998. The Sadiola Hill Mine: A lower Proterozoic gold deposit in the Kinieba window-Mali, West Africa. *Unpublished report to Anglo American*, 6.

Bossière, G., Bonkoungou, I., Peucat, J.J., and Pupin, J.P. (1996). Origin and age of Paleoproterozoic conglomerates and sandstones of the Tarkwaian Group in Burkina Faso, West Africa. *Precambrian Research 80*, 153-172.

Dabo, M., and Aïfa, T., 2010. *Structural styles and tectonic evolution of the Kolia-Boboti sedimentary Basin, Kédougou-Kéniéba inlier, eastern Senegal. Comptes Rendus Geoscience 342*, 796-805.

Dabo, M., and Aifa, T. (2011). Late eburnean deformation in the Kolia-Boboti sedimentary basin, Kedougou-Kenieba Inlier, Senegal. *Journal of African Earth Sciences 60*, 106-116.

Debat, P., Diallo, DP, Ngom, PM, Rollet, M. and Seyler, M. (1984). The series of Mako in its central and southern parts (eastern Senegal, West Africa). Information on the evolution of the volcano-sedimentary series and preliminary geochemical data on post-tectonic magmatic formations. *Journal of African Earth Sciences 2*, 71-79.

Dia, A., van Schmus, W.R., and Kröner, A. (1997). Isotopic constraints on the age and formation of a Palaeoproterozoic volcanic arc complex in the Kedougou Inlier, eastern Senegal, West Africa. *Journal of African Earth Sciences 24*, 197–213.

Dioh, E., Béziat, D., Debat, P., Grégoire, M., and Ngom, P.M. (2006). Diversity of the Paleoproterozoic granitoids of the Kedougou Inlier (eastern Senegal): Petrographical and geochemical constraints. *Journal of African Earth Sciences*, *44*, 351-371.

Ennih, N. and Liegeois. (2008a). The Boundaries of the West African Craton (IGCP485). *Geological Society of London Special Publication 297*, 536.

Fellenius, W. (1936). *Calculation of the Stability of Earth Dams, Trans. 2nd Cong. on Large Dams 4*, 445.

Gueye, M., Siegesmund, S., Wemmer, K., Pawlig, S., Drobe, M., Nolte, N., and Layer, P. (2007). New evidence for an early birimien evolution in the West African Craton: An example from the Kedougou-Kéniéba Inlier, southeast Senegal. *South African Journal of Geology 110*, 511-534.

Gueye, M., Ngom, P.M., Diéne, M., Thiam, Y., Siegesmund, S., Wemmer, K., and Pawling, S. (2008). Intrusive rocks and tectono-metamorphic evolution of the Mako Paleoproterozoic belt (Eastern Senegal, West Africa). *Journal of Africa Earth Sciences 50*, 88-110.

Groves, D.I., Goldfarb, R.J., Gebre-Mariam, M., Hangemann, S.G., and Robert, F. (1998). Oregenic gold deposit: A proposed classification in the context of their crustal distribution and relationship to other gold deposit types. *Ore Geology Reviews 13*, 7-27.

Hanssen, E., Kaisin, J., Mounkoro, B., and Hill, J. (1998). *Sadiola sulphide drilling project*. Unpublished, report to IAMGOLD Corporation on behalf of SEMOS, 87.

Hasting, D., 1982. On the tectonics and metallogenesis of West Africa: A model incorporating new geophysical data. *Geoexploration 20*, 295-327.

Hein, K.A.A. (2008). Geology of the Sadiola open cast and ancillary pits, Mali. *Final company report to SEMOS S.A. Mali*, 18.

Hein, K.A.A., and Tshibubudze, A., 2007a. Sadiola Ore Genesis Model, Sadiola Mine and satellite pits, *Mali. Preliminary company report to Société D'Exploitation des Mines d'Or de Sadiola S.A. (SEMOS), Mali, June 2007*, 16.

Hein, K.A.A., and Tshibubudze, A., 2007b. Sadiola Ore Genesis Model, Sadiola Mine and satellite pits, Mali. *Final company report to Société D'Exploitation des Mines d'Or de Sadiola S.A. (SEMOS), Mali, August 2007*, 15.

Hirdes, W., and Davis, D.W. (2002). U-Pb Geochronology of Paleoproterozoic rocks in the southern part of the Kedougou-Kéniéba Inlier, Senegal, West Africa: evidence for diachronous accretionary development of the Eburnean province. *Precambrian Research 118,* 83–99.

Hoek, E., Carranza-Torres, C., and Corkum, B., (2002). *Hoek-Brown criterion – 2002 edition*. Proc. NARMS-TAC Conference, Toronto, 2002, *1*, 267-273.

IAMGold Corporation. (2007). "Joint Management Information Circular, April 30th"

Kadio, E., Coulibaly, Y., Allialy, M.E., Kouamelan, A.N., and Pothin, K.B.K. (2010). On the occurrence of gold mineralizations in southeastern Ivory Coast. *Journal of African Earth Sciences 57*, 423-430.

Laubscher, D.H. (1990). *A geomechanics classification system for the rating of rock mass in mine design*. J. S. Afr. Inst. Min. Metall., *90*, Oct. 1990, 257-273.

Lawrence DM, Treloar PJ, Rankin AH, Harbidge P, and Holliday J. (2013). *The Geology and Mineralogy of the Loulo Mining District, Mali, West Africa*. Evidence for Two Distinct Styles of Orogenic Gold Mineralization. Economic Geology *108,* 199-227

Ledru, P., Pons, J., Mile´si, J.P., Feybesse, J.L., and Johan, V. (1991). Transcurrent tectonics and polycyclic evolution in the Lower Proterozoic of Senegal-Mali. *Precambrian Research 50*, 337–354.

Leube, A., Hirdes, W., Mauer, R., and Kesse, G.O. (1990).The early Proterozoic Birimian Supergroup of Ghana and some aspects of its associated gold mineralization. *Precambrian Research 46*, 139-165.

Liégeois, J.P., Claessens, W., Camara, D., and Klerkx, J., 1991. *Short-lived Eburnian orogeny in southern Mali*. Geology, tectonics, U-Pb and Rb-Sr geochronology. Precamb. Res., 50, 111-136.

Macfarlane, A., Crow, M.J., Arthurs, J.W., Wilkinson, A.F., and Aucott, J.W., 1981. The geology and mineral resources of northern Sierra Leone. *Overseas Mem. Inst. Geol. Sci. 7*, 103.

Mamadou, 2017. Rapport de Relations litho-structurales avec la minéralisation aurifère du gisement de Sadiola.

Matabane, M. (2008). The geology of the FE3 open cast, Sadiola, Mali: Stratigraphy, structure and intrusive rocks. *Honours thesis, University of the Witwatersrand, Johannesburg*, 56.

Matthias, I.R., and Hein, K.A.A. (2002). Character, morphology and origin of gold from the selected mines in the Yatela and Sadiola goldfield, Mali, West Africa. In: Poster Presentation to the WAXI Sponsors Meeting, Ouagadougou, Burkina Faso, 28 March to 1 April 2011

Meinert, L.D. (1992). Skarns and Skarn Deposits. *Journal of the Geological Association of Canada 19*, 4.

Milési, J.P., Feybesse, J.L., Ledru, P., Dommanget, A., Ouedraogo, M.F., Marcoux, E., Prost, A., Vinchon, C., Sylvain, J.P., Johan, V., Tegyey, M., Calvez, J.Y., and Lagny, P., 1989. *Minéralisations aurifères de l'Afrique de l'Ouest, leurs relations avec l'évolution litho-structurale au Protérozoïque inférieur*. Carte géologique au 1/2.000.000. Chronique de la recherche minière 497, 3–98.

Milési, J.P., Ledru, P., Feybesse, J.L., Dommanget, A., and Marcoux, E. (1992). Early proterozoic ore deposits and tectonics of the Birimian orogenic belt, West Africa. *Precambrian Research 58*, 305–344.

Pawling, S., Gueye, M., Klischies, R., Schwarz, S., Wemmer, K., and Siegesmund, S. (2006). Geochemical and Sr-Nd isotopic data on the Birimian of the Kedougou-

Kenieba Inlier (eastern Senegal): Implications on the Palaeoproterozoic evolution of the West African Craton. *South African Journal of Geology 109*, 411-427.

Potrel, A., Peucat, J.J., and Fanning, C.M., 1998. Archean crustal evolution of the West African Craton: example of the Amsaga Area, (Requibat Rise). U-Pb and Sm-Nd evidence for the crustal growth and recycling. *Precambrian Research 90*, 107-117.

Ranson, R.L., 1998. *Structural modelling of the Sadiola Hill Gold Deposit, Mali, MSc thesis*, University of Exeter, England.

Robins, P.S. (2006). The quantification of grade uncertainty, and associated risk, and their influence on pit optimization for the Sadiola deep sulphide prefeasibility project. *MSc thesis, University of the Witwatersrand, Johannesburg,* 139.

Rocscience. (2002), *Slide v.5.0 – 2D Limit Equilibrium Slope Stability Analysis*.

Rocscience. (2002), *Swedge v.5.010 – 3D Limit Equilibrium Analysis of Wedge Failures.*

Rocscience. (2002), *Phase2 v.6.0 – Finite Element Analysis for Excavations and Slopes.*

Rocscience. (2003), Dips v.5.106 – Statistical Analysis of Orientations of Structural Data.

Rocscience. (2008), Rockplane v.2.041 – 3D Limit Equilibrium Stability Analysis of Planar Failures.

Ryan, T.M., and Pryor, P.R. (2000). *Designing Catch Benches and Interramps Slopes*. In Slope Stability in Surface Mining, Hustrulid, McCarter & Van Zyl (Eds.), SME, Chapter 3, 27-38.

SEMOS. (2009). *Sadiola Deep Sulphide Project. Pre-Feasibility Study*. SEMOS report, October 2009.

Sibson, R.H., and Poulsen, F.R.K. (1988). High-angle reverse faults, fluid-pressure cycling, and mesothermal gold-quartz deposit. Geological Society of America *16*, 551-555.

SRK (Steffen, Robertson and Kirsten). (2000). *Mining Geotechnical Evaluation and Slope Design for the Cut III Pit, Sadiola.* SRK Report prepared for AngloGold. Report No 199542/1, May 2000.

SRK (Steffen, Robertson and Kirsten). (2009). *Feasibility Level Mining Geotechnical Investigation for the Sadiola Deep Sulphide Project, Republic of Mali*. SRK Report prepared for AngloGold Ashanti. Report No 398529, March 2009.

SRK (Steffen, Robertson and Kirsten). (2010). *Sadiola Mine Deep Sulphide Pit Slope Study Final Report*. Report No 413514-1 Rev1, August 2010

Theron, S.J., 1997a. The intrusive and extrusive rocks from the Sadiola concession areas: *A petrographical and geochemical study, 6 February 1997, Unpublished AARL Gold and Base Metal Unit Report No. M96X5071*, 50.

Voet, H.W., 1997. Cross folding at Sadiola hill mine and the possible extent of the orebody to the south. *Unpublished, report to Anglo American Corporation of South Africa Limited, File 13/147/500(a), 19 November 1997*, 3.

WAXI. (2013). Confidential Final Report, P934A West African Exploration Initiative. Stage 2, 924.

Witschard, F. (1965). *Contribution to the geological and petrological study metallogenic granite massifs Senegal Oriental. Memories BRGM 44*, 171.

APPENDICES

WAC = West African Craton

KKI = Kedougou-Kenieba Inlier

MTZ = Main Transcurrent Shear Zone

SEMOS = Société D'Exploitation des Mines d'Or de Sadiola

SFZ = Sadiola Fracture Zone

QFP = Quartz-Feldspar-Porphyry

PPE = Personal Protective Equipment

QAQC = Quality Analyze, Quality Control

Sp = Stock pile

F = Finger

FE = Farabakouta East

USCS = Unified Soil Classification System

UCS = Uniaxial Compressive Strength

TCS = Triaxial Compression Strength

IS50 = Point Load Strength

SHS = Shear Box Strength

IRS = Intact Rock Strength

GSI = Geological Strength Index

JCr = Joint Condition rating

FFr = Fracture Frequency rating

DIORw = weathered diorite

DIOR = Diorites

DCMB = Decarbonated Marble

CAMB = Carbonated marbles

MGWK = Meta-sandstones

Sap = Saprolite

SZ = Shear zone

RFA = residual friction angle

CV = Coefficient of Variations

LEM = Limit Equilibrium Method

FEM = Finite Element Model

PoO = Probability of Ocurrence

LFB = Length of Failed Bench

LB = Length of Bench

FoS = Factors of Safety

SRF = Stress Reduction Factors

R_c = Compressive strength

F_{max} = Breaking load

R_t = Tensile strength

T_{max} = Maximum Tensile Force

C_{sam} = Cohesion of a sample

Φ_{sam} = Friction angle of a sample

C_m = Cohesion of a rock mass

Φ_m = Internal friction angle of a rock mass

γ = Unit weight

GC = Grade Control

SRK = Steffen, Robertson and Kirsten company

Mi = Material Index

WAXI = West African Exploration Initiative